THE JOURNAL OF THE INSTITUTION OF ENGINEERS, MALAYSIA

KDN PP5476/10/2012 (030203)
ISSN 0126-513X
Vol. 73, No. 3
September 2012

IEM JOURNAL

Vol. 73, No. 3, September 2012
KDN PP5476/10/2012 (030203) ISSN 0126-513X

CONTENTS

1 Selecting A Design Of Sustainable Inland Container Ship For Bangladesh Based On Economical And Environmental Performances
by N. M. Golam Zakaria, K. Shahriar Iqbal, M. Imran Khaled and M. Milon Khan

7 CNTs/SnO_2 And CNTs/MnO_2 Nanocomposites For The Fabrication Of The Electrodes For Supercapacitors
by Ir. Dr Ng Kok Chiang and Dr Daniel Jewell

14 Numerical And Experimental Study On Wave Propagation In The Open Atmosphere
by Mohammad Ali Jinnah and Mohammad Monjurul Ehsan

23 An Analytical Study Of Fluid Tank System For Reducing The Rolling Of A Ship
by Gazi Md. Khalil, Md. Shahjada Tarafder and Md. Shahidul Islam

33 Frequency Analysis Of Annual Runoff In Peninsular Malaysia Using A Regional Approach Based On L-Moments
by Aminuddin Mohd. Baki, Ismail Atan and Nora Farina Mohd. Halim

39 Referees Form

41 Information for Authors

THE INSTITUTION OF ENGINEERS, MALAYSIA
Bangunan Ingenieur, Lots 60 & 62, Jalan 52/4,
P.O.Box 223 (Jalan Sultan),
46720 Petaling Jaya, Selangor Darul Ehsan.
Tel: 03-7968 4001/4002
Fax: 03-7957 7678
E-mail: sec@iem.org.my **Homepage:** http://www.myiem.org.my

Printed by: RED CARD MARKETING (M) SDN. BHD. (622849-V)
No. 20, Jalan TPK 1/2, Seksyen 1, Taman Perindustrian Kinrara,
47100 Puchong, Selangor Darul Ehsan.
Tel: 603-8075 6773 (Hunting Line) **Fax:** 603-8075 1937, 8075 1987
Website: www.redcard.com.my

Mailer: PERFECT MAIL SERVICES (648839-P)
14 Jalan TSB 2, Taman Perindustrian Sungai Buloh,
Sungai Buloh, Selangor Darul Ehsan.
Tel: 603-6156 5288

PRINT QUANTITY: *5,500 Copies*

SELECTING A DESIGN OF SUSTAINABLE INLAND CONTAINER SHIP FOR BANGLADESH BASED ON ECONOMICAL AND ENVIRONMENTAL PERFORMANCES

(Date received: 14.12.11/Date accepted: 15.10.12)

N. M. Golam Zakaria[1], K. Shahriar Iqbal[2], M. Imran Khaled[3] and M. Milon Khan[4]

[1]Department of Naval Architecture and Marine Engineering,
Bangladesh University of Engineering and Technology, Dhaka, Bangladesh
E-mail: [1]gzakaria@name.buet.ac.bd, [2]ksiqbal@yahoo.com, [3]imrankhaled@yahoo.com, [4]milon_1871@yahoo.com

ABSTRACT

A sustainable design of a container ship from alternative options has been selected for inland shipping in Bangladesh. In this selection process commercial attractiveness of these vessels were compared at first by using net present values (NPV) of the investment as well as assessing the required freight rate (RFR) for carrying unit container. Environmental impact assessment (EIA), another important parameter nowadays, has also been assessed to analyse the consequences imposed by all the models on environment throughout the lifetime. Before making the final selection, their service qualities were also discussed. Considering all parameters, the ship with hatch cover has been found to be the best option for inland waterways in Bangladesh.

Keywords: *Economic performance, environmental impact assessment, ship design, global warming*

1.0 INTRODUCTION

Bangladesh is going to add a new fleet of container ships in her inland waterways in order to enhance the mobility of containers from and to the country's sea ports. It will definitely ease pressure on road and train transportation for delivering container. To do so inland container ports and the container handling facilities are being developed. New container ships are being owned by some public and private entrepreneurs.

In most of the cases commercial attractiveness of ships are considered for choosing the project. A design selected on the basis of only economic performance may not sustain for long. People all over the world have become more aware of their consumption of goods and services and their impact on the natural resources and quality of environment. As a result, new stricter regulation is coming day by day to tackle global and local issues like climate change, ozone layer depletion etc. Such regulations often increase the cost of operation. So it is always wise to take these possibilities into account while planning to launch a new project.

The main objective of this paper is to focus on selecting a design considering not only the commercial attractiveness but also the environmental burden imposed by the ships. The quality of service is also considered in this selection process.

Hasegawa and Iqbal [1], Iqbal and Hasegawa [2] and Iqbal and Shill [3] adopted methodology to compare inland water and road transportation systems to find the best option for carrying cargo and passenger. This method included comparison of economical benefit, environmental burden imposed and service quality rendered by the transportation systems. In this paper similar methodology was used to compare alternative design of container ships. Here the environmental impact assessment was carried more in depth using the software SimaPro [4].

2.0 METHODOLOGY

For economic analysis net present values (NPV) of the investment after considering the total price of the ships and operating costs throughout its entire life span has been estimated for a number of alternative designs of container ships suitable for inland waterways of Bangladesh for the proposed Dhaka-Chittagong route. The minimum freight charges required to carry a container (TEU) between the same route, that is, required freight rate (RFR) [5], are also estimated and compared to find the commercial attractiveness. In all the cases 12% rate of return (RR) on the investment was taken into account.

Environmental impact assessment (EIA) is the technical qualitative and quantitative characterization and assessment of the consequences of absorption and emission of various materials and substances from and to the environment. The impact analysis addresses ecological and human health consequences and resource depletion and could be divided into three sub-phases:

- Classification: sorting of parameters into environmental effect categories.
- Characterisation: calculation of the potential contribution of the environmental loading to each effect category.
- Valuation: assessment of the total environmental impact of the product life cycle.

In this study SimaPro, an EIA database software, was used to assess the consequences on the environment carried by the alternative container ships in their whole life cycle. The effect categories considered here included carcinogens, respiratory organics/inorganics, climate change, radiation, ozone layer depletion, aquatic acidification/eutrophication, land use, mineral extraction, fossil fuel extraction, etc. These effect categories have impacts on resources, human health, global warming, habitat alteration, biological diversity and other hazards. Assessing the potential contribution of the ships to all these impact types, total damages were assessed and compared to find which one will impose minimum burden to our environment.

Finally discussing the service quality available from the alternative ships, the best alternative was proposed for the inland shipping in Bangladesh.

3.0 MODEL CONSIDERED

Four model designs of container ships were considered in this analysis. Although, the choice of primary parameters/hull form coefficients is a matter of design style and tradition, but due consideration must be given if there is any constraints in that route. In this study, a dimensional constraint on the limit of length, breadth, draught and air draught has been imposed compatible with the proposed route. For example, a constraint on length is set by the dimensions of regulatory body's restriction considering river width, maneuverability of ship to turn in this narrow waterway etc. A limit on draft for the vessels is set by the existing availability of the depth of water in the ports as well as navigability of approaches throughout the season to which the ship is intended to trade.

The particulars of the models shown in Table 1 have been selected after considering all the constraints. A typical General Arrangement of container ship has been shown in Figure1. Figure 2 shows the different components of life cycle assessment of ships and Table 2 contains the amount of some of the materials and energy used in various phases of the ships' life cycle. The figures shown in the tables were the major input data in this analysis.

Table 1: Particulars of Selected Container Ships Considered

Ship Type	Length (M)	Breadth (M)	Depth (M)	Speed (KN)	Engine Power (KW)	Capacity (TEUs)
Closed Top Container Ship (With hatch cover)	75.5	13.15	6.2	10	1130	108
Open Top Container Ship (without hatch cover)	75.4	13.15	8.0	10	1130	108
Deckloading Container Ship	75.4	15.66	4.2	10	1140	100
Deckloading Container Ship	75.1	13.15	4.2	10	910	80

Table 2: Materials and Energy Consumption during Construction, Maintenance and Operation of four selected container ships

Ship Type	Construction and Maintenance Phase				Operation Phase	
	Material			Energy		
	Hull	Machinery	Outfitting			
	Low alloy Steel (kg)	Ferrochromium High Carbon Steel (kg)	Brass (kg)	Electricity (MJ)	Diesel (kg)	Lub Oil (kg)
With hatchcover	8.33E5	6.95E4	7.5E3	1.53E6	1.47E7	2.92E5
Without hatchcover	8.94E5	6.95E4	7.5E3	1.63E6	1.47E7	2.92E5
Deckloading (B = 15.66m)	8.74E5	6.95E4	7.5E3	1.6E6	1.48E7	2.95E5
Deckloading (B = 13.15m)	8.25E5	6.95E4	7.5E3	1.52E6	1.26E7	2.49E5

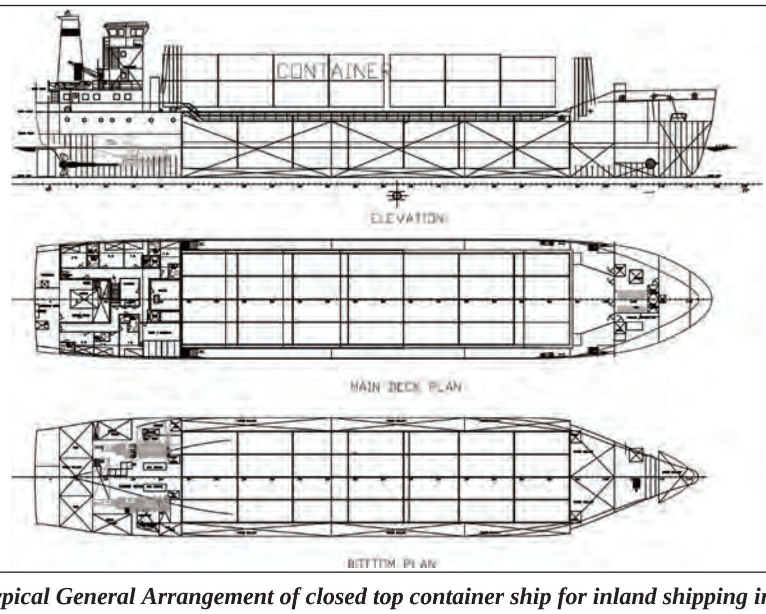

Figure 1: Typical General Arrangement of closed top container ship for inland shipping in Bangladesh

4.0 ECONOMIC PERFORMANCE OF THE MODEL SHIPS

Considering 30 years life time, required freight rate (RFR), that is, minimum freight charge required to attain 12% rate of return on investment as first cost of ship and operating cost, was estimated for carrying 1 TEU container through a distance of 307 km between Dhaka and Chittagong. Fifteen off-hire days per annum for maintenance was taken into account in this estimation. Net present value (NPV), another parameter for comparison of economic performance, was also estimated here to find economically the most attractive ship model. For this estimation 8000 Tk./TEU, which is the current rate charged by railway, was considered.

Both the parameters were calculated according to I.L. Buxton [5]. The Results are shown in Figure 3 and Figure 4.

The ship with hatch-cover showed the best performance, that is, the minimum required freight rate of Tk. 6035/TEU and the highest net present value of Tk. 365,149,000. All with 12% rate of return on investment. The ship without hatch-cover was the next. The worst among the four was the ship with deck loading and 13.15m breadth. This is because the ship with hatch-cover had the capacity of 108 TEUs and comparatively low construction cost. The construction costs of the deck-loading type ships were comparatively higher due to its heavy deck construction to withstand the containers' weight.

5.0 ENVIRONMENTAL IMPACT ASSESSMENT

Environmental impact assessment of the models were carried out using the software SimaPro. Amount of some major materials and energy required to construct and operate the model ships were used as input to the system. The percentage of the materials which were considered to be recycled was also used as input. SimaPro developed life cycle model of the ship with the inputs and outputs from and to the environment. The life cycle model of the container ship with deck-loading and 15.66m breadth is shown in Figure 2. Similar models were generated for other three ship models. Then, using SimaPro, the environmental burden imposed by the ships were assessed. The results were shown in Figure 5 as the comparison of environmental impacts for four different models, Figure 6 as the damage assessment and Figure 7 as the single score of the consequences of environmental burden. In these results the impacts on human health, ecosystem quality, climate change and the use of resources are shown. The best option from the environmental point of view was the ship with deck-loading and 13.15m breadth and the worst was the ship with deck-loading and 15.66m breadth. The impacts imposed by two other ships are very close in magnitude, with only a very little better result for ship with hatch-cover [6].

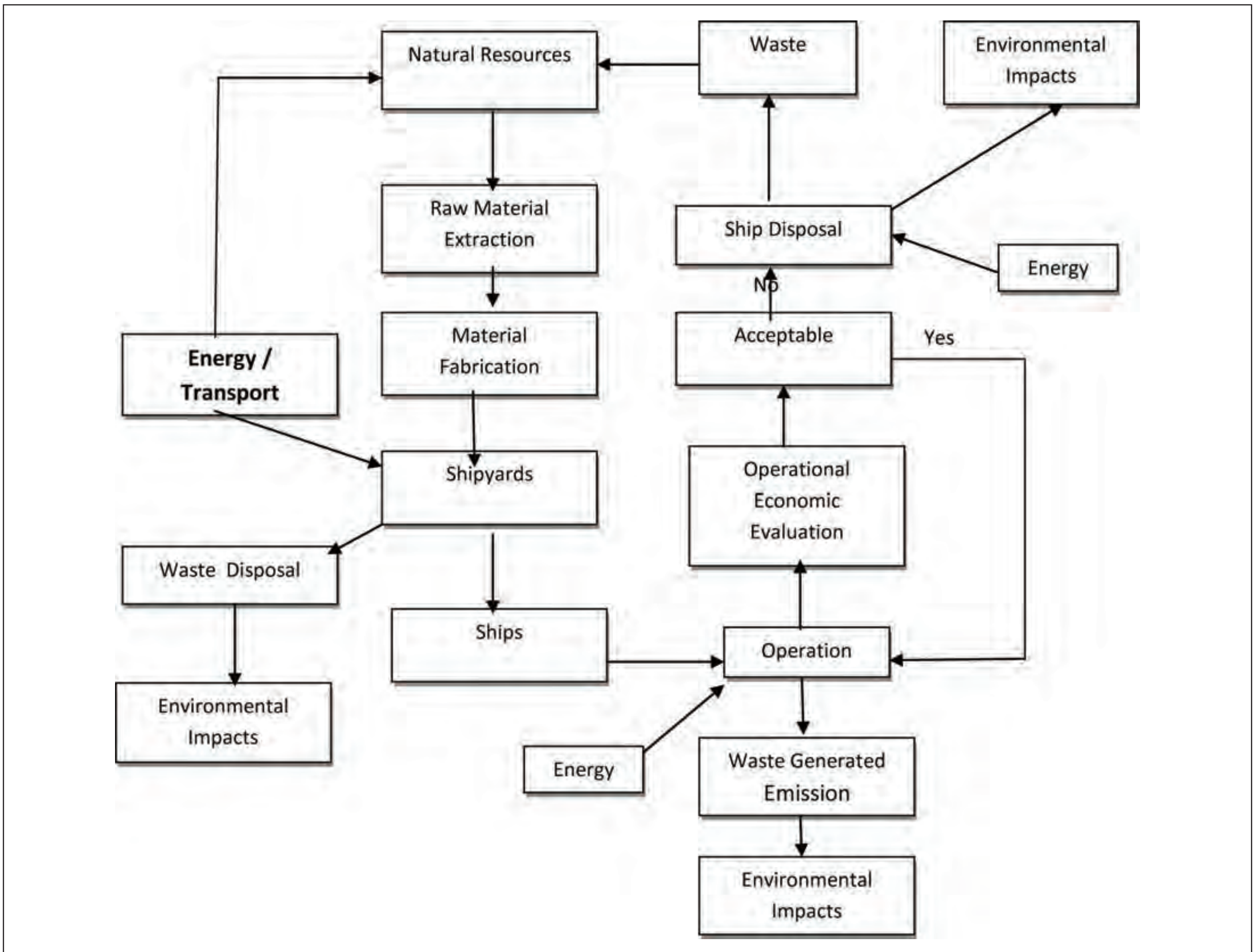

Figure 2: Life cycle assessment of container ships

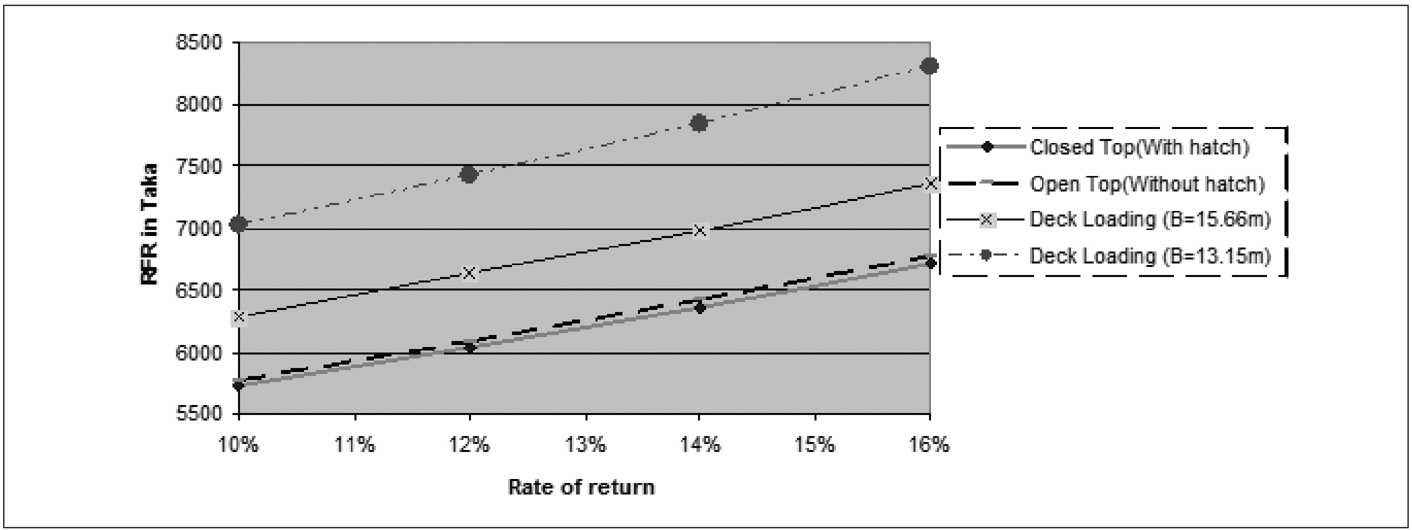

Figure 3: Required freight rate for carrying 1 TEU between Dhaka and Chittagong by alternative container ships

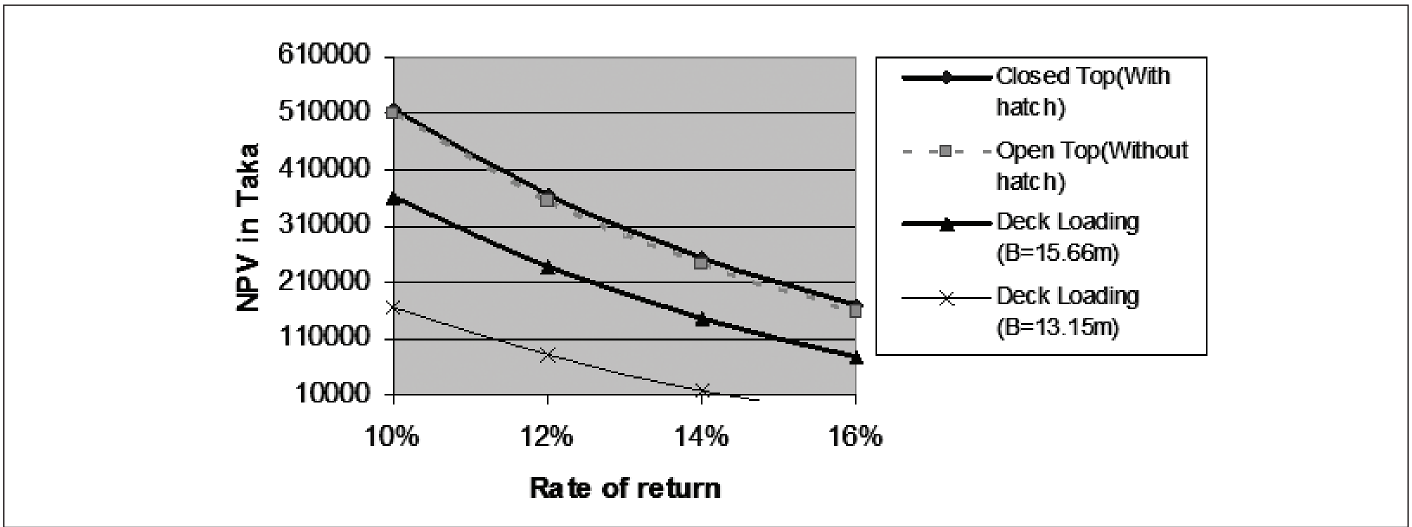

Figure 4: Net present value of the cash flow for carrying containers between Dhaka and Chittagong by alternative container ships

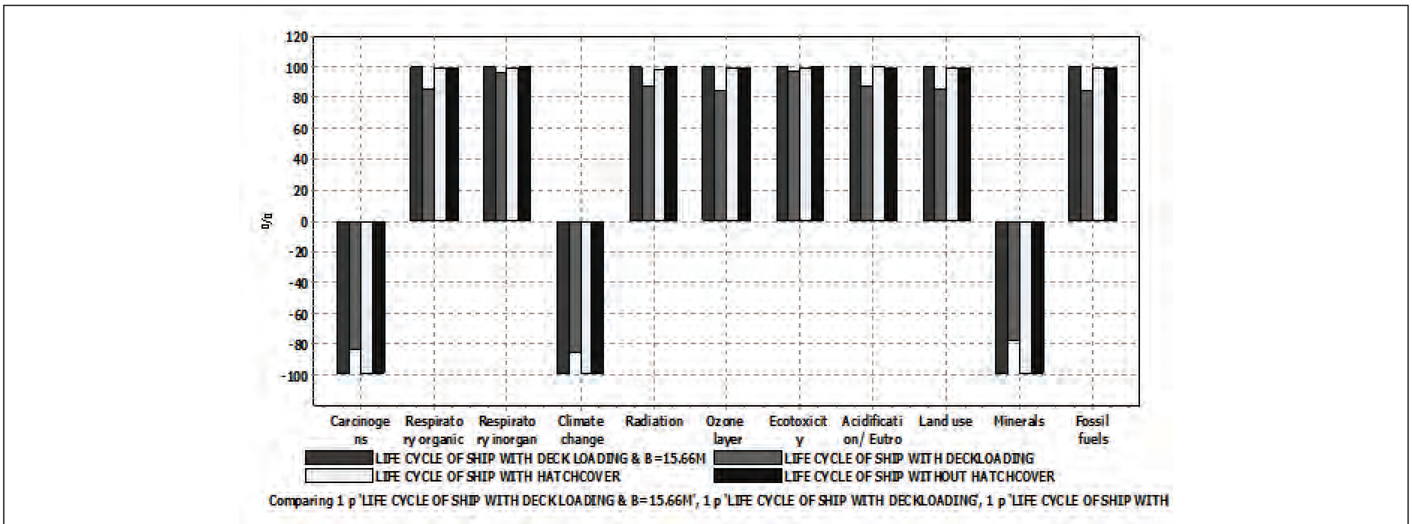

Figure 5: Comparison of environmental impacts for four model ships

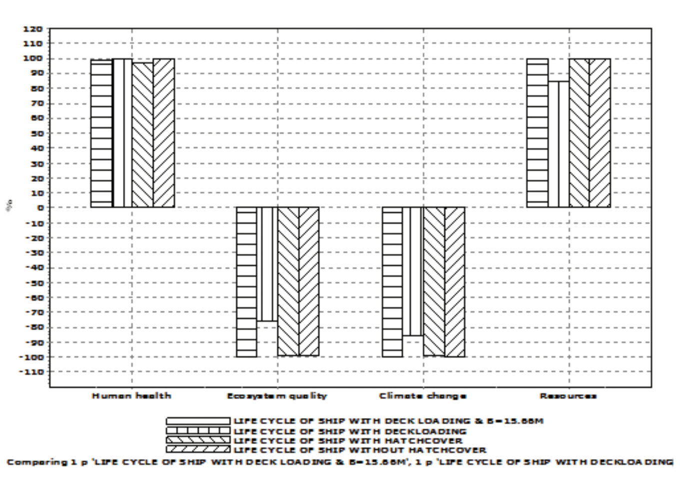

Figure 6: Damage assessment of four model ships' life cycle

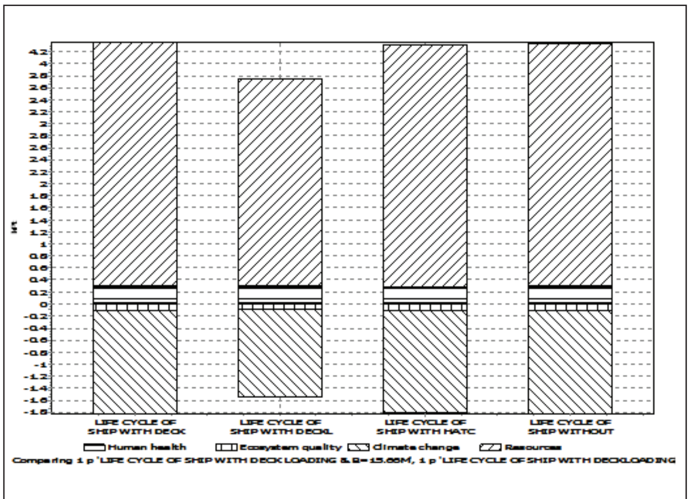

Figure 7: Single score of the consequences of environmental burden of four model ships

6.0 SERVICE QUALITY

For loading and unloading of the containers, deck-loading type ships will be favourable. But it deserves special cares against the flooding of sea water in the hold during a coastal navigation in rough sea condition and hence the vessel shall need an extra ship's depth to keep the freeboard. On the other hand ship with hatch-cover will protect the containers from adverse weather condition and from the hull strength point of view, it will enhance the longitudinal and tensional strength of ship. Among the models considered here the ship with and without hatch-cover have more capacity of carrying containers, which is 108 TEUs.

7.0 CONCLUSION

Analysing three different criterion like economic benefit, environmental burden imposed and service quality, the ship with hatch-cover would be the best option among the models of the container ships considered. The following reasons were in support of this option:

- it would require minimum freight rate to attain specific rate of return on investment,
- it would ensure maximum net present value of the total cash flow in its life time,
- though the ship with deck-loading and 13.15m breadth showed minimum damage to the environment, the ship with hatch-cover got more capacity of carrying 108 TEUs containers.
- the loading – unloading facility is in favour of deck-loading type container ship, but the ship with hatch-cover would protect the containers from damage occurred by bad weather.

There are uncertainties in such analysis. One should be aware of these uncertainties while using such model for comparison of different projects. The reasons behind these uncertainties are usually due to:

- uncertain data,
- uncertainties on the correctness of the model,
- uncertainties caused by incompleteness of the model,
- different opinion on weights of various impact categories, etc. ■

REFERENCES

[1] Hasegawa K. and Iqbal K.S. (2000). "Inland Transportation System Planning by Life Cycle Impact Assessment: A Case Study." Journal of Marine Science and Technology, Springer-Verlag Tokyo, Vol. 5, pp 1-8.

[2] Iqbal K.S. and Hasegawa K. (2001). "Inland Transportation System Planning by Life Cycle Impact Assessment: A Case Study, (second report: single comparison index)." Journal of Marine Science and Technology, Springer-Verlag Tokyo, Vol. 6, pp 83-92.

[3] Iqbal K.S. and Shill S.K. (2005). "A Comparative Study of Two Passenger Transportation Systems between Two Bangladeshi Cities." Journal of Naval Architecture and Marine Engineering, vol. 2, no. 2, pp 1-10.

[4] PRe Consultants, SimaPro (Environmental Impact Assessment Database Software),Website: *http://www.pre.nl*, accessed on June 15, 2010.

[5] Buxton, I.L. (1976). Engineering Economics and Ship Design, published by British Ship Research Association, UK.

[6] Khan M.M., and Khaled M. I. (2011). Cost estimation, economical analysis and environmental analysis of inland container ships for Bangladesh, Undergraduate Thesis submitted to Naval Architecture and Marine Engineering Dept, BUET, Bangladesh.

PROFILES

DR N.M. GOLAM ZAKARIA is working as an associate professor in the department of Naval Architecture and Marine Engineering of Bangladesh University and Engineering & Technology (BUET), Dhaka, Bangladesh. He obtained his Ph.D. from Japan in 2006. His field of specialisations is seakeeping, ship safety, shipbuilding and Green ship recycling.

DR KHO. SHAHRIAR IQBAL is working as a Professor in the in the department of Naval Architecture and Marine Engineering of Bangladesh University and Engineering & Technology (BUET), Dhaka, Bangladesh. His field of specializations is marine environment and pollution, marine transportation and ship recycling.

MR. MD. IMRAN KHALED is working with Bangladesh Navy as a Lieutenant. He completed his B.Sc. Engg. from Bangladesh University of Engineering & Technology under the department of Naval Architecture and Marine Engineering on February 2011.

MR. MD. MILON KHAN is working with Bangladesh Navy as a Lieutenant. He completed his B.Sc. Engg. from Bangladesh University of Engineering & Technology under the department of Naval Architecture and Marine Engineering on February 2011.

CNTs/SnO_2 AND CNTs/MnO_2 NANOCOMPOSITES FOR THE FABRICATION OF THE ELECTRODES FOR SUPERCAPACITORS

(Date received: 10.05.12/Date accepted: 09.11.12)

Ir. Dr Ng Kok Chiang*[1], Dr Daniel Jewell[2]

[1]MyBig Sdn. Bhd., No. 1, Jalan P4/7, Seksyen 4, Bandar Teknologi Kajang, 43500 Semenyih, Selangor, Malaysia.
[2]Department of Materials Science and Metallurgy, New Museums Site, Pembroke Street, University of Cambridge, Cambridge CB2 3QZ, United Kingdom.
*E-mail: [1]*kokchiang.ng@leonghing.com*

ABSTRACT

The development of next generation high-energy and high-power aqueous supercapacitors is vital in an era when power demand has peaked. In terms of engineering related issues at the micro level, the major area urgently requiring attention is the development of new nanocomposite materials. This article reports on nanocomposites which demonstrate superiority in terms of three-dimensional structure and which possess electrical conductivity equivalent to metallic conductors as a result of CNTs which complement the high redox-active properties of the transition metal oxides. Such combined contributions, when applied in supercapacitors, lead to increased charge storage capabilities and exceptional cycling stability. Two nanocomposites, namely, CNTs/SnO_2 and CNTs/MnO_2, were synthesised their physicochemical properties examined by X-ray diffraction, scanning electron microscopy, cyclic voltammetry and galvanostatic charge-discharge. The nanocomposites show superior results in terms of charge-storage mechanisms, cycle life, and electrochemical kinetics. Uniquely, in this paper, CNTs/SnO_2 nanocomposites were also reported as an alternative negative electrode material to the commonly used activated carbon in asymmetrical supercapacitors.

Keywords: *Energy Storage, Fabrication, Nanocomposites, Supercapacitors*

1.0 INTRODUCTION

Energy efficient and robust power devices are key to overcoming the daunting challenges of climate change and the depletion of the earth's fossil fuels. As a result of an extensively diversified and globalised energy market, electrochemical capacitors, which are also known as supercapacitors, are becoming one of the vital energy-storage devices of the 21st century. This is because electrochemical capacitors bridge the crucial performance disparity between high energy-density fuel cells or batteries and high power-density traditional capacitors. The necessary developmental advances can be achieved through innovations in pseudo-capacitive nanocomposites of transition metal oxides and carbon nanotubes (CNTs) which combine both ion adsorptions (interfacial capacitance) and fast redox reactions (pseudo-capacitance) for energy storage.

In addition to enhancing the core performance of supercapacitors, there is also a need to develop materials which offer an alternative to activated carbon as a negative electrode material in asymmetric aqueous electrochemical capacitors. There have already been many studies of probable positive electrode materials for supercapacitors, especially those with very good pseudo-capacitive properties as they are able to outperform the traditional electrical-double layer storage mechanism. The simple logic therefore is to search for a low cost metal oxide that is active in the negative potential range, such as tin oxide (SnO_2) which has been examined extensively as the negative electrode material in lithium ion batteries [1-4]. Lithium ion battery research has already progressed to combining SnO_2 [5, 6] and CNTs as a promising anode candidate, owing to the excellent mechanical and electrical properties of CNTs [7-9], SnO_2 has only recently been studied in supercapacitors as the positive electrode material [5-9].

In order to address these separate challenges, two different nanocomposite materials have been synthesised. In the case of core performance improvement, a carbon nanotube manganese oxide nanocomposite (denoted CNTs/MnO_2) was synthesised by the redox deposition method[1]. In this approach $KMnO_4$ was used as an oxidant which would react with the CNTs, to be reduced to an insoluble form of MnO_2 in an aqueous solution. This precipitate then anchors itself onto the surface of the CNTs to form the CNTs/MnO_2 nanocomposite [10-14]. Such composites were previously reported to exhibit very high electrode specific capacitance (≥ 5.0 F/cm^2) in the positive potential range [10].

For the production of a new negative electrode material for aqueous asymmetric supercapacitors, a nanocomposite of carbon nanotubes and tin oxide (denoted CNTs/SnO_2) was synthesised in which tin oxides were coated on the surface of individual CNTs. Good understanding of the science of materials is important for practicing engineers to fully comprehend the nature, capabilities, and ratings of energy devices that are increasingly being built with these advanced nanocomposite materials.

2.0 METHODOLOGY

CNTs/MnO_2 nanocomposite synthesis – The CNTs/MnO_2 nanocomposite was synthesised via spontaneous redox deposition of MnO_2 on the CNTs in the $KMnO_4$ aqueous solution as previously reported[2]. In this synthesis, one gram of $KMnO_4$

(Fluka ≥99.0% (RT)) was dissolved in 50.0 mL of deionised water in an Erlenmeyer flask before the addition of acid-treated CNTs (to form a nanocomposite of CNTs/MnO_2 of 4:6 w/w). The resulting mixture was continuously stirred for nine days in the covered flask until the purple colour disappeared. During and after the reaction, clear solutions gradually appeared with the product settling to the bottom of the flask. The resulting nanocomposite was filtered, washed and dried in the oven overnight at 60˚C.

CNTs/SnO_2 nanocomposite synthesis – In the synthesis of the CNTs/SnO_2, 1.0 g of tin (II) chloride dihydrate (Fisher 97+%) was dissolved in 50.0 mL of deionised H_2O in an Erlenmeyer flask and 1.0 mL of HCl (38%) was added and stirred continuously for 1.0 hour to dissolve the tin (II) chloride. Then, the acid-treated CNTs were added to the solution and stirred for 24 hours at room temperature to form a nanocomposite of CNTs/SnO_2 of 4:6 w/w. The resulting mixture was then filtered, washed and dried overnight at 60˚C in a conventional oven.

Chemical and structural characterizations – The nanocomposites, all in the powder form, were characterized by X-ray diffraction (XRD, Hiltonbrooks DG3 generator plus Philips PW1050/25 goniometer, CuKα radiation), an environmental scanning electron microscope (SEM, Philips FEI XL30 FEG-ESEM), a low resolution TEM (LR-TEM, JEOL 2000FX), and a high resolution TEM (HRTEM, JEOL 2100F).

Preparation of the electrode and electrochemical analysis – The nanocomposite (34.2 mg) with a binder (3.0 mg, 60% w.t. aqueous emulsion of polytetrafluoroethylene, PTFE, Aldrich) was thoroughly dispersed in 4.0 mL of deionised water. The mixture (10.0 µL, with 0.0855 mg of the nanocomposite) was drop-cast onto a graphite disc working electrode (0.5 cm in diameter) using an electronic micropipette (EDP3 Rainin LTS, 10-100 µL, with wide orifice tips). Upon evaporation, the resulting thin film (13.44 µm on average thickness) on the electrode was dried in a desiccator overnight before electrochemical tests (AUTOLAB PGSTAT30) in a one-compartment three-electrode cell with the Ag/AgCl (3.0 M KCl) reference electrode and a graphite counter electrode at room temperature.

3.0 RESULTS AND DISCUSSIONS

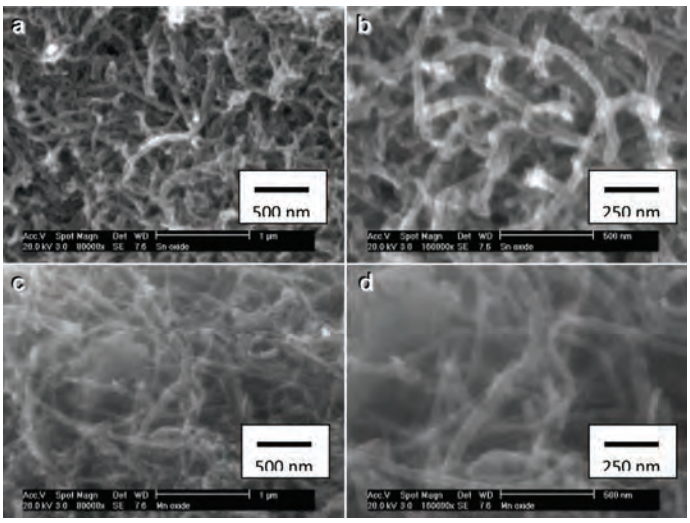

Figure 1: SEM images of the nanocomposites at different magnifications, i.e. 80,000x and 160,000x (a, b) CNTs/SnO_2 and (c, d) CNTs/MnO_2

Figure 1 shows the SEM images of the acid-treated CNTs after SnO_2 (a, b) and MnO_2 deposition (c, d) at two magnifications as indicated. The images of the CNTs/SnO_2 and CNTs/MnO_2 nanocomposites show that they retained the bundle nature and the three-dimensional entangled structures originating from the as-received CNTs. This shows that the SnO_2 and MnO_2 deposits did not block the opening and the porous structure which is inherent to the CNTs. The porosity can be observed as the dark spots in Figure 1 which are also the spaces created due to the nature of the CNTs. Maintaining such configurations assists the movement of the ions into and out of the positive and negative electrodes of the nanocomposites as mentioned previously. The SEM images of the nanocomposites demonstrate that thin coatings of the metal oxides exist around the CNTs. The jagged and consistent coarse surfaces, especially for the CNTs/SnO_2 nanocomposite, illustrate the evenly distributed SnO_2 on the surface of individual CNTs throughout the structure. The coating can only be further confirmed and substantiated by TEM images in Figure 2, 3, and 4 in the subsequence sections.

As for the SEM analysis, the TEM images of the overall CNTs/SnO_2 60% w.t. confirmed that the nanocomposite retained the bundle nature of the CNTs as can be seen in Figure 2(a). It is noted that almost all the CNTs or CNT bundles in the sample are individually coated with thin and uniform layers of SnO_2. Enlarging the image of the end of one of the nanocomposite's fibrils reveals a very thin coating of nanocrystalline SnO_2 of about 5 nm width as can be observed in Figure 2(d). This also demonstrates the nature of the open-ended CNT the fact that the nanocrystalline SnO_2 is coated onto the CNT even to the very tip. It is also notable, as shown from the bundle in Figure 2(a), that separate SnO_2 agglomerates (away from the CNTs) were not seen. Instead, the SnO_2 nano-grains nucleate only on the surface of the CNTs. Finally, it can be observed that the CNT's walls and cavities are only vaguely visible in Figure 2(a-c) which may be due to the interference of thicker oxide coatings that made it difficult to resolve the structures by TEM [10].

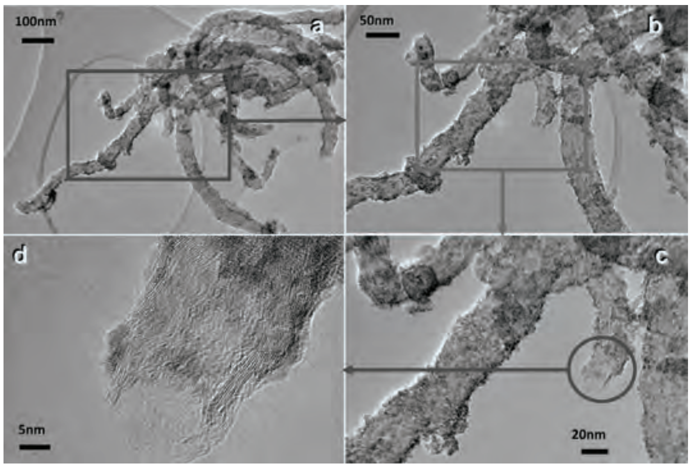

Figure 2: TEM images of the CNTs/SnO_2 60% w.t. nanocomposite; (a) and (b) overviews of the fully SnO_2-coated CNTs, (c) and (d) TEM images of enlarged micrographs depicting the open-ended tube of a CNT coated with a nanocrystalline coating SnO_2

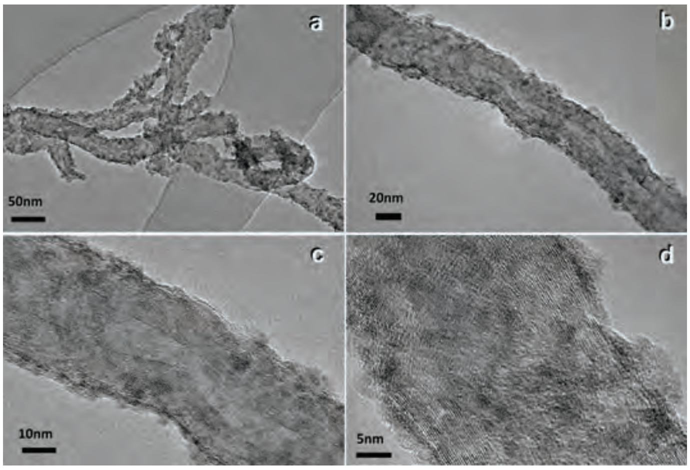

Figure 3: Closed-up examination of various other strands of the coated CNTs/SnO_2 60% w.t. nanocomposite; (a) tangled SnO_2 coated CNTs, (b) and (c) a mid-portion of the nanocomposite fibril coated with SnO_2 and (d) densely coated with nanocrystalline particles of SnO_2 on the surface of the CNT

Figure 3(a) shows more strands of CNTs coated uniformly with SnO_2 throughout. Figure 3(b, c) present typical TEM images of mid portions of SnO_2 coated CNTs where the parallel and long fringes are from the CNT walls (the grapheme layers) are clearly distinguishable from those almost randomly originated from the nanocrystalline SnO_2. It should also be noted that the structure of the CNTs remain intact. No corrosion was observed in the deposition of SnO_2 onto the CNT as compared to that caused by the $KMnO_4$ in the deposition of MnO_2 onto the CNTs. This can be clearly seen in the bundled nanocomposites in Figure 3 (a, b) and the long nanocomposite fibril in Figure 3(b) as well as the deposition of SnO_2 at the very end of the CNT in Figure 3(d). Such preservation of the CNTs structure may be attributed to the fact that SnO_2 deposition resulted from the reaction between the Sn^{2+} ion and an oxidant, such as dissolved oxygen gas in the synthesis solution, without attacking the CNTs [15]. In Figure 3(d), on the enlarged portion of one of the nanocomposite fibrils the observed SnO_2 nanoparticles are rounded with diameters of about 4 nm and are distributed evenly on the surface of the CNT. These SnO_2 nanoparticulates also densely populate the CNT surface and show fringes on each of them, confirming nanocrystallinity.

Figure 4(a) shows the overview of the well-dispersed CNTs/MnO_2 60%w.t. nanocomposite on the carbon-holey grids examined under the TEM. In all the TEM images of the CNTs/MnO_2 60% w.t. nanocomposite, the surfaces of the CNTs are well covered with MnO_2 deposits. Figure 4(c) and (d) depict uneven depositions of nano-layers of MnO_2 on the CNTs while (e) and (f), enlarged views, show that the CNT walls remained intact even with the presence of the thick layer of MnO_2 on the surface of the CNT. It was previously reported that the mechanism behind the deposition results in the formation of thick MnO_2 coatings on the CNTs [10, 11].

In short, the growth of MnO_2 continues even after the surface of the CNTs are fully covered with MnO_2 deposit in accordance with the 'MEC' (microelectrochemical cell) principle, i.e. electrons are moved from the defect sites of the CNTs to other sites in contact with MnO_4^- where the anion is reduced to MnO_2 as in any electrodeposition process. Thus, the thick coating and no separated precipitation from the CNT structure is observed. Figure 4(b) and (d) also show the broken and short-ended characteristics of the CNT indicating that corrosion by $KMnO_4$ in the reduction to the insoluble MnO_2 might have taken place. The layered structure of the MnO_2 as can be seen in the enlarged TEM images of (e) and (f), would be excellent for retaining the facile transport pathways for both protons and electrons [16] as in the case of ruthenium dioxide, according to the following reaction (1) [11, 17-20]:

$$MnO_x(OH)_y + \delta H^+ + \delta^+ \rightleftharpoons MnO_{x-\delta}(OH)_{y+\delta} \qquad (1)$$

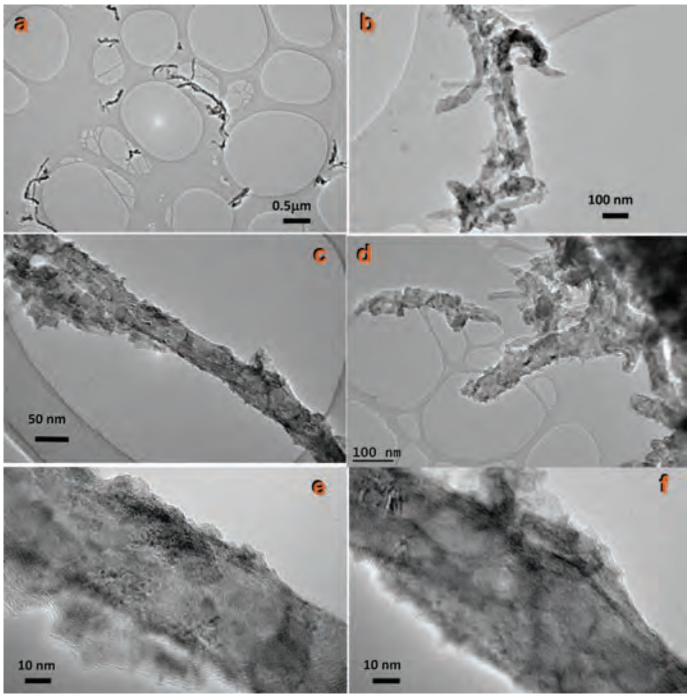

Figure 4: TEM images of the CNTs/MnO_2 60% w.t. nanocomposite

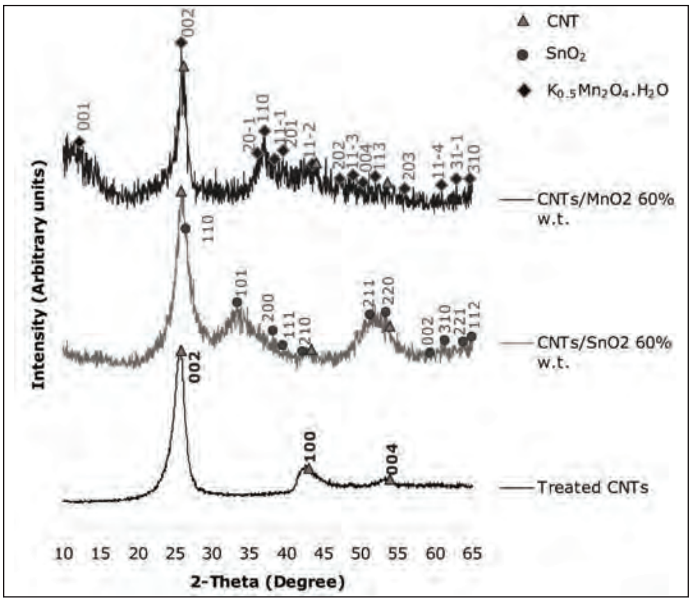

Figure 5: XRD spectrum of the nanocomposites and the acid-treated CNTs

The XRD patterns of the nanocomposites reveal the presence of cassiterite-type SnO_2 (JCPDS 41-1445) in the CNTs/SnO_2 60% w.t. nanocomposite. The broad peaks are consistent with the nanoparticles being small (4 nm in diameter) as discussed in the TEM section before. The lattices are a = 4.738 Å, b = 4.738 Å and c = 3.187 Å. The peaks corresponding to the identification of the cassiterite-type SnO_2 are shown with the green round markers with their indexes. The XRD traces of the CNTs/MnO_2 60% w.t. nanocomposite show the peaks which correspond to monoclinic birnessite-type MnO_2 (JCPDS 42-1317) with lattices of a = 5.150 Å, b = 2.844 Å and c = 7.159 Å. There are three peaks from the acid-treated CNTs as indicated by the yellow triangular markers. The XRD patterns of the CNTs/SnO_2, CNTs/MnO_2, and acid-treated CNTs are presented in Figure 5.

MnO_2 and CNTs are complementary in properties where the three-dimensional structure of their nanocomposite, due to the presence of CNT [21], provides the mesoporous cavity for ion movements. MnO_2 is also known for its low cost and large pseudo-capacitance but has the disadvantage of being resistive [22]. Thus, a nano-layer of MnO_2 on CNT would improve the ion conduction in the MnO_2 phase [10]. The same improvement can be deduced for the CNTs/SnO_2 60% w.t. nanocomposite although SnO_2 is more conducting than MnO_2 (10^2 ~ 10^3 S/cm for SnO_2 vs. 10 ~ 10^2 S/cm for MnO_2) [23-24].

Sn has two stable valences, Sn(IV) and Sn(II), which is the basis for the redox chemistry of solid SnO_2. Thus, the charge storage mechanism for the transition metal oxides was applied to SnO_2 at positive potentials in a recent study [6]. However, no study has reported on using SnO_2 as the negative electrode in supercapacitors. To fill in this gap, the CNTs/SnO_2 nanocomposite was further studied by cyclic voltammetry at different potential ranges. The cyclic voltammogram recorded in a wide potential range, i.e. -0.8 to 0.9 V (vs. Ag/AgCl), is fairly rectangular in the overall shape, although a broad oxidation and reduction peak couple appears around 0.10 V. The peak currents varied linearly with the scan rates. These features are strong evidence of the same electrode reaction being responsible for the current flow in the tested potential range, which is in agreement with the behaviour of pseudo-capacitive materials.

When the potential range was narrowed to only positive or only negative potentials, the recorded cyclic voltammograms retained the respective partial features of the cyclic voltammogram recorded in the wide potential range. The capacitance values derived from the cyclic voltammograms in both positive and negative regions were very much the same, which again is evidence of the same electrode reaction being responsible for the pseudo-capacitance of SnO_2 in the wide potential range of 1.7 V as shown in Figure 6. It is worth pointing out that the cyclic voltammograms in Figure 6 suggest the possibility of using the CNTs/SnO_2 to make a symmetrical 1.7 V supercapacitor. However, because the specific capacitance of CNTs/SnO_2 is only about half of that of CNTs/MnO_2, it was decided to use the latter as positive electrode in the asymmetric supercapacitor.

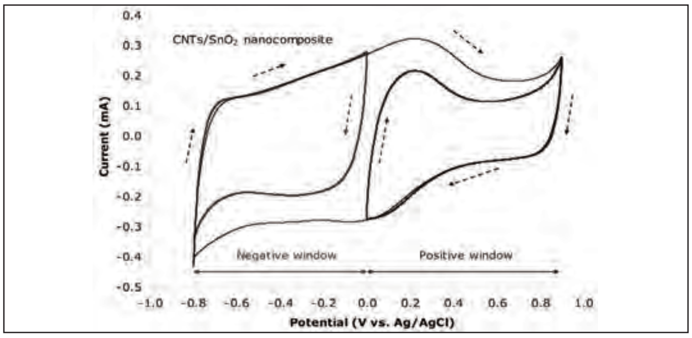

Figure 6: Cyclic voltammograms of the CNTs/SnO_2 in 2.0 M KCl recorded in different potential ranges

Summarising the relevant literature [5, 6] and the aforementioned findings from this work, the charge storage mechanism of the CNTs/SnO_2 nanocomposite can be expressed as equations (2), (3), and (4) below;

Oxidation:

$$Sn(IV)_{(x+y)}OOK_xH_y \rightarrow Sn(IV)O_2 + xK^+ + yH^+ + (x+y)e^- \qquad (2)$$

Reduction:

$$Sn(IV)O_2 + xK^+ + yH^+ + (x+y)e^- \rightarrow Sn(IV)_{(x+y)}OOK_xH_y \qquad (3)$$

Redox:

$$SnO_2 + xK^+ + yH^+ + (x+y)e^- \rightleftharpoons SnOOK_xH_y \qquad (4)$$

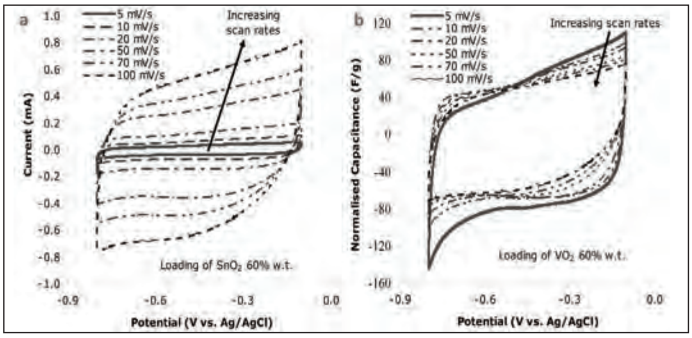

Figure 7: Cyclic voltammograms and mass-normalised capacitance vs. potential (vs. Ag/AgCl) of the CNTs/SnO_2 60% w.t. nanocomposite at various scan rates (5, 10, 20, 50, 70 and 100 mV/s) in 2.0 M KCl. Arrow indicates increasing scan rates

Figure 7 shows the cyclic voltammograms of the CNTs/SnO_2 60% w.t. and its corresponding potential dependent normalised capacitance curves according to $C = \frac{I}{s}$. The cyclic voltammograms are rectangular and relatively symmetric in current which can be compared with an ideal capacitor. Besides, the increase in the currents of the voltammograms with insignificant changes to their rectangular shapes with increasing scan rate also shows the good electrochemical properties of the nanocomposites and a high rate capability of charge-discharge of the nanocomposite. Figure 7(b) depicts the increase in the mass specific capacitance which is calculated using equation $C = \frac{I}{s}$ with respect to the decrease in scan rate and is in line with the slow response of the mass transfer process in fast scan rates, where ions have limited time to move in and out of the pores of the nanocomposites. It is also interesting to note that the negative ends of the potential windows of the cyclic voltammograms of the CNTs/SnO_2 nanocomposite at various scan rates reach a potential of -0.8 V (vs. Ag/AgCl). This is more negative than the current onset potential (ca. -0.5 V) for hydrogen evolution as observed on the cyclic voltammogram of a platinum electrode in the same aqueous electrolyte. This is indicative of overpotential for hydrogen evolution on the CNTs/SnO_2 electrodes.

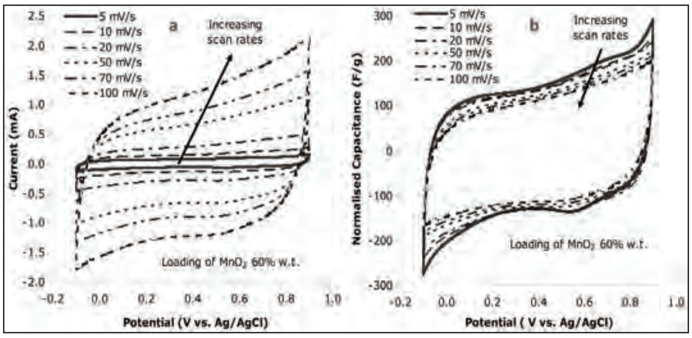

Figure 8: Cyclic voltammograms and mass-normalised capacitance vs. potential (vs. Ag/AgCl) of the $CNTs/MnO_2$ 60% w.t. nanocomposite at various scan rates (5, 10, 20, 50, 70 and 100 mV/s) in 2.0 M KCl. Arrow indicates increasing scan rates. Mass of the $CNTs/MnO_2$ 60% w.t. nanocomposite on the electrode: 0.10 mg

Figure 8 shows the cyclic voltammograms and the corresponding potential dependent normalised capacitance of the $CNTs/MnO_2$ 60% w.t. nanocomposite at different scan rates. The arrows in the figures indicate the direction of the current change with increasing scan rate. The cyclic voltammograms grow larger with increasing scan rate. Even at a fast scan rate of 100 mV/s, the nanocomposite still shows a relatively rectangular cyclic voltammogram, indicating the high rate capability and high reversibility of the redox reaction of the MnO_2 deposited on the CNTs. The charge storage mechanism of the MnO_2 can be explained with reference to the widely accepted understanding of charge transfer reactions in solid transition metal oxides which are usually semiconductors.

The multiple valences of transition metals, e.g. Mn(IV), Mn(II) and Mn(II), are the thermodynamic reason for their ability to undergo electron transfer reactions. To maintain neutrality upon electron transfer into the solid oxide phase, intercalation and adsorption of either or both protons (H^+) and alkali cations (Li^+, Na^+, or K^+) from the electrolyte is necessary [11]. In the $CNTs/MnO_2$ 60% w.t. electrode, both protons and alkali cations have been found to be involved in the redox transition between M(IV) and Mn(III) [11, 25, 26]. During the positive and negative potential sweeps, reversible oxidation and reduction reactions take place in the MnO_2 explained below in the presence of the K^+ cations and H^+ protons from the 2.0 M KCl in equations (5), (6), and (7) below [11, 19, 27];

Oxidation:

$$\mathrm{Mn(III)}_{(x+y)}\mathrm{Mn(IV)}_{1-(x+y)}\mathrm{OOK}_x\mathrm{H}_y \rightarrow \mathrm{Mn(IV)O_2} + x\mathrm{K}^+ + y\mathrm{H}^+ + (x+y)e^- \quad (5)$$

Reduction:

$$\mathrm{Mn(IV)O_2} + x\mathrm{K}^+ + y\mathrm{H}^+ + (x+y)e^- \rightarrow \mathrm{Mn(III)}_{(x+y)}\mathrm{Mn(IV)}_{1-(x+y)}\mathrm{OOK}_x\mathrm{H}_y \quad (6)$$

Redox:

$$\mathrm{MnO_2} + x\mathrm{K}^+ + y\mathrm{H}^+ + (x+y)e^- \rightleftharpoons \mathrm{MnOOK}_x\mathrm{H}_y \quad (7)$$

The variation in the mass specific capacitance of the $CNTs/MnO_2$ 60% w.t. nanocomposite with the scan rate in the potential range of -0.1 to 0.9 V is shown in Figure 8(b). At the lowest scan rate of 5 mV/s, the largest normalised capacitance plot is evident as compared to all the other scan rates. The specific capacitance decreases gradually with the increasing scan rate as can be seen. The decrease in specific capacitance was due to the incomplete mass transport process, thus, the incomplete redox reactions, adsorption/desorption, and intercalation/deintercalation of cations or protons in the higher scan rates. The highest average mass specific capacitance at the scan rate of 5 mV/s can be calculated also, utilising the average charge accumulated in the positive and negative sweep of the cyclic voltammogram and is found to be 138.20 F/g in the defined potential range of -0.1 to 0.9 V. A further examination of the electrochemical properties of the nanocomposite was carried out with the galvanostatic charge-discharge technique, and the results are presented in Figure 9.

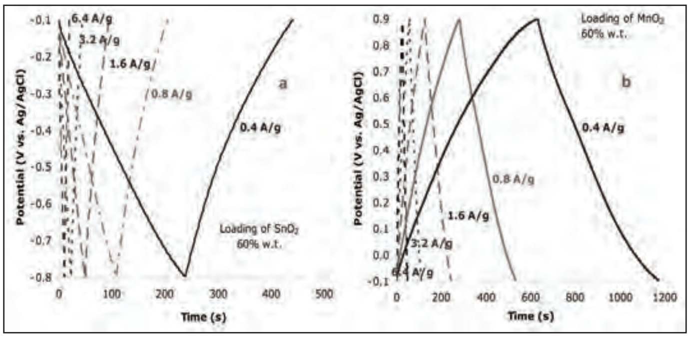

Figure 9: (a) Potential-time plots from the galvanostatic charge-discharge test of the $CNTs/SnO_2$ 60% w.t. nanocomposites and (b) the $CNTs/MnO_2$ 60% w.t. nanocomposites at different normalised currents (0.4, 0.8, 1.6, 3.2, and 6.4 A/g) in 2.0 M KCl

Figure 9(a) shows the potential-time plots from the galvanostatic charge-discharge test of the $CNTs/SnO_2$ 60% w.t. nanocomposites at different normalised currents of 0.4, 0.8, 1.6, 3.2 and 6.4 A/g. The potential-time plot of $CNTs/SnO_2$ 60% w.t. is compared with that of $CNTs/VO_2$ 60% w.t. and the acid-treated CNTs at the normalised current of 0.4 A/g. At the lowest normalised current applied, i.e. 0.4 A/g, a specific capacitance of 130.19 F/g is obtained for the range of -0.8 to -0.1 V against Ag/AgCl. Given that at the same normalised current and potential range, acid-treated CNTs recorded a specific capacitance of 35.11 F/g in the negative range, the specific capacitance of the SnO_2, CM-oxide, assuming proportional contribution can be found to be 193.57 F/g. The potential-time plots from the galvanostatic charge-discharge test of the $CNTs/MnO_2$ 60% w.t. nanocomposite in the Figure 9(b) show linear variation of the potential with respect to time in the potential range of -0.1 to 0.9 V (vs. Ag/AgCl), indicating good capacitive behaviour for all the normalised currents applied, i.e. 0.4, 0.8, 1.6, 3.2 and 6.4 A/g. Even at a higher normalised current of 6.4 A/g, a specific capacitance of 162.00 F/g was recorded for the $CNTs/MnO_2$ 60% w.t. nanocomposite. At the lowest normalised current of 0.4 A/g, the $CNTs/MnO_2$ 60% w.t. nanocomposite registered a capacitance of 236.62 F/g while the acid-treated CNTs recorded a specific capacitance of 41.21 F/g in the positive range. Assuming proportional contribution, the specific capacitance of the MnO_2, $C_{M\text{-}oxide}$ can be determined to be 366.89 F/g.

4.0 CONCLUSION

$CNTs/SnO_2$ 60% w.t. and $CNTs/MnO_2$ 60% w.t. have been successfully synthesised via hydro-oxidation deposition of SnO_2 on the CNTs and reduction of $KMnO_4$ by CNTs i.e. redox and deposition, respectively. The SEM images for the $CNTs/SnO_2$ revealed jagged surface morphology while the TEM images confirmed the evenly distributed SnO_2 nanoparticulates on the surface of the CNTs throughout the structure. TEM images validated the existence of uneven coatings MnO_2 on the surface of the CNTs. XRD patterns reveal the presence of SnO_2 (JCPDS 41-1445) and birnessite-MnO_2 (JCPDS 42-1317) in the CNTs/SnO_2 and CNTs/MnO_2 nanocomposites, respectively. CNTs/SnO_2 exhibited an overpotential for hydrogen evolution as no gas evolution was observed for a potential as negative as -0.8 V (vs. Ag/AgCl) while the CNTs/MnO_2 showed an oxygen overpotential on the positive range extending above the potential of the evolution of oxygen at 0.6 V (vs. Ag/AgCl). The maximum values of mass specific capacitance achieved by the CNTs/SnO_2 60% w.t. and the CNTs/MnO_2 60% w.t. were 130.19 F/g and 236.62 F/g respectively at the normalised current of 0.4 A/g. These values correspond to the specific capacitance ($C_{M\text{-}oxide}$) of (assuming proportional contribution) 193.57 and 366.89 F/g for SnO_2 and MnO_2 respectively. The knowledge of the capacitance achievable by these nanocomposite materials can be utilised to build desirable supercapacitors of any sizes to be used in the UPS back-up system or possibly replacing diesel standby generators in the case of blackout. Thus, the results reported in this article on these nanocomposite materials show that they are capable of constructing the next generation supercapacitors which is crucial as we face the energy crisis in the present and in the future and when the engineering world needs more efficient yet environmental-friendly energy storage devices. ■

REFERENCES

[1] Wan K., *et al.* (1998). "Tin-based oxide anode for lithium-ion batteries with low irreversible capacity." Journal of Power Sources. 75(1): pp 9-12.

[2] Mohamedi M., *et al.* (2001). "Amorphous tin oxide films: Preparation and characterization as an anode active material for lithium ion batteries." Electrochimica Acta. 46(8): pp 1161-1168.

[3] Yuan L., *et al.* (2006). "Nano-structured spherical porous SnO_2 anodes for lithium-ion batteries." Journal of Power Sources. 159(1): pp345-348.

[4] Mei L., *et al.* (2007). "Core-shell and hollow microspheres composed of tin oxide nanocrystals as anode materials for lithium-ion batteries." Electrochemical and Solid-State Letters, 2007. 10(8): pp K33-K37.

[5] Rajendra P.K. and Miura N. (2004). "Electrochemical synthesis and characterization of nanostructured tin oxide for electrochemical redox supercapacitors." Electrochemistry Communications. 6(8): pp 849-852.

[6] Wu M., *et al.* (2008). Cathodic deposition and characterization of tin oxide coatings on graphite for electrochemical supercapacitors. Journal of Power Sources. 175(1): pp 669-674.

[7] Wang Z., Chen G., and Xia D. (2008) "Coating of multi-walled carbon nanotube with SnO_2 films of controlled thickness and its application for Li-ion battery." Journal of Power Sources. 184(2): pp 432-436.

[8] Xie J. and Varadan V.K. (2005). "Synthesis and characterization of high surface area tin oxide/functionalized carbon nanotubes composite as anode materials." Materials Chemistry and Physics. 91(2-3): pp 274-280.

[9] Du N., *et al.* (2009). "Synthesis of polycrystalline SnO_2 nanotubes on carbon nanotube template for anode material of lithium-ion battery." Materials Research Bulletin. 44(1): pp 211-215.

[10] Jin X., *et al.* (2007). "Nanoscale microelectrochemical cells on carbon nanotubes." Small. 3(9): pp 1513-1517.

[11] Wu M., *et al.* (2004). "Redox deposition of manganese oxide on graphite for supercapacitors." Electrochemistry Communications. 6(5): pp 499-504.

[12] Dong X., *et al.* (2006). "MnO_2-embedded-in-mesoporous-carbon-wall structure for use as electrochemical capacitors." The Journal of Physical Chemistry B. 110(12): pp 6015-6019.

[13] Huang X., *et al.* (2007). "Preparation and properties of manganese oxide/carbon composites by reduction of potassium permanganate with acetylene black." Journal of The Electrochemical Society. 154(1): pp A26-A33.

[14] Ma S.B., *et al.* (2007). "Synthesis and characterization of manganese dioxide spontaneously coated on carbon nanotubes." Carbon. 45(2): pp 375-382.

[15] Han W.Q. and Zettl A. (2003). Coating single-walled carbon nanotubes with tin oxide. Nano Letters. 3(5): pp 681-683.

[16] McKeown D.A., *et al.* (1999) "Structure of hydrous ruthenium oxides: Implications for charge storage." The Journal of Physical Chemistry B. 103(23): pp 4825-4832.

[17] Hu C.C. and Tsou T.W. (2002). "Ideal capacitive behavior of hydrous manganese oxide prepared by anodic deposition." Electrochemistry Communications. 4(2): pp 105-109.

[18] Conway B.E. (1991). "Transition from "Supercapacitor" to "Battery" behavior in electrochemical energy storage." Journal of The Electrochemical Society. 138(6): pp 1539-1548.

[19] Hu C.C. and Tsou T.W. (2003). The optimization of specific capacitance of amorphous manganese oxide for electrochemical supercapacitors using experimental strategies. Journal of Power Sources. 115(1): pp 179-186.

[20] Ghaem M., *et al.* (2008). "Charge storage mechanism of sonochemically prepared MnO_2 as supercapacitor electrode: Effects of physisorbed water and proton conduction." Electrochimica Acta. 53(14): pp 4607-4614.

[21] Peng C., *et al.* (2008). "Carbon nanotube and conducting polymer composites for supercapacitors." Progress in Natural Science. 18(7): pp 777-788.

[22] Hashmi S. and Updahyaya H. (2002). "MnO_2-polypyrrole conducting polymer composite electrodes for electrochemical redox supercapacitors." Ionics. 8(3): pp 272-277.

[23] Wu N.L., Han C.Y., and Kuo S.L. (2002). " Enhanced performance of SnO_2 xerogel electrochemical capacitor prepared by novel crystallization process." Journal of Power Sources. 109(2): pp 418-421.

[24] Glicksman R. and Morehouse C.K. (1956). "Resistivity studies of various Leclanché cathode materials." Journal of The Electrochemical Society.103(3): pp 149-153.

[25] Khomenko V., Raymundo-Piñero E., and Béguin F. (2006). "Optimisation of an asymmetric manganese oxide/activated carbon capacitor working at 2 V in aqueous medium." Journal of Power Sources. 153(1): pp 183-190.

[26] Lee H.Y. and Goodenough J.B. (1999). " Supercapacitor behavior with KCl electrolyte." Journal of Solid State Chemistry. 144(1): pp 220-223.

[27] Pourbaix M. (1966). "Atlas of electrochemical equilibria in aqueous solutions." Pergamon Press, New York.

PROFILES

IR. DR NG KOK CHIANG graduated from the University of Western Australia with first class honours in Bachelor of Engineering in Electrical & Electronics and Bachelor of Commerce majoring in Accounting, Investment Finance (Derivatives), and Managerial Accounting. He then furthered his studies to the University of Nottingham, UK and graduated with a PhD in Energy Storage Engineering having worked on nanomaterials and nanocomposites for advanced supercapacitors for renewable energy storage for three and a half years. Ir. Dr Ng Kok Chiang in his course of research and work had liaised with various organisations such as E.ON (Power and Gas), Lockheed Martin, Jaguar/Land Rover (supercapacitors in automotive industry/electric cars), Battelle (lab management and commercialisation), Malaysia Rubber Board (energy management) and MOSTI (Fabrication of Advanced Supercapacitors).

He is currently the Chief Technology Officer with MyBIG Sdn. Bhd. involved in various research and prototyping projects in collaboration with various Malaysian Government Agencies and research bodies. Two of the most prominent solutions founded were the advanced switching mechanism for the Nexcap storage incorporated in the Sunopy solar system to efficient capturing of the energy from the solar power.

DR DANIEL A. JEWELL is a Research Associate in the Department of Materials Science and Metallurgy at the University of Cambridge. He received his MEng degree in Engineering at the University of Nottingham, England, UK, where he also completed his PhD in Engineering on the world renowned FFC-Cambridge Process under the supervision of Professor George Chen, one of the inventors.

Since 2009 he has been the primary researcher on the Chinuka Process at the University of Cambridge in collaboration with Professor Derek Fray and White Mountain Titanium Corporation.

Daniel's primary research focus is titanium extraction, but he is also experienced in the manufacture and testing of supercapacitors, and the electrochemical production of carbon.

NUMERICAL AND EXPERIMENTAL STUDY ON WAVE PROPAGATION IN THE OPEN ATMOSPHERE

(Date received: 25.03.12/Date accepted: 24.11.12)

Mohammad Ali Jinnah[1] and Mohammad Monjurul Ehsan[2]

MCE Department, Islamic University of Technology (IUT),
Board Bazar, Gazipur-1704, Bangladesh
E-mail: [1]jinnah@iut-dhaka.edu, [2]mme.ehsan@gmail.com

ABSTRACT

In the present research works, wave propagation in the open atmosphere has been investigated both numerically and experimentally. Two-dimensional (2D) numerical code has been developed to solve the Euler equations for the upstream and downstream parameters during the shock wave propagation in the open atmosphere. It is observed that due to decay of the shock strength, all parameters (velocity, pressure and density) in the upstream of the shock wave are decreased as increasing the travel time of the wave in the open atmosphere. It is seen from the numerical images that the propagation of the shock front in the open atmosphere is spherical in shape. An experiment has been conducted by a horizontal shock tube to generate subsonic wave as well as shock wave with supersonic speed by rupturing different types of diaphragms. The properties of diaphragm are the major factors to generate shock wave in the shock tube. It is observed that the properties of diaphragm like toughness and brittleness are the best properties in the present case. In the present experiment, transparent Raksin sheet and used X-ray film are selected as the diaphragm where used X-ray film has the better rupturing quality as compare to Raksin sheet. For measuring the wave speed, a time measuring technique has been developed to measure the wave travel time in the open atmosphere and it is simple in use and accurate in measurement as compare to other complicated technique like wave visualization by High Speed Video camera. During the wave propagation in the open atmosphere, the wave speed decreases and the decay of the wave strength is observed.

Keywords: *Euler equations, Open Atmosphere, Shock wave, Wave decay, Wave visualization*

1.0 INTRODUCTION

For the study of wave propagation in the open atmosphere, an experiment has been conducted to measure the wave speed during the propagation in the open atmosphere. The measurement of wave speed and the determination of its location in the open atmosphere is one of the complex experimental works in the laboratory. In the present research works, a technique has been developed to measure the wave propagation time between two locations and it is very simple in use and accurate in measurement as compare to other existing methods. The measurement of the wave speed is used to investigate the decay of the wave strength as well as the decay of the shock wave strength in the open atmosphere. Both experimental and numerical investigation is essential to improve the understanding of the decay phenomena of the shock strength during interaction with objects in the open atmosphere. A numerical code has been developed to solve the Euler equations for the non-viscous flow field in the open atmosphere and the present code is one of the modified versions of the code developed by Jinnah and Takayama [1]. Many researchers had been used optical techniques to visualize the wave propagation for measuring the wave speed and the location of the wave. Widely used qualitative and semi-quantitative optical flow diagnostics are shadowgraph, schlieren, and interferometry but the application of some of these techniques to supersonic and hypersonic flows can be highly challenging due to the high velocity, strong gradients and restricted optical access generally encountered. Doig *et al*. [2] conducted experiment where direction-indicating color schlieren flow visualization was used to determine optically the general effectiveness of the methods. Multiple images were taken during a single tunnel run, which allowed, to some extent, confirmation of the general steadiness of the flow.

Laser-based techniques such as laser Doppler anemometry and particle image velocimetry are well established for investigation of supersonic flows, but as yet their use in hypersonic flows has been limited. Other relevant measurement techniques include particle tracking velocimetry, Doppler global velocimetry, laser-two-focus anemometry, background oriented schlieren and laser induced fluorescence methods, molecular tagging velocimetry for velocity measurement and thermo-graphic phosphor thermometry for surface temperature measurement. Laser measurement techniques are becoming more commonly applied to many areas of thermo-fluids and heat transfer. An area of their application, which presents highly challenging requirements, is in the measurement of aerospace flows. High speed camera can also be used for the flow visualization to analysis the structure of the wave. In the shock wave research laboratory, Tohoku University Japan, the speed of projectile was measured by Shimadzu's HPV-1 High Speed Video Camera.

In the study of metal-high explosive detonation wave interaction, by the pin technique, it was desirable to obtain time measurements to an accuracy of less than 1 microsecond (*μsec*) over a total time interval of 5 *μsec*. Commercial instruments capable of a high degree of time resolution were not available and a special instrument was developed for this purpose. Kobiera *et al*. [3] conducted experiment on the shock wave propagation through the test section and the shock wave causes a disturbance of the droplets; this process was visualized by a schlieren system and recorded by a high-speed camera. Pianthong *et al*. [4] conducted experiment with the use of the shadowgraph method, showing the projectile traveling inside and leaving the pressure relief section at a velocity of about 1100 *m/s*.

In the present method, a logic circuit has been developed to detect the metal to metal touch pulses for triggering which is finally used to open and close the gate to allow and stop the crystal frequency for counting. Using the number of pulse counted, the traveling time between the trigger points is calculated for the subsonic or supersonic objects. Normally the propagation time of the logic gates is not more then 20 nanoseconds, so the accuracy level of the measured time by the present technique will be less then 0.006%. The obtained experimental results are compared with the numerical results by solving the Euler equations for shock wave propagation in the open atmosphere and it is observed that the simulation results are satisfactory for the wave propagation in the open atmosphere. The present numerical technique can be used for designing aero-mechanism system such as supersonic aircraft by determining the shock wave interaction effects with objects and its decay phenomena during propagation in the open atmosphere.

2.0 EXPERIMENTAL SETUP

Experiments are carried out in a single diaphragm horizontal shock tube in the Fluid Mechanics Laboratory of the Islamic University of Technology (IUT). Figure 1 shows a schematic illustration of the horizontal shock tube consisting of 150 *mm* diameter and 1.5 *m* long high pressure chamber made of mild steel. High pressure chamber is the driver section of the shock tube and the driven section of the shock tube is 100 *mm* diameter and 5 *m* long. A diaphragm is used between two flanges of the driver section and the driven section of the shock tube and

Figure 2: Photograph of post-shocked high speed air delivered from end section of the shock tube

tightly fastens by nut-bolt with proper gasket. The diaphragm is separated the high pressure chamber from atmospheric pressure. Inserting the air (or N_2) pressure inside the high pressure chamber, chamber pressure gradually increases and due to high pressure of the chamber, the diaphragm feels tension force and at certain instant it starts rupture. Due to sudden rupture, the fluid from the high pressure chamber starts to flow with high velocity and when the flow velocity reaches to exceed sonic limit, the shock wave generates after travelling certain distance in the driven section. In the present experiment, the shock wave is allowed to propagate in the open atmosphere, even though it is not safe for human beings if the shock wave strength overcomes the moderate Mach number. After propagating the shock wave in the open atmosphere, the post-shocked high speed air delivered from the end section of the shock tube, which is shown in Figure 2. High pressure fluid, whose pressure is less than chamber pressure, drives the shock front. The rupture of the diaphragm in the shock tube depends on the diaphragm properties and it is observed that better toughness, slightly brittle property of the diaphragm can able to generate stronger shock wave. On the other hand, in smaller diameter shock tubes, diaphragms are ruptured relatively uniform and quickly and then incident shock formation distance is relatively short and its

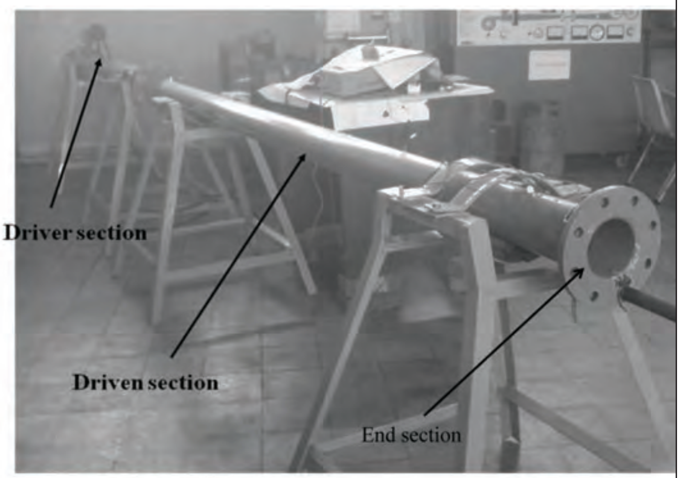

Figure 1: Simple shock tube photograph, constructed in Fluid Mechanics Lab on IUT where driver section and driven section are shown

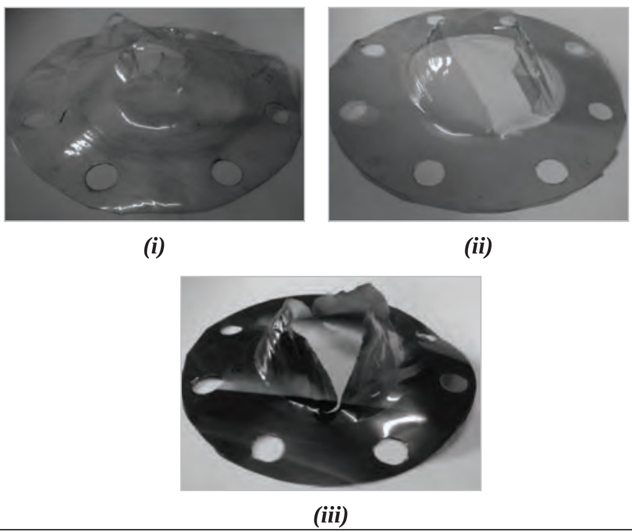

Figure 3: Rupturing characteristics of different diaphragms of (i) Thick polythene; (ii) Raksin; (iii) Used X-ray film

frontal shape is planar. However, in a large size shock tube under study, large diameter plastic diaphragm such as Mylar ones tend to rupture non-uniformly to generate three dimensionally distorted shock fronts. In the present experiment, three types of diaphragm are used where ductile typed thick polythene diaphragm is not suitable to generate shock wave. Raksin sheet and used X-ray film are suitable to use as a diaphragm for generating shock wave in the driven section of the shock tube. Rupturing characteristics of different diaphragms are observed in the experiments which are shown in Figures 3(i)-(iii). Ductile typed thick polythene diaphragm starts continuous deformation as increasing the chamber pressure and it is continuing to deform upto the rupturing of the diaphragm. So such types of diaphragm rupturing fail to create supersonic velocity suddenly at the driven section which finally does not generate shock wave. Due to toughness and brittleness of the Raksin sheet and used X-ray film, the deformation is not linear as increasing the chamber pressure and the rupturing happened suddenly making large ruptured area. Due to sudden diaphragm ruptured, a fluid column from high pressure chamber starts to move through driven section and creates shock wave after travelling certain distance in the driven section. At the same time, an expansion wave, known as expansion fan, moves through high pressure chamber, as a result, a contact surface is created which is moved behind the shock wave with lower velocity, as shown in Figure 4. Figure 4 gives an *x-t* diagram for a typical shock wave indicating the available test time in the test section of the shock tube. The test time is terminated by the arrival of the reflected expansion wave head from the driver end as indicated in Figure 4 and the arrival of the contact surface terminates the test time for the reflection of the incident shock waves from the driven end section if the end wall present at the end section. In the present case, the incident wave propagates in the open atmosphere from the driven end section because of the absence of the end wall.

In the present experiment, the constructed shock tube is used to generate shock wave at the outlet of the shock tube. The chamber pressure of the shock tube is taken in the range of 3.5 – 4.5 kg/cm^2 and due to sudden rupture of the diaphragm, a wave generates in the shock tube which travels with subsonic or supersonic speed depending on the pressure inside the chamber during rupturing. If the chamber pressure increases, a shock wave generates after diaphragm rupturing. A time measuring device is

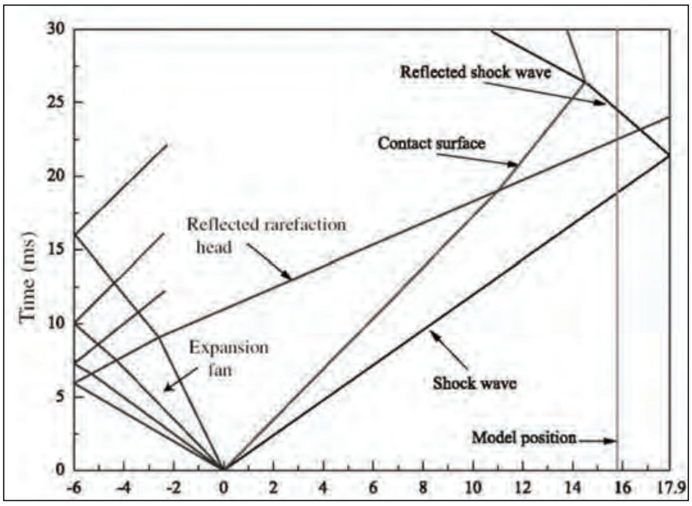

Figure 4: A typical x-t diagram for the relative direction of the shock wave and expansion wave propagation after the rupture of diaphragm

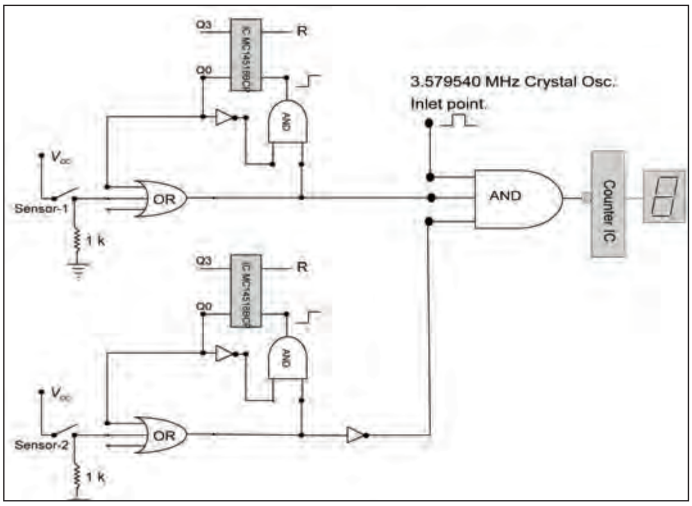

Figure 5: Circuit layout use to construct time measuring device

used to measure the travel time of the wave propagation in the open atmosphere. The logic circuit for the time measuring device has been developed by using two sensing points as shown in Figure 5. In sensing point-1, a metal wire carrying sufficient voltage when touches another metal wire then a voltage signal generates in that wire which causes to change the state of the AND gate to open and allow to pass the crystal frequency through it. Similarly in sensing point-2, shown in Figure 5, a digital signal closes the AND gate not to pass the crystal frequency through it. In this sensing technique, a direct metal to metal contact sensing is more efficient as compare to other sensing devices, like pressure transducers, Electro-optic sensors, Infrared sensors, Magnetic sensors etc and here is not necessary to change the signal, like light, heat, magnetic signal into electric voltage signal. Using the number of pulse counted, the traveling time of the wave between two sensing points is calculated.

Two trigger points (Trigger-1 and Trigger-2) are installed 61.5 *cm* apart in the shock tube to measure the incident wave Mach number. Similarly other four trigger points are also installed at different positions by the supporting rod, shown in **Figure 6**, in the open atmosphere to calculate the wave speeds during the propagation in the open atmosphere and the calculated traveling time between different triggers are recorded. Trigger-2 is installed at the end point of the shock tube where $x = 0.0$ *cm* and all other trigger distances are measured from Trigger-2. Here the distance of the Trigger-3 from Trigger-2 is 9 *cm*, shown in **Figure 6-7**. Similarly from Trigger-2, the distance of

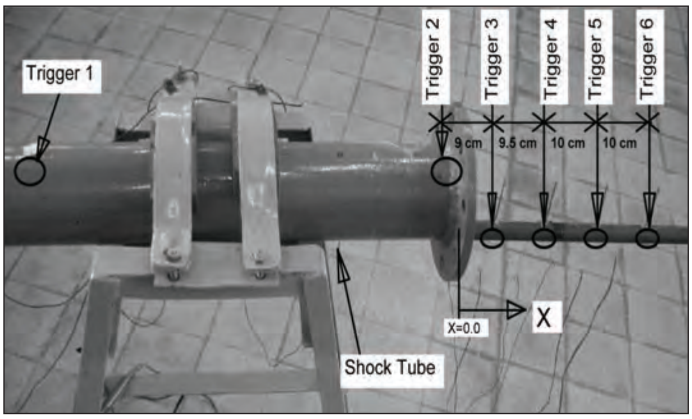

Figure 6: A schematic illustration of the horizontal shock tube where the relative distances between different trigger points are given

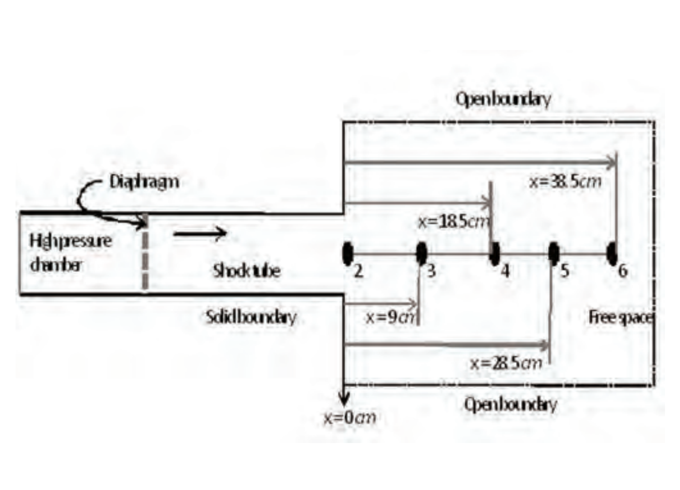

Figure 7: Schematic diagram of the Shock tube and the position of trigger points

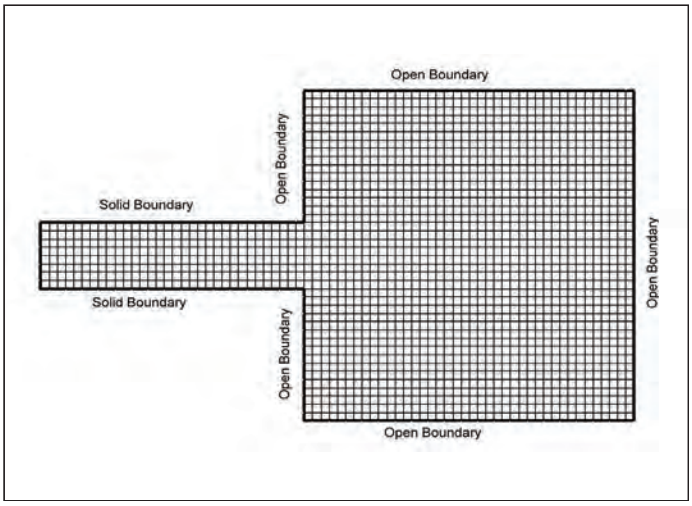

Figure 8: 2D numerical grids of the shock tube and the free space where solid boundaries are taken for shock tube and open boundaries are taken for free space

Trigger-4 is 18.5 *cm*, the distance of Trigger-5 is 28.5 *cm* and the distance of Trigger-6 is 38.5 *cm* respectively which are shown in **Figure 6-7**.

3.0 NUMERICAL SIMULATION

3.1 Problem Specifications

In the present simulation, the results obtained by solving two-dimensional (2D) Euler equations are used to compare with experimental results. The valid 2D numerical code has been developed to solve the Euler equations for the shock wave propagation in the open atmosphere and the extended 3D code was used by Jinnah and Takayama [1] to compute the outcomes of the shock/turbulence interaction. The governing equation is,

$$\frac{\partial Q}{\partial t}+\frac{\partial F}{\partial x}+\frac{\partial G}{\partial y}=0$$

Where $Q = [\,\rho,\ \rho u,\ \rho v,\ e],$

$$F = [\,\rho u,\ \rho u^2,\ \rho uv,\ u(e+p)],$$

$$G = [\,\rho v,\ \rho uv,\ \rho v^2,\ v(e+p)]$$

Here Q is the vector of conservative variables which contains mass, momentum and energy. All variables are calculated in per unit volume. ρ is taken as the mass per unit volume. Two momentum terms in two-dimensional Cartesian coordinates system are ρu, and ρv per unit volume. F and G are the two inviscid flux vectors in x- and y- axis respectively. Each flux vectors contain mass flux, momentum flux and energy flux. ρu is the mass flux and ρu^2, ρuv are the momentum flux and $u(e+p)$ is the energy flux in the x-axis. Similarly ρv is the mass flux and ρuv, ρv^2 are the momentum flux and $v(e+p)$ is the energy flux in the y-axis. Also ρ is the fluid density and u, v are velocity components in each direction of Cartesian coordinates. While e is the total energy per unit volume, pressure p can be expressed by the following state equation for ideal gas

$p=(\gamma-1)[e-\frac{1}{2}\rho(u^2+v^2)]$ where γ is the ratio of specific heats.

The governing equation described above for compressible inviscous flow is discretised by the finite volume method. A second order, upwind Godunov scheme of Flux vector splitting method is used to discrete the inviscid flux terms where HLL-Reimann solver is used for shock capturing in the flow. Two dimensional cells with adaptive grid systems are used for these computations.

The initial two-dimensional grid systems are shown in **Figure 8**. The physical size of each cell before adaptation is equal to 13 x 13 (*mm*). The grid adaptation is one of the improved and computational time saving techniques, which is used in these computations. The grid adaptation is performed by two procedures, one is refinement procedure and another is coarsening procedure. The refinement and coarsening operations are handled separately in computation.

3.2 Boundary Conditions

The upstream of incident shock wave is set as inflow boundary condition, the properties and velocities of which are calculated from Rankine-Hugoniot conditions with incident shock Mach number. The downstream inflow boundary conditions, shown in **Figure 8**, are open boundary conditions and the wall surfaces of the shock tube are used as solid boundary where the gradients normal to the surface are taken zero.

4.0 RESULTS AND DISCUSSION

In the present research work, the investigation on wave propagation in the open atmosphere from the end section of the shock tube is focused mainly to observe the decay of the wave strength. Both experimentally and numerically, the decay of the wave strength measures during propagation and finally a comparison test is performed between numerical results and experimental results. The numerical images are used to visualize the density contour in the flow field during the shock wave propagation in the open atmosphere. It is observed from the density contour of the wave that the number of lines near shock front decreases gradually as increasing the distance of the shock front from the end section of the shock tube. The density contour behind the shock front shows that each line indicates the uniform density along the line and the two adjacent lines measure the density gradient of the flow field. Here there have approximately 60 contour lines considered between maximum and minimum density in the field and the density contours step is 0.01 which are shown in **Figure 9(i)–(viii)**. Similarly the density fringes are visualized numerically to investigate the wave propagation phenomena in the open atmosphere which are shown in **Figure 10(i)–(viii)**. Many researchers used Double exposure holographic interferometry to visualize experimentally the density fringes for the shock wave interaction with different objects, like Wedge, Cone and Cylinder etc. Other researchers used Laser beam to take two consequent exposures on the same photo film within few nanoseconds. Because of double shot on the same photo film, the word double exposure was used. Numata *et al*. [5] conducted their experiments to observe the shock wave reflection from a skewed wedge by using the holographic interferometry. A series of experiments was carried out in order to investigate the initial transient flow in the nozzle by Saito *et al*. [6]. In their experiment the flow was visualized by using the double exposure laser holographic interferometry and a comparison test was conducted on density fringes of the flow field obtained by experimentally and numerically. In the present computation, the density fringes are used to explain the wave propagation characteristics and to get the complete idea on the spherical expansion of the shock front in the open atmosphere.

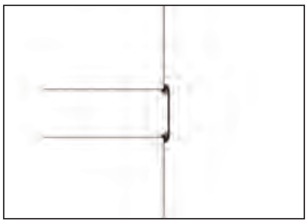

(i) Near end section of the shock tube, $x = 0$ *cm*, density contours step 0.01

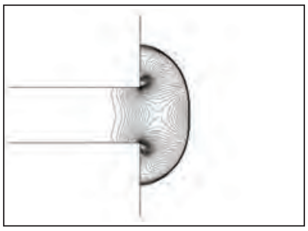

(ii) Shock front position at $x = 9.0$ *cm*, density contours step 0.01

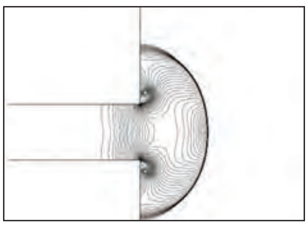

(iii) Shock front position at $x = 13.75$ *cm*, density contours step 0.01

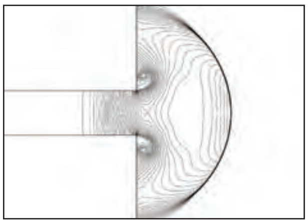

(iv) Shock front position at $x = 18.5$ *mm*, density contours step 0.01

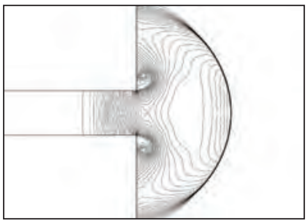

(v) Shock front position at $x = 23.5$ *mm*, density contours step 0.01

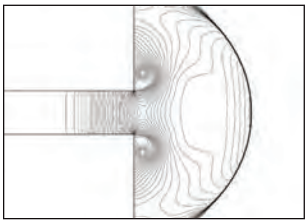

(vi) Shock front position at $x = 28.5$ *mm*, density contours step 0.01

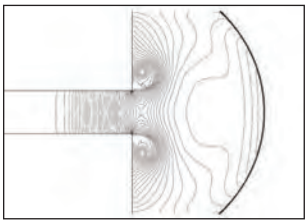

(vii) Shock front position at $x = 33.5$ *mm*, density contour step 0.01

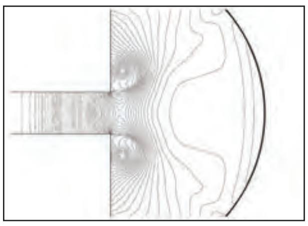

(viii) Shock front position at $x = 38.5$ *mm*, density contour step 0.01

Figure 9: Numerical results of the density fringes at different locations of the shock front in the open Atmosphere for moderate shock propagation

(i) Near end section of the shock tube, x = 0.0 *cm*, density fringes step 0.1

ii) Shock front position at x = 9.0 *cm*, density fringes step 0.1

(iii) Shock front position at x = 13.75 *cm*, density fringes step 0.1

(iv) Shock front position at x = 18.5 *cm*, density fringes step 0.1

(v) Shock front position at x = 23.5 *cm*, density fringes step 0.1

(vi) Shock front position at x = 28.5 *cm*, density fringes step 0.1

(vii) Shock front position at x = 33.5 *cm*, density fringes step 0.1

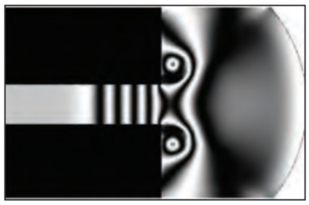

(viii) Shock front position at x = 38.5 *cm*, density fringes step 0.1

Figure 10: Numerical results of the density fringes at different locations of the shock front in the open Atmosphere for moderate shock propagation

The present time measuring technique is used successfully in experiment to investigate the wave propagation in the open atmosphere. The sensing point-1 as shown in **Figure 5**, is installed at the end section of the shock tube where at trigger-2, *x = 0 cm*, shown in **Figure 7**. Similarly sensing point-2, shown in **Figure 5**, is installed at a point in the free space where the distance from the end section of trigger-3 *is x = 9 cm*, shown in **Figure 7**. During the wave propagation over these triggers, the device is captured frequency which is directly proportional to the travelled time of the wave from trigger-2 to trigger-3. The captured frequency is converted into travelled time by dividing the known crystal frequency. Here the known crystal frequency is 3579540 Hz, that means, 1 second is equivalent to 3579540 pulses. Similarly by installing sensing point-1 and sensing point-2 of the device at the points where trigger-2, *x = 0 cm* and trigger-6, *x = 38.5 cm* respectively, the captured frequency is recorded during the wave propagation between these trigger points and the captured frequency is then converted into travelled time of the wave.

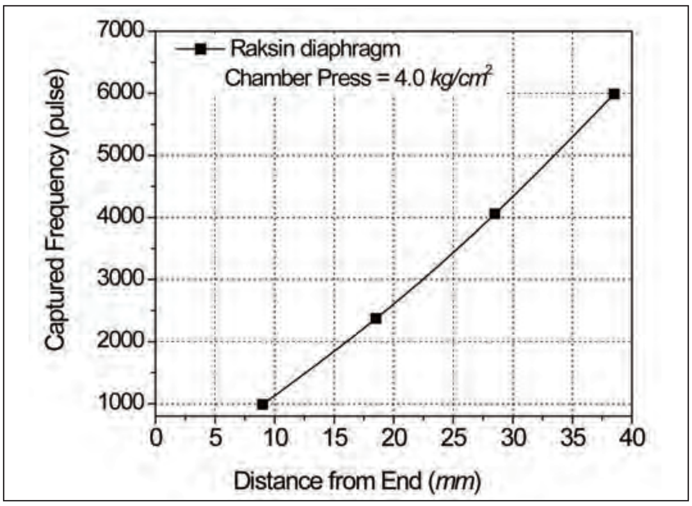

Figure 11: Captured frequency recorded experimentally during the wave travels between different trigger points in the open Atmosphere (Here 1 sec = 3579540 pulses)

Figure 11 shows captured frequencies recorded experimentally during the wave propagation over the points in the open atmosphere where the position of the trigger points are, *x = 0 cm*, *x = 9 cm*, *x = 18.5 cm*, *x = 28.5 cm* and *x = 38.5 cm*, shown in **Figure 7** and here Raksin sheet is used as a diaphragm in the shock tube. The average wave speeds (U_{av}) are determined by the ratio of the distance between two trigger points to the wave travelled time of this distance and the wave speed between any two trigger points is considered as the wave speed at the mid point of the two trigger points. In case of Raksin diaphragm, **Figure 12** shows the average wave speed (U_{av}) variations from the end of the shock tube in the open atmosphere. Here the maximum wave speed is *326 m/s* at position, *x = 4.5 cm* which is the mid point between the trigger points, *x = 0 cm* and *x = 9 cm*. As compare to the local sound velocity, the wave speed is subsonic. So it is concluded that the rupture of the Raksin diaphragm generates subsonic wave at the end point of the shock tube and as increasing the travel distance by the wave, the wave strength decreases during propagation in the open atmosphere which is shown in **Figure 12**.

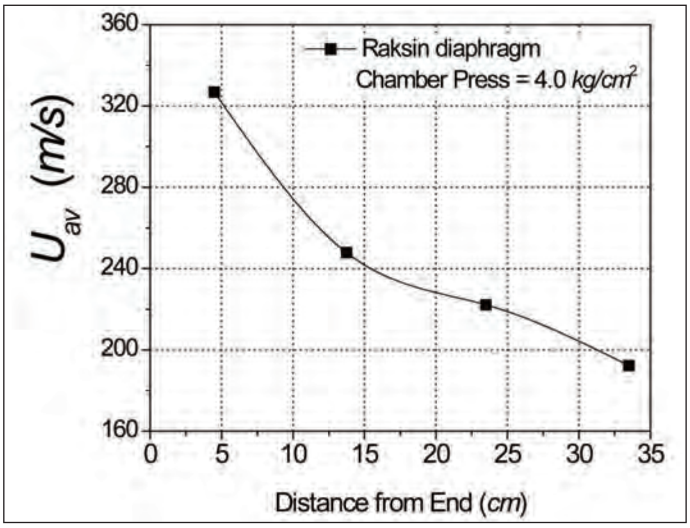

Figure 12: Experimental results of the average wave speed at different locations of the shock front in the open Atmosphere (Here rupture of Raksin diaphragm generates subsonic wave at the end of shock tube)

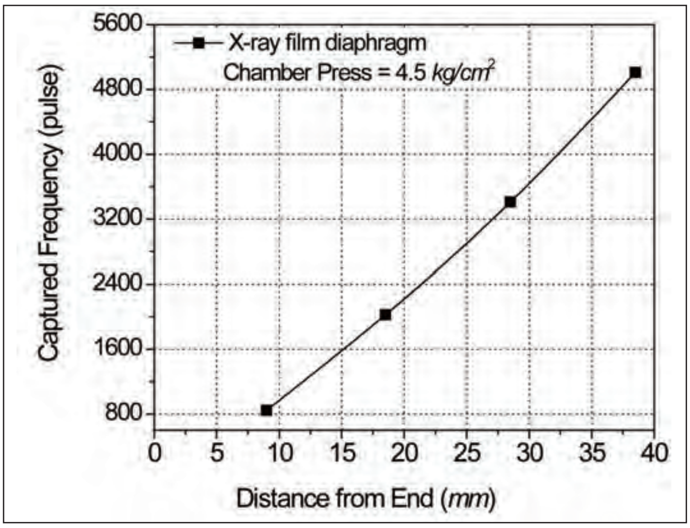

Figure 13: Captured frequency recorded experimentally during the wave travels between different trigger points in the open Atmosphere (Here 1 sec = 3579540 pulses)

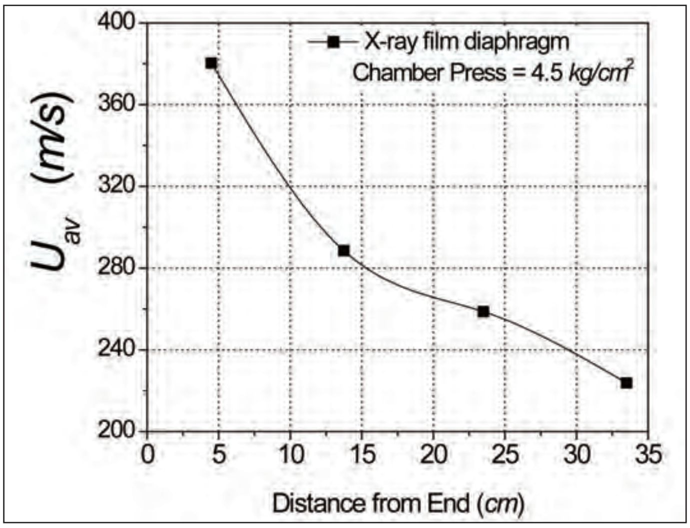

Figure 14: Experimental results of the average wave speed at different locations of the shock front in the open Atmosphere (Here rupture of used X-ray film diaphragm generates supersonic wave at the end of shock tube)

Similarly **Figure 13** shows captured frequencies recorded experimentally during the wave propagation over the points in the open atmosphere where the position of the trigger points are *x = 0 cm*, *x = 9 cm*, *x = 18.5 cm*, *x = 28.5 cm* and *x = 38.5 cm*, shown in **Figure 7** and here used X-ray film is used as a diaphragm in the shock tube. In case of used X-ray film, **Figure 14** shows the average wave speed (U_{av}) variations from the end of the shock tube in the open atmosphere. Here the maximum wave speed is *380 m/s* at position, *x = 4.5 cm* which is the mid point between the trigger points, *x = 0 cm* and *x = 9 cm*. As compare to the local sound velocity, the wave speed is supersonic. So it is concluded that the rupture of the used X-ray film diaphragm generates shock wave at the end point of the shock tube and as increasing the travel distance by the wave, the shock wave strength decreases to subsonic wave during propagation in the open atmosphere which is shown in **Figure 12**.

The decay of the wave propagation is determined both experimentally and numerically during the wave propagation over the trigger points in the open atmosphere and **Figure 15** shows the profile of the percentage of decay at different trigger points when Raksin sheet is used as a diaphragm in the shock tube. It is observed that initially the percentage of decay increases obtained by experiment as compare to the numerical results. It is observed that the percentage of the decay increases as increasing the distance from the end point of the shock tube. It is also observed that the decay obtained from experiment has the good agreement with the numerical results.

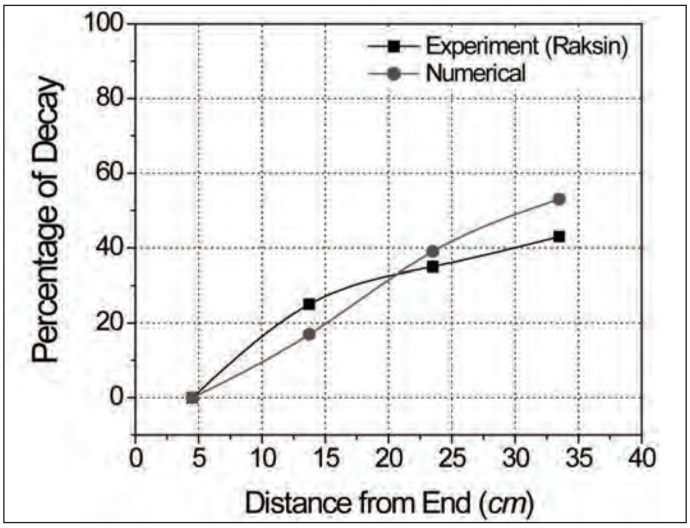

Figure 15: Comparison between Experimental results and Numerical results of the percentage of decay of the wave propagation in the open Atmosphere (Here rupture of Raksin diaphragm generates subsonic wave at the end of shock tube)

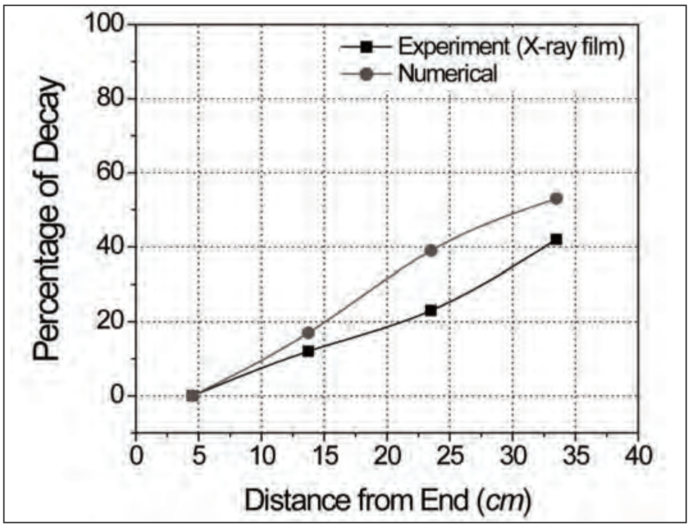

Figure 16: Comparison between Experimental results and Numerical results of the percentage of decay of the wave propagation in the open Atmosphere. (Here rupture of used X-ray film diaphragm generates supersonic wave at the end of shock tube)

Figure 16 shows the profile of the percentage of decay at different trigger points when used X-ray film is used as a diaphragm in the shock tube. It is observed that initially the percentage of decay decreases obtained by experiment as compare to the numerical results. It is observed that the percentage of the decay increases as increasing the distance from the end point of the shock tube. It is also observed that the decay obtained from experiment has the good agreement with the numerical results. So it is concluded that the decay of subsonic wave and supersonic wave has the same nature during the propagation in the open atmosphere and such type of decay observes due to spherical expansion of the wave in the open atmosphere. The decay of shock wave may differ with subsonic wave due to rapid compression and expansion happened during shock wave propagation but the percentage of decay is same after propagating far distance in the open atmosphere.

5.0 CONCLUSION

In the present experimental works, shock wave has been generated by rupturing different types of diaphragms in the shock tube. The rupturing properties of diaphragm are the major factors to generate shock wave in the shock tube. It is observed that used X-ray film gives the better performance as compare to Raksin sheet for rupturing purposes and the properties like toughness and brittleness are the best properties of the diaphragm.

For calculating the wave speed in the open atmosphere, the present time measuring technique is simple in use and accurate in measurement as compare to other complicated technique like wave visualization technique. During the wave propagation in the open atmosphere, the wave speed decreases as increasing the travel time. So decreasing the wave speed indicates that the decay of the wave strength is the normal phenomenon during propagation in the open atmosphere. In the present research, the decay of the wave strength obtained from experimental results has the good agreement with numerical results. ■

REFERENCES

[1] Jinnah MA and Takayama K. (2011) Numerical and Experimental Study of Shock/Turbulent Flow Interaction – A Code Validation Test. Journal IEM, Vol. 72, No.4: 37-46.

[2] Doig GC, Barber TJ, Leonardi E, Neely J and Kleine H. (2008) Methods for investigating supersonic ground effect in a blowdown wind tunnel, Shock Waves, 18: 155-15.

[3] Kobiera A, Szymczyk J, Wola'nski P and Kuhl A. (2009) Study of the shock-induced acceleration of hexane droplets, Shock Waves, 18: 475-85.

[4] Pianthong K, Zakrzewski S, Behnia M and Milton BE. (2002) Supersonic liquid jets: Their generation and shock wave characteristics, Shock Waves, 11: 457-66.

[5] Numata D, Ohtani K and Takayama K. (2009) Diffuse holographic interferometric observation of shock wave reflection from a skewed wedge, Shock Waves, 19: 103-112.

[6] Saito T and Takayama K. (1999) Numerical simulations of nozzle starting process, Shock Waves, 9: 73-79.

PROFILES

DR MOHAMMAD ALI JINNAH is an Associate Professor in Department of Mechanical and Chemical Engineering, Islamic University of Technology (An Organ of the OIC), Bangladesh. He obtained his Ph.D. from Tohoku University, Sendai, Japan in 2005 specialising in Shock Wave interaction with turbulent flow.

MR. MOHAMMAD MONJURUL EHSAN is a Lecturer in Department of Mechanical and Chemical Engineering, Islamic University of Technology (An Organ of the OIC), Bangladesh. He obtained his M.Sc. Engg degree from IUT in 2012 specialising in Shock Wave propagation in Open Atmosphere.

AN ANALYTICAL STUDY OF FLUID TANK SYSTEM FOR REDUCING THE ROLLING OF A SHIP

(Date received: 18.07.12/Date accepted: 24.11.12)

Gazi Md. Khalil[1], Md. Shahjada Tarafder[2] and Md. Shahidul Islam[3]

Department of Naval Architecture and Marine Engineering,
Bangladesh University of Engineering and Technology, Dhaka-1000, Bangladesh
E-mail: [1]khalil@name.buet.ac.bd, [2]shahjada68@yahoo.com, [3]shahid777@name.buet.ac.bd

ABSTRACT

There have long been attempts to reduce the rolling of ships, prompted by a desire to increase comfort of travel, improve weapon control measures, extend the operation of aircraft, and so on. In many passenger and naval ships anti-rolling tanks are fitted in order to reduce rolling. Anti-rolling tank systems operate on the principle that a fluid, usually water, moves from one tank to another and generates a moment on the ship that counteracts the rolling motion. The principal aim of the present paper is to explain the characteristics of oscillation of fluid in anti-rolling tanks. Using the principle of conservation of energy, a detailed theoretical analysis is performed for the oscillation of water in two identical circular tanks connected by a narrow pipe. A new expression is derived for the frequency of oscillation of water as a function of the diameter of the circular tanks, the depth of water in the tanks, and the length and diameter of the connecting pipe. Subsequently, the expression for the frequency of oscillation of water is modified for the case of two identical rectangular tanks. Then it is analytically demonstrated how the aforesaid tank system can be used to neutralize the rolling motion of a ship. Based on the aforesaid theoretical analysis, a computer program is developed in FORTRAN 95 *and executed on the* DELL OPTIPLEX 780 *computer. The computational results are plotted in order to show how the frequency of oscillation of water is influenced by the diameter of the tanks, the depth of water in the tanks, geometry of the tanks and the length-to-diameter ratio of the connecting pipe. The present theoretical analysis is expected to be useful in the design of anti-rolling tanks which will effectively reduce the rolling motions of a ship.*

Keywords: *Anti-Rolling Tank, Connecting Pipe, Depth of Water, Diameter of Tanks, Frequency of Oscillation, Identical Tanks, U-Tank*

1.0 INTRODUCTION

A ship moving on the surface of a sea is almost always in oscillatory motion. There are six fundamental forms of ship motions. These motions are heaving, swaying, surging, rolling, pitching and yawing. All six motions are oscillatory in nature. The first three are linear motions, heaving being the vertical motion of the ship, whilst swaying and surging are respectively the athwartship motion and the fore-and-aft motion. Rolling is a rotation about a longitudinal axis, while pitching is a rotation about a transverse axis and yawing is a rotation about a vertical axis.

The motions of ships and the control of these motions have been the focal point of extensive research over the years. A ship in a seaway undergoes complex motions that may reduce the operational range of the ship and can be uncomfortable or even dangerous for the crew. In certain circumstances, the captain may be forced to alter the course or slow the ship to reduce large motions and thus reduce the combat readiness of naval vessels, cause the loss of containers on cargo vessels, and reduce the operational parameters of various ships. In extreme cases, the ship may capsize.

If a ship could possibly roll among waves unresisted, that is, without being subject to any resistance from wind or water and having her natural period of rolling synchronizing with that of the waves, the effect would be that the continued impulses given by the synchronizing waves would eventually capsize her, whatever might be her stability.

The great value of bilge keels in increasing resistance and reducing rolling has frequently been proved by experiments with models and experience with ships in service. Bilge keels produce good results upon large ships but the effect is equally apparent upon smaller craft with a short period.

Various other methods have been adopted in the past to reduce rolling. In some passenger and naval ships anti-rolling tanks were fitted and in a few a type of gyroscope has been fitted. Whatever method is tried, whether by external fittings such as bilge keels, fins, etc., or internal appliances, the principal object is to absorb the energy imparted to the ship by the wave motion, and the degree of violence of the rolling depends on the rate at which the resisting medium can keep pace in absorbing the energy which the waves are imparting to the ship.

There have been many types of internal tanks designed to produce counter-rolling moments, and they have been tried with varied degrees of success. No attempt will be made here to describe all these various systems. Rather, it would be more pertinent to single out one of the most successful of this type of anti-rolling device which was originally developed by Frahm in 1911. The famous Frahm tank consists basically of a U-shaped tank system transversely arranged from side to side (*Figure 1*). Actually, the system is composed of two reservoirs (one on the port side and the other one on the starboard side) connected by a horizontal duct. The horizontal duct is of a smaller sectional area than the reservoirs. The fluctuating column of water within the reservoirs comprises an oscillatory system, possessing a definite natural period of oscillation. For the effective operation of the

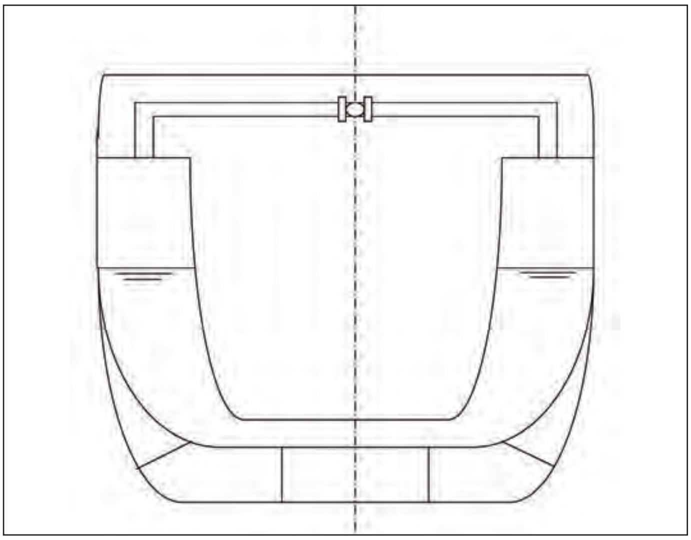

Figure 1: Schematic diagram of Frahm's tank

reservoirs, it is essential that the period of oscillation of the water column within the reservoirs be equal to the period of rolling of the vessel in still water. This is attained by the proper choice of dimensions for the section of the connecting water canal. As the vessel experiences a resonant, regular sea, there arises the phenomenon of dual resonance between the action of the waves and the rocking of the vessel, and between the motions of the vessel and the oscillations of the water in the reservoirs. The oscillations of the vessel lag, in phase, the oscillations of the exciting force by $\pi/2$, and the oscillations of the water within the reservoirs lag the oscillations of the vessel by $\pi/2$. As a result, the lag between the phase of the oscillations of the water and the phase of the exciting moment comprises π, and the stabilizing moment created by the oscillation of the water bears a sign opposite to that of the exciting moment of the wave action (Blagoveshchensky, 1962).

The reservoirs are connected across the top by an air line whose dimensions are also critical in affecting the period of the water in the system. This air line is equipped with valves which, upon adjustment, can control the amount of water transferred between reservoirs and the phase relation between the roll of the ship and the transfer of the water. The phase lag is adjusted so that when the ship is rolling to port the water in the tank is rolling to starboard. This type of tank contains no mechanical apparatus at all, although the water passes through structural constrictions as it passes from side to side, and is efficient only when the quantity of water in motion has been carefully calculated (Walton and Baxter, 1970).

In recent years, there has been a significant interest in U-tanks in relation to their potential for reducing the likelihood of ship parametric roll resonance. Holden *et al*. (2011) presented two novel nonlinear models of U-shaped anti-roll tanks for ships, and their linearization. The models were derived using Lagrangian mechanics. This formulation not only simplifies the modeling process, but also allows one to obtain models that satisfy energy-related physical properties. The proposed nonlinear models and their linearization were validated using model-scale experimental data.

There are many more researchers who have made important contributions towards the improvement of anti-rolling tanks. Some of them are Watanabe (1930), Vasta *et al*. (1961), Okada and Takagi (1965), Watanabe *et al*. (1966), Webster (1967), Takaishi (1971), Barr and Aukudinov (1977), Cox and Lloyd (1977), Webster *et al*. (1988), Honkanen (1990), Yamaguchi and Shinkai (1992), Lee and Vassalos (1996), Hsueh and Lee (1997), Treakle (1998), Gawad *et al*. (2001), Tanizawa *et al*. (2003), Moaleji and Greig (2007), Umeda *et al*. (2008), Marzouk and Nayfeh (2009), Winden (2009), Holden *et al*. (2011), etc.

Many researchers have studied the design of anti-rolling tanks. However, most of them concentrated on studying the performance of anti-roll tanks in damping the rolling motion of the ship. Little attention has been paid to the fluid motion inside the tank itself. Another important issue is the tank tuning. Proper tuning of the anti-rolling tank, to match the ship's natural frequency, is very important in reducing the rolling motion. This paper concentrates on the most familiar type, which is the U-tube passive tank as a mechanical absorber of rolling motion. A detailed mathematical analysis of the oscillation of water in two identical tanks connected by a narrow duct is presented. An expression is derived for the frequency of oscillation of water as a function of the diameter of the tanks, the depth of water in the tanks, and the length and diameter of the connecting duct. The present theoretical model is expected to be useful in the design of anti-rolling tanks which will effectively reduce rolling motions of a ship.

2.0 THEORETICAL ANALYSIS

Consider two identical circular cylindrical tanks of cross-sectional area A. The tanks are connected at their bottom by a pipe of length L and cross-sectional area a, as shown in *Figure 2*. The tanks are filled with water, and depth of water in each tank is h.

Suppose that oscillatory motion occurs in the tanks due to some external disturbance. In such a case, the water level will fall in one tank, with a corresponding rise in the other. The head of water, causing flow in the pipe, will be the difference between the two water levels.

Let the water level in Tank 1 fall down by y. Then the water level in Tank 2 will rise up by y. Let x be the horizontal displacement of water in the pipe. The volume of water that has passed from Tank 1 is Ay. From constancy of volume of water, the volume of water can be written as Equation (1)

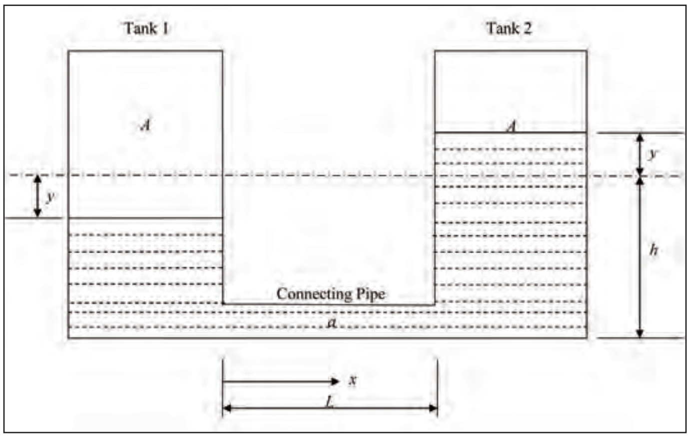

Figure 2: Natural oscillations of water in two identical tanks

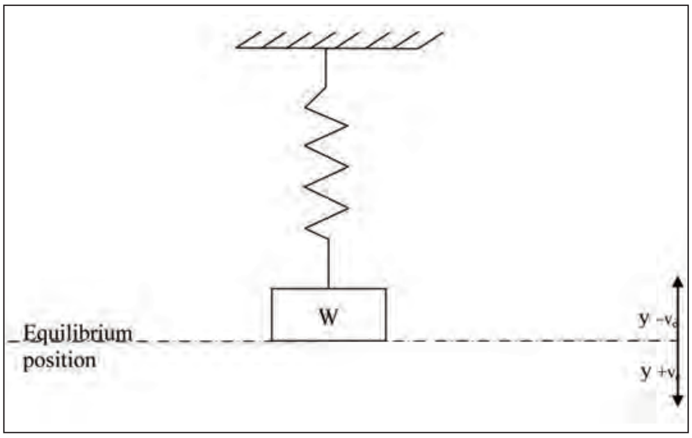

Figure 3: Simple spring-mass system

$$Ay = ax \tag{1}$$

$$\therefore x = \frac{Ay}{a} \tag{2}$$

Using the principle of conservation of energy, natural frequencies of oscillating systems can be conveniently determined. The simplest case of a free, natural oscillation is that of a weight suspended on a spring, as shown in *Figure 3*. When the weight is disturbed from its position of equilibrium, a restoring force is applied by the change in length of the spring and free oscillations are sustained by the elastic force in the spring alone. For the oscillating system, the energy is partly kinetic and partly potential. The kinetic energy (T) is associated with the velocity of the mass and the potential energy (U) is due to the strain energy stored in the spring. Thus,

$$T + U = \text{Total energy} = \text{constant} \tag{3}$$

Therefore, the rate of change of energy is zero.

$$\frac{d}{dt}(T+U) = 0 \tag{4}$$

The kinetic energy of the mass is given by

$$T = \frac{1}{2}mv^2 = \frac{1}{2}m\dot{y}^2 \tag{5}$$

The potential energy of the system is due to strain energy stored in the spring and is given by

$$U = \int_0^y ky\,dy = \frac{1}{2}ky^2 \tag{6}$$

where k is the spring constant.

The expression for the potential energy of the water oscillating in the tanks is as shown in Equation (7). In case of oscillation, the water falls in one tank, with a corresponding rise in the other. The restoring force (F) is due to the difference between the two water levels. Thus, it can be written as:

$$F = 2Ay\rho g \tag{7}$$

where ρ is the density of water.

In this problem there is no specific "spring", but still the force of gravity tends to restore the water level to an equilibrium position. Thus we have a "gravity spring", of which the spring constant by definition is the force per unit deflection.

$$F = ky$$

$$\therefore k = \frac{F}{y} = \frac{2Ay\rho g}{y} = 2A\rho g \tag{8}$$

Equation (6) and Eqn (8) can be combined and rewritten as:

$$U = \frac{1}{2}(2A\rho g)y^2$$

$$\therefore U = A\rho g y^2 \tag{9}$$

Differentiating Eqn (9) with respect to time t,

$$\frac{dU}{dt} = 2A\rho g y\frac{dy}{dt} = 2A\rho g y\dot{y} \tag{10}$$

The kinetic energy of the oscillating mass of water is given by

$$T = \frac{1}{2}Ah\rho\left(\frac{dy}{dt}\right)^2 + \frac{1}{2}Ah\rho\left(\frac{dy}{dt}\right)^2 + \frac{1}{2}aL\rho\left(\frac{dx}{dt}\right)^2$$

$$\text{or, } T = Ah\rho\left(\frac{dy}{dt}\right)^2 + \frac{1}{2}aL\rho\left(\frac{dx}{dt}\right)^2 \tag{11}$$

Equation (2) and Eqn (11) can be combined and rewritten as:

$$T = Ah\rho\left(\frac{dy}{dt}\right)^2 + \frac{1}{2}aL\rho\left(\frac{A}{a}\right)^2\left(\frac{dy}{dt}\right)^2$$

$$\text{or, } T = Ah\rho\dot{y}^2 + \frac{1}{2}aL\rho\left(\frac{A}{a}\right)^2\dot{y}^2$$

$$\text{or, } T = \frac{1}{2}\rho\left[2Ah + aL\left(\frac{A}{a}\right)^2\right]\dot{y}^2 \tag{12}$$

Differentiating both sides of Eqn (12) with respect to time t,

$$\frac{dT}{dt} = \frac{1}{2}\rho\left[2Ah + aL(A/a)^2\right]2\dot{y}\ddot{y}$$

$$\text{or, } \frac{dT}{dt} = \rho\left[2Ah + aL(A/a)^2\right]\dot{y}\ddot{y} \tag{13}$$

From Eqn (4), Eqn (10) and Eqn (13),

$$\rho\left[2Ah + aL(A/a)^2\right]\dot{y}\ddot{y} + 2A\rho g y\dot{y} = 0$$

Dividing the above expression by $\rho\dot{y}$ throughout,

$$\left[2Ah + aL(A/a)^2\right]\ddot{y} + 2Agy = 0 \tag{14}$$

$$\text{or,}\ \ \ddot{y} + \left[\frac{2Ag}{2Ah + aL(A/a)^2}\right]y = 0$$

$$\text{or,}\ \ \ddot{y} + p^2 y = 0 \tag{15}$$

where p is the natural frequency of oscillation in radian per second. Thus,

$$p^2 = \frac{2Ag}{2Ah + aL(A/a)^2}$$

$$\text{or,}\ \ p^2 = \frac{2g}{2h + L(A/a)} \tag{16}$$

Let D be the diameter of each tank and d the diameter of the connecting pipe. Therefore,

$$A = \frac{\pi D^2}{4}$$

$$a = \frac{\pi d^2}{4}$$

$$\therefore \frac{A}{a} = \frac{\pi D^2}{4} \times \frac{4}{\pi d^2} = \left(\frac{D}{d}\right)^2 \tag{17}$$

From Eqn (16) and Eqn (17), it can be written as:

$$p^2 = \left[\frac{2g}{2h + L(D/d)^2}\right] \tag{18}$$

$$\text{or,}\ \ p = \left[\frac{2g}{2h + L(D/d)^2}\right]^{1/2} \text{rad/sec} \tag{19}$$

We know that

$$p = 2\pi N$$

where N is the frequency of oscillation in cycles per second.

$$\therefore\ \ N = \frac{1}{2\pi}\left[\frac{2g}{2h + L(D/d)^2}\right]^{1/2} \text{cycles/sec} \tag{20}$$

Consider a very special case when the diameter of the connecting pipe is equal to the diameter of the twin tank, that is, $D = d$. Then Eqn (20) reduces to

$$N = \frac{1}{2\pi}\left[\frac{2g}{2h + L}\right]^{1/2} \text{cycles/sec} \tag{21}$$

Then consider two rectangular tanks in place of the aforesaid circular cylindrical tanks. The length and breadth of each tank is D and the depth of water is h. The two tanks are connected by a pipe of diameter d. Therefore, it can be written as:

$$A = D \times D = D^2 \text{ and}$$

$$a = \frac{\pi d^2}{4}$$

$$\therefore \frac{A}{a} = \frac{D^2}{\pi d^2/4} = \frac{4}{\pi}\left(\frac{D}{d}\right)^2 \tag{22}$$

Combining Eqn (16) and Eqn (22), it can be shown that:

$$p^2 = \frac{2g}{2h + \frac{4L}{\pi}\left(\frac{D}{d}\right)^2}$$

$$\therefore p = \left[\frac{2g}{2h + \frac{4L}{\pi}\left(\frac{D}{d}\right)^2}\right]^{1/2} \text{rad/sec}$$

$$N = \frac{1}{2\pi}\left[\frac{2g}{2h + \frac{4L}{\pi}\left(\frac{D}{d}\right)^2}\right]^{1/2} \text{cycles/sec} \tag{23}$$

Consider a U-tank of uniform cross-sectional area A, as shown in *Figure 4*. The tank is filled with water. Let the total length of the water column be L', and the density of water be ρ. If the water oscillates back and forth, the mass in motion is $\rho AL'$. The force of gravity tends to restore the water level to an equilibrium position. Suppose that the water level in one arm of

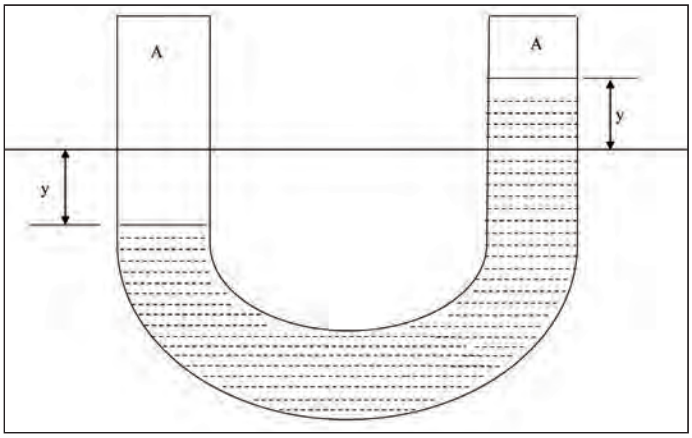

Figure 4: Natural oscillations of water in a U-tank

the U-tank is raised by y, then it will fall in the other arm by y. This gives an unbalanced weight of $2y$ water column. Thus the inertia force (Fi) and the restoring force (F) can be expressed as follows:

$$F_i = AL'\rho\ddot{y}$$

$$F = 2Ay\rho g$$

According to Newton's law of motion,

$$AL'\rho\ddot{y} = -2Ay\rho g$$

$$\text{or, } AL'\rho\ddot{y} + 2Ay\rho g = 0$$

$$\text{or, } \ddot{y} + \left(\frac{2g}{L'}\right)y = 0 \tag{24}$$

Equation (24) is of the well-known form:

$$\ddot{y} + p^2 y = 0$$

where
$$p^2 = \frac{2g}{L'} \tag{25}$$

Thus the frequency of oscillation can be expressed as

$$p = \left(\frac{2g}{L'}\right)^{1/2} \text{rad/sec}$$

and (26)

$$N = \frac{1}{2\pi}\left(\frac{2g}{L'}\right)^{1/2} \text{cycles/sec} \tag{27}$$

It may be noted that Eqn (21) gives an expression for the frequency of oscillation of water in two identical circular tanks when the diameter of each tank is equal to that of the connecting pipe. Then Eqn (27) provides an expression for the frequency of oscillation of water in a simple U-tank. A careful observation reveals that there is no fundamental difference between these two expressions, although they are independently derived. This confirms the validity of the present theoretical analysis.

Let us now discuss how the aforesaid tank system can be used to neutralize the rolling motion of a ship. Suppose these two tanks are installed in a ship, one on the starboard and the other on the port side and are connected by a pipe. In case of rolling, the water will roll from side to side with a period similar to that of the ship but exactly opposite in phase, that is, when the ship is rolling to port the water in the tank will be rolling to starboard. In *Figure 5* the main spring-mass system (k_1, m_1) is the analogue of the ship and the small spring-mass system (k_2, m_2) is the analogue of the anti-rolling tanks. A sinusoidal wave exciting force $P \sin \omega t$ acts on the main mass m_1.

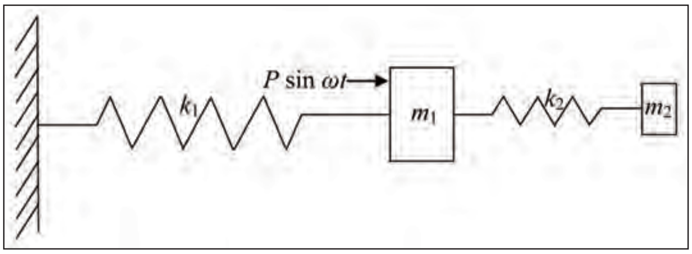

Figure 5: Equivalent spring-mass system of a ship under rolling-motion

The equation of motion can be written as

$$m_1 \frac{d^2 x_1}{dt^2} = k_2(x_2 - x_1) - k_1 x_1 + P \sin \omega t \tag{28}$$

$$m_2 \frac{d^2 x_2}{dt^2} = -k_2(x_2 - x_1) \tag{29}$$

The Cardinal Principle of forced vibration of a linear system is that a harmonic force acting on a linear system produces a harmonic motion of the same frequency but with a phase shift. Since the system under consideration is undamped, the phase angles can be taken as constant and equal to zero. Hence, the solution of Eqn (28) and Eqn (29) can be written in the form

$$x_1 = a_1 \sin \omega t \tag{30}$$

$$x_2 = a_2 \sin \omega t \tag{31}$$

Using Eqn (30) and Eqn (31) in Eqn (28) and Eqn (29), it can be shown that:

$$a_1(-m_1\omega^2 + k_1 + k_2) - a_2 k_2 = P \tag{32}$$

$$-a_1 k_2 + a_2(-m_2\omega^2 + k_2) = 0 \tag{33}$$

Defining

$$\left.\begin{aligned} \frac{k_1}{m_1} &= p_1^2 \\ \frac{k_2}{m_2} &= p_2^2 \\ \frac{P}{k_1} &= x_s \\ \frac{m_2}{m_1} &= \mu \end{aligned}\right\} \tag{34}$$

and rewriting Eqn (32) and Eqn (33) as

$$a_1\left(1 + \frac{k_2}{k_1} - \frac{\omega^2}{p_1^2}\right) - a_2\left(\frac{k_2}{k_1}\right) = x_s \tag{35}$$

$$a_1 - a_2\left(1 - \frac{\omega^2}{p_2^2}\right) = 0 \tag{36}$$

Solving Eqn (35) and Eqn (36),

$$\frac{a_1}{x_s} = \frac{\left(1 - \frac{\omega^2}{p_2^2}\right)}{\left[\left(1 - \frac{\omega^2}{p_2^2}\right)\left(1 + \frac{k_2}{k_1} - \frac{\omega^2}{p_1^2}\right) - \frac{k_2}{k_1}\right]} \tag{37}$$

$$\frac{a_2}{x_s} = \frac{1}{\left[\left(1 - \frac{\omega^2}{p_2^2}\right)\left(1 + \frac{k_2}{k_1} - \frac{\omega^2}{p_1^2}\right) - \frac{k_2}{k_1}\right]} \tag{38}$$

Assuming the reduction factor

$$\Delta = \left[\left(1 - \frac{\omega^2}{p_2^2}\right)\left(1 + \frac{k_2}{k_1} - \frac{\omega^2}{p_1^2}\right) - \frac{k_2}{k_1}\right] \tag{39}$$

In Eqn (37) and Eqn (38), the magnification factors of the main mass ($\underline{a}_1$) and the anti-rolling tank ($\underline{a}_2$) can be written as:

$$\underline{a}_1 = \frac{a_1}{x_s} = \frac{\left(1 - \frac{\omega^2}{p_2^2}\right)}{\Delta} \tag{40}$$

$$\underline{a}_2 = \frac{a_2}{x_s} = \frac{1}{\Delta} \tag{41}$$

Equation (40) gives us the condition for reducing the rolling motion of the ship to zero. If p_2 is made equal to ω (that is, the frequency of the anti-rolling tank is made equal to the frequency of the wave exciting force), then a_1 becomes zero. Thus the rolling motion of the ship does not exist any more.

If p_2 is made equal to ω then Eqn (34) and Eqn (39) lead to:

$$\Delta = -\frac{k_2}{k_1} = -\frac{p_2^2}{p_1^2}\frac{m_2}{m_1} = -\frac{\omega^2}{p_1^2}\mu \tag{42}$$

Combining Eqn (41) and Eqn (42):

$$\underline{a}_2 = -\frac{p_1^2}{\omega^2 \mu} \tag{43}$$

3.0 RESULTS AND DISCUSSION

A detailed mathematical analysis of the oscillations of water in two identical tanks connected by a narrow pipe is presented in the preceding section. Based on the aforesaid theoretical analysis, a computer program is developed in FORTRAN 95 and executed on the DELL OPTIPLEX 780 computer. It may be noted that all computations are performed initially for a pair of identical circular tanks and then for a pair of identical rectangular tanks whose length and breadth are equal to the diameter of the circular tanks. The computational results are then plotted in order to show the characteristics of oscillation of water in circular as well as rectangular tanks.

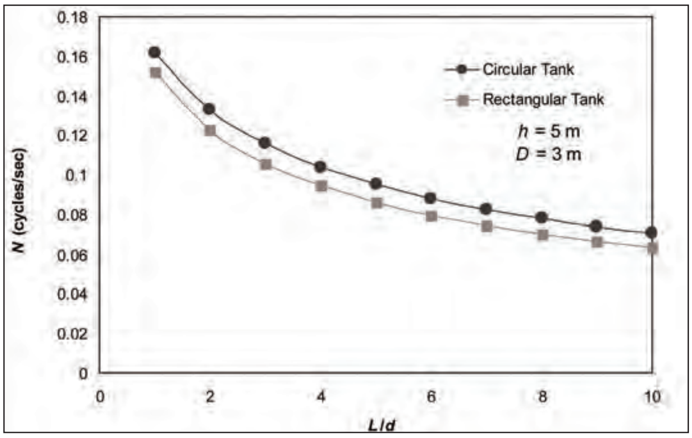

Figure 6: Variation of the frequency of oscillation (N) with the length-to-diameter ratio (L/d) of the connecting pipe when the depth of water (h) is 5 m and the diameter of each tank (D) is 3 m

Figure 6 shows the variation of the frequency of oscillation of water (*N*) with the length-to-diameter ratio (*L*/*d*) of the connecting pipe. The computations are performed assuming that the diameter of each tank (*D*) is 3 m and the depth of water (*h*) is 5 m. It is observed that the frequency of oscillation of water attains a high value (0.16 cycles/second) when the length-to-diameter ratio of the connecting pipe is equal to unity, and then gradually decreases as the length-to-diameter ratio increases. The frequency of oscillation is 0.08 cycles/second when *L/d* is 10. The frequencies of oscillation of water in the rectangular tanks are always found to be lower than those in the circular tanks. In the case of rectangular tanks, *N* is equal to 0.15 cycle/second when *L/d* is equal to 1 and *N* is equal to 0.07 cycle/second when *L/d* is equal to 10. It may be noted that Attwood *et al*. (1953) have provided a very useful table containing the rolling periods of different types of ships namely, battleship, fleet aircraft carrier, cruiser, destroyer and liner. Typical periods of rolling are found to vary from 7.5 seconds to 24 seconds. In other words, the frequency of rolling varies from 0.042 to 0.133 cycle/second. Thus the frequencies of oscillation

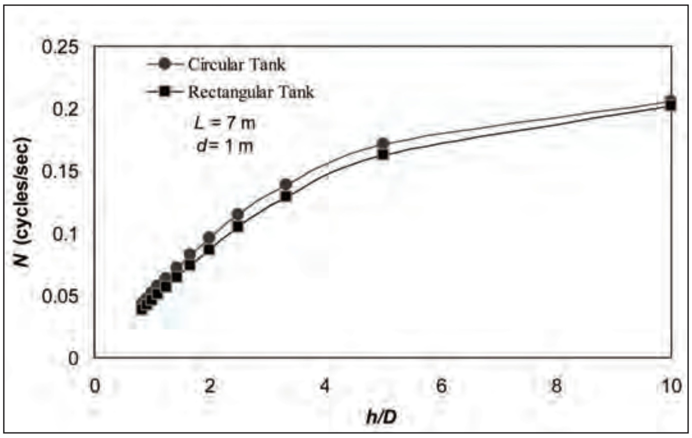

Figure 7: Variation of the frequency of oscillation (N) with the non-dimensional depth of water (h/D) in the tanks when the length of the connecting pipe (L) is 7 m and its diameter (d) is 1 m

of water obtained from the present theoretical analysis are found to be in complete agreement with the range of frequencies of rolling reported by Attwood *et al*.

Figure 7 shows the variation of the frequency of oscillation of water (N) with the non-dimensional depth of water (h/D) in the tanks. The computations are performed assuming that the length (L) and diameter (d) of the connecting pipe are 7 m and 1 m respectively. It is observed that the frequency of oscillation of water increases almost linearly with the increase of non-dimensional depth of water in the tanks. This observation on the variation of the frequency of oscillation of water holds good for both the circular and the rectangular tanks. However, the frequencies of oscillation of water in the circular tanks are always found to be higher than those in the rectangular tanks.

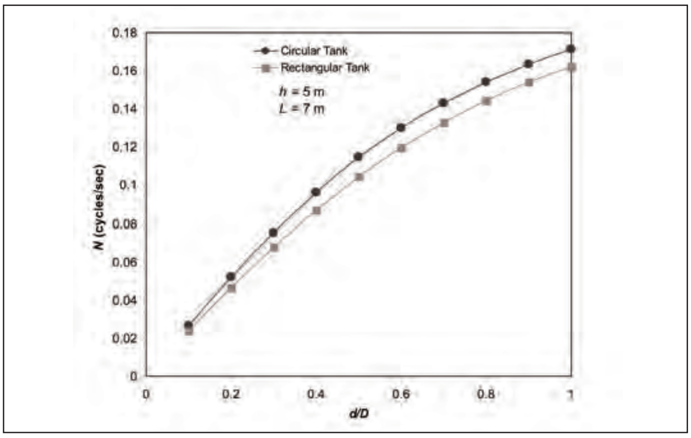

Figure 8: Variation of the frequency of oscillation (N) with the non-dimensional diameter (d/D) of the connecting pipe when the depth of water (h) is 5 m and length of the pipe (L) is 7 m

Figure 8 shows the variation of the frequency of oscillation of water (N) with the non-dimensional diameter (d/D) of the connecting pipe. The computations are performed assuming that the depth of water (h) is 5 m and the length of the connecting pipe (L) is 7 m. It is observed that the frequency of oscillation of water rapidly increases with the increase of non-dimensional diameter and attains the maximum value when $d/D = 1$. It is interesting to note that the maximum value of frequency of oscillation of water is obtained when the diameter of the connecting pipe is equal to that of the twin tank. This statement is equally true for both the circular and the rectangular tanks. However, the frequencies of oscillation of water in the circular tanks are always higher than those in the rectangular tanks.

Figure 9 shows the variation of the frequency of oscillation of water (N) with the non-dimensional length of the connecting pipe (L/D) when the depth of water (h) is 5 m and the diameter of the connecting pipe (d) is 1 m. It is observed that the frequency of oscillation of water decreases with increase in non-dimensional length of the connecting pipe. The variation is, however, not linear. The frequency of oscillation decreases rapidly up to $L/D = 6$ and after that the rate of reduction is quite low. The frequency curves for both the rectangular tanks and the circular tanks exhibit similar trend. However, it must be noted that the frequency of oscillation of water in circular tanks is always greater than that in rectangular tanks.

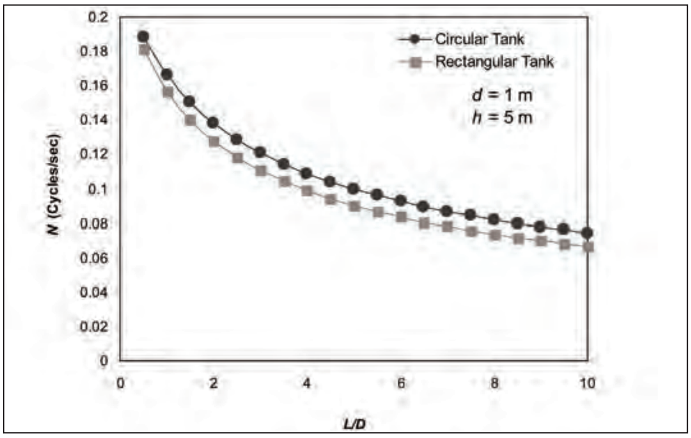

Figure 9: Variation of the frequency of oscillation (N) with the non-dimensional length of the connecting pipe (L/D) when the depth of water (h) is 5 m and the diameter of the connecting pipe (d) is 1 m

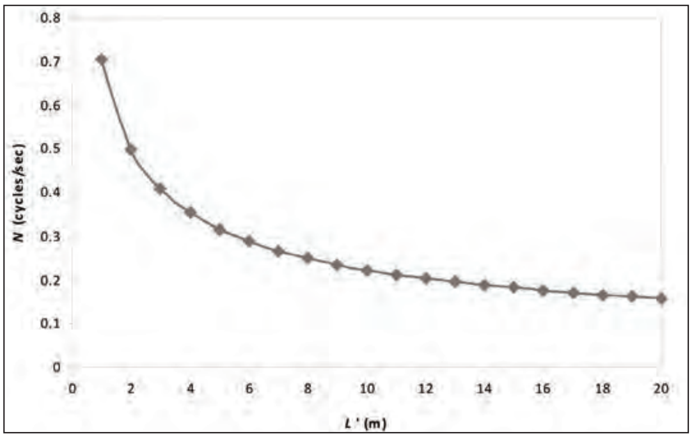

Figure 10: Variation of the frequency of oscillation (N) with the total length of water column (L') in the U-tank

Figure 10 shows the variation of frequency of oscillation of water (N) with the total length of the water column (L') in the U-tank. It is observed that the frequency of oscillation of water decreases at a sharp rate with the increase of the total length of the water column up to $L' = 15$ m. However, the frequency of oscillation does not remarkably change when the length of the water column exceeds 15 m.

Equation (40) provides the condition for the complete elimination of rolling motion of a ship. If the frequency of the anti-rolling tank (p_2) is made equal to the frequency of the wave force (ω), then a_1 becomes zero. Thus the rolling motion of the ship does not exist any more.

Figure 11 is plotted to show the relationship between the magnification factor of the anti-rolling tank ($\underline{a}_2$) and the mass ratio (μ) when the frequency of oscillation of the ship is equal to the frequency of the wave (exciting) force and the frequency of the anti-rolling tank. Actually, when the frequency of the wave (exciting) force equals the frequency of the ship, then resonance occurs. This is the worst case scenario and the main subject of interest. This figure shows the relationship between the magnification factor of the anti-rolling tank ($\underline{a}_2$) and the mass ratio (μ). From this figure it is evident that as μ increase, i.e., the mass of anti-rolling tank increases, $\underline{a}_2$ decreases. But a large mass overboard will reduce the stability. So, one must be careful in choosing an appropriate mass of anti-rolling tank.

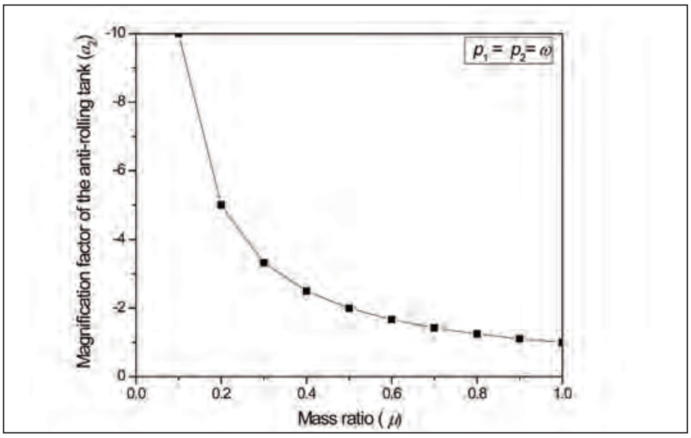

Figure 11: Relationship between the magnification factor of the anti-rolling tank ($\underline{a}_2$) and the mass ratio (μ)

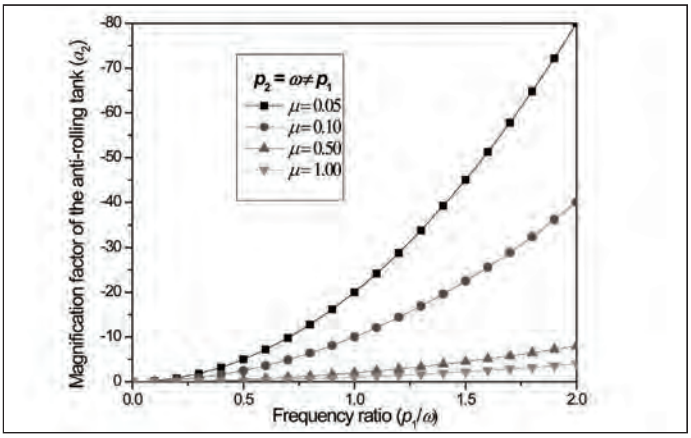

Figure 12: Relationship between the magnification factor of the anti-rolling tank ($\underline{a}_2$) and the frequency ratio (p_1/ω)

Figure 12 is plotted for the case when the frequency of the ship is not equal to the frequency of the exciting force and the frequency of the anti-rolling tank is tuned to that of the exciting force. It shows the relationship between the magnification factor of the anti-rolling tank ($\underline{a}_2$) and the frequency ratio (p_1/ω) for different values of the mass ratio (μ). For a given value of μ, $\underline{a}_2$ increases with the increase of p_1/ω. For a given system p_1 or ω can not be changed, so $\underline{a}_2$ can be controlled only by changing the mass ratio (μ).

NOMENCLATURE	
A	cross sectional area of the tank
a	cross sectional area of the connecting pipe
a_1	amplitude of oscillation of the ship
a_2	amplitude of oscillation of water in the U-tank
$\underline{a}_1$	magnification factor of the ship
$\underline{a}_2$	magnification factor of the U-tank
D	diameter of the circular tank
d	diameter of the pipe connecting the two tanks
F	restoring force
Fi	inertia force
g	acceleration due to gravity
h	depth of water in the tanks
k	spring constant
k_1	spring constant of the ship
k_2	spring constant of the U-tank system
L	length of the pipe connecting the two tanks
L'	total length of the water column in the U-tank
N	frequency of oscillation of water (cycles/sec)
m_1	mass of the ship
m_2	mass of the water in the U-tank
P	exciting force
p	frequency of oscillation of water (rad/sec)
p_1	frequency of oscillation of the ship
p_2	frequency of oscillation of water in the U-tank
T	kinetic energy
U	potential energy
x	coordinate measured along the horizontal axis
x_s	ratio of the exciting force to the spring constant of the ship
y	vertical displacement of the water level
Δ	reduction factor
μ	ratio of the mass of water in the U-tank to the mass of the ship (m_2/m_1)
ρ	mass density of water
ω	frequency of the exciting force

3.0 CONCLUSION

This paper presents an analytical study of the oscillation of water in two identical tanks connected by a narrow pipe. It also analyses how this fluid tank system can be used for reducing the rolling of a ship. The following conclusions can be drawn from the present work:

(a) Using the principle of conservation of energy, a detailed theoretical analysis is performed for the oscillation of water in two identical circular tanks connected by a narrow pipe. A new expression is derived for the frequency of oscillation of water as a function of the diameter of the circular tanks, the depth of water in the tanks, and the length and diameter of the connecting pipe. Subsequently, the expression for the frequency of oscillation water is modified for the case of two identical rectangular tanks.

(b) The frequency of oscillation of water in the circular tanks is always found to be higher than that in equivalent rectangular tanks. But the frequency curves exhibit similar trend for both circular and rectangular tanks.

(c) The frequency of oscillation of water decreases with increase in length-to-diameter ratio (L/d) of the connecting pipe.

(d) It is observed that the range of frequencies of oscillation of water is 0.08 cycle/second to 0.16 cycle/second for the circular tanks whereas the range is from 0.07 to 0.15 cycle/second for the rectangular tanks. The aforesaid range of frequencies is in complete agreement with the values of rolling frequency of ships presented by Attwood *et al*. (1953).

(e) The frequency of oscillation of water increases almost linearly with the increase in non-dimensional depth of water (h/D) in the tanks.

(f) The frequency of oscillation of water increases sharply with the increase of the non-dimensional diameter (d/D) of the connecting pipe. The twin tank system behaves like a U-tank when $d = D$.

(g) The frequency of oscillation of water decreases at a sharp rate with the increase of the total length water column (L') in the U-tank.

(h) If the frequency of the anti-rolling tank (p_2) is made equal to the frequency of the wave force (ω), the rolling motion of the ship is reduced to zero.

(i) The amplitude of oscillation of water in the anti-rolling tank a_2 can be controlled by changing the ratio of the mass of water in the tank to the mass of the ship (m_2/m_1).

(j) The present theoretical model is expected to be useful in the design of anti-rolling tanks which will effectively reduce rolling motions of a ship. ■

REFERENCES

[1] Attwood, E.L., Pengelly, H.S. and Sims, A.J. (1953), *Theoretical Naval Architecture*, William Clowes and Sons, Ltd, London, p. 343.

[2] Barr, R.A. and Aukudinov, V.K. (1977), Ship rolling, its prediction and reduction using roll stabilization, *Marine Technology,* Vol. 14, No. 1, pp. 19-41.

[3] Blagoveshchensky, S.N. (1962), *Theory of Ship Motions*, Vol. 2, Dover Publications, New York, pp. 509-513.

[4] Cox, G.G. and Lloyd, A.R. (1977), Hydrodynamic design basis for navy ship roll motion stabilization, *SNAME Transactions,* Vol. 85, pp. 51-93.

[5] Frahm, H. (1911), Results of trials of anti-rolling tanks at sea, *Transactions of the Institution of Naval Architects*, Vol. 53, pp. 183-201.

[6] Gawad, A.F.A., Ragab, S.A., Nayfeh, A.H. and Mook, D.T. (2001), Roll stabilization by anti-roll passive tanks, *Ocean Engineering*, Vol. 28, pp. 457-469.

[7] Holden, C., Perez, T. and Fossen, T.I. (2011), A Lagrangian approach to nonlinear modeling of anti-roll tanks, *Ocean Engineering*, Vol. 38, pp. 341-359.

[8] Honkanen, M.G. (1990), Heel and roll control by water tank, *The Naval Architect*, May 1990, pp. E215-E216.

[9] Hsueh, W.J. and Lee, Y.J. (1997), A design for ship stabilization by activated antiroll tanks, *Journal of Marine Science and Technology*, Vol. 2, pp. 77-86.

[10] Lee, B.S. and Vassalos, D. (1996), An investigation into the stabilization effects of anti-roll tanks with flow obstructions, *International Shipbuilding Progress*, Vol. 43, No. 433, pp. 70-88.

[11] Marzouk, O.A. and Nayfeh, A.H. (2009), Control of ship roll using passive and active anti-roll tanks, *Ocean Engineering,* Vol. 36, pp. 661-671.

[12] Moaleji, R. and Greig, A.R. (2007), On the development of ship anti-roll tanks, *Ocean Engineering*, Vol. 34, Issue 1, pp. 103-121.

[13] Okada, S. and Takagi, M. (1965), Dynamical stability of the ships equipped with an anti-rolling tank, *Journal of Zosen Kiokai,* Vol. 117, pp. 85-92.

[14] Takaishi, Y. (1971), A model experiment on the effect of an anti-rolling tank of ship in oblique seas, *Journal of Kansai Society of Naval Architects,* Japan, pp. 158-179.

[15] Tanizawa, K., Taguchi, H. and Sawada, H. (2003), Application of NWT to the design of ART, *Proceedings of The Thirteenth International Offshore and Polar Engineering Conference,* Honolulu, Hawaii, USA, May 25-30, 2003, pp. 307-314.

[16] Treakle, T.W. (1998), *A Time-Domain Numerical Study of Passive and Active Anti-Roll Tanks to Reduce Ship Motions,* Master Thesis, Virginia Polytechnic Institute and State University, USA.

[17] Umeda, N., Hashimoto, H., Minegaki, S. and Matsuda, A (2008), An investigation of different methods for the prevention of parametric rolling, *Journal of Marine Technology Society,* Vol. 13, pp. 16-23.

[18] Vasta, J., Giddings, A.J., Taplin, A. and Stillwell, J. (1961), Roll stabilization by means of passive tanks, *SNAME Transactions,* Vol. 69, pp. 411-460.

[19] Walton, T. and Baxter, B. (1970), *Know Your Own Ship,* Twenty-eighth Edition, Charles Griffin & Company Limited, London, pp. 269-271.

[20] Watanabe, Y. (1930), On the design of anti-rolling tank, *Journal of Society of Naval Architects of Japan*, Vol. 46, pp. 125-153.

[21] Watanabe, S., Sakao, M., Komaru, S., Yamanouchi, Y. and Ando, S. (1966), An experimental study on anti-rolling tanks, *Journal of Kansai Society of Naval Architects*, Japan, Vol. 120, pp. 27-33.

[22] Webster, W.C. (1967), Analysis of the control of activated anti-roll tanks, *SNAME Transactions*, Vol. 74, pp. 296-331.

[23] Webster, W.C., Dalzell, J.F. and Barr, R.A. (1988), Prediction and measurement of the performance of free-flooding ship anti-rolling tanks, *SNAME Transactions*, Vol. 96, pp. 333-364.

[24] Winden, B. (2009), *Anti Roll Tanks in Pure Car and Truck Carriers*, Master Thesis, KTH Centre for Naval Architecture, Stockholm, Sweden.

[25] Yamaguchi, S. and Shinkai, A. (1992), Characteristic analysis of anti-rolling tanks by using a numerical simulation on the basis of the finite difference method, *Transactions of the West Japan Society of Naval Architects*, No. 84, pp. 153-162.

PROFILES

PROFESSOR GAZI MD. KHALIL has been serving as a teacher in the Department of Naval Architecture and Marine Engineering, Bangladesh University of Engineering and Technology, Dhaka since April 1973. He served as the Head of the same department for a period of eight years. Dr. Khalil received a fellowship of The Matsumae International Foundation, Japan and carried out post-doctoral research in the Department of Naval Architecture, University of Tokyo in 1987. He specialized in Wave Forces on Offshore Structures. He published more than 100 research papers in various national and international journals and proceedings of conferences.

DR MD. SHAHJADA TARAFDER is now working as a Professor in the Department of Naval Architecture and Marine Engineering of Bangladesh University of Engineering and Technology, Dhaka. Dr. Tarafder obtained the Degree of B. Sc. Engg. in 1994 and M. Sc. Engg. in 1996 from the same university. He obtained the Degree of Doctor of Engineering from Yokohama National University, Japan in 2002.

DR MD. SHAHIDUL ISLAM is now working as an Associate Professor in the Department of Naval Architecture and Marine Engineering of Bangladesh University of Engineering and Technology, Dhaka. He obtained his Doctor of Engineering degree from Yokohama National University in December 2005. His research interest includes mesh generation, finite element analysis, ship structures etc. and has published a number of papers in various national and international journals and proceedings of the conferences.

FREQUENCY ANALYSIS OF ANNUAL RUNOFF IN PENINSULAR MALAYSIA USING A REGIONAL APPROACH BASED ON L-MOMENTS

(Date received: 10.05.12/Date accepted: 22.12.12)

Aminuddin Mohd. Baki[1], Ismail Atan[2] and Nora Farina Mohd. Halim[3]

Faculty of Civil Engineering, Universiti Teknologi MARA (UiTM)
40450 Shah Alam, Selangor, Malaysia.
E-mail: [1]amin_ba_ki@yahoo.co.uk, [2]ismailatan585@gmail.com, [3]norafarina@ymail.com

ABSTRACT

Estimation of runoff is very important for flood estimation. Thus, runoff is very important in designing and managing water resources projects involving natural hazards. Region refers to a set of sites of which is expected to have data drawn in a synonymous frequency distribution. In this study, a regional frequency analysis of annual runoff in Peninsular Malaysia has been conducted and was based on the theory of L-Moments as developed by Hosking and Wallis [1] is a very reliable method for assessing exceedance probabilities of extreme environmental events when data is available from more than one site. The General Logistics (GLO) and Generalized Extreme Value (GEV) were found to be suitable for the region in peninsular Malaysia [2]. The best fit distributions of annual runoff in Malaysia are determined based on L-moment ratio diagram and statistical tests. Numerical analysis was performed on some stations in every state in Peninsular Malaysia. Thus, the analysis performed are using data from homogeneous regions established using L-moments procedure. From the analysis, probability plots and comparison between at site and regional estimation shows that most of the station are almost the same and lies on the 45^o lines meaning that the site are fitted distribution.

Keywords: *Homogeneous, L-Moment, Regionalisation, Regional Frequency Analysis*

1.0 INTRODUCTION

Flooding occurs when a watercourse is unable to convey the quantity of runoff flowing downstream. The frequency with which this occurs is described by a return period. Regionalization is the procedure to find natural groups of watersheds with homogeneous hydrologic response, and finds applications in hydrologic design, planning and management of water resources systems [3]. The regional frequency analysis is widely used in flood analysis. The approach based on the theory of L-moments was developed by Hosking and Wallis [1] is a very reliable method for assessing exceedance probabilities of extreme environmental events when data is available from more than one site. The method of L-moments is analogous to the method of ordinary moments. The main advantage of L-moments is that, being a linear combination of data, they are less influenced by outliers.

In recent years, researchers either hydrologist or engineer used different procedures because of the different parameters used and resulting to the different results. The reliability of the estimate are largely depends on the quality and the length of the hydrological records used in the analysis. The accuracy is the parameter that most design engineer had problem in analyses that can cause errors in estimation of hydrological parameters. Frequency analysis method using data from single site will limit the prediction value and lead to a large sampling errors [4].

This paper contains the application of the methodology proposed by Hosking and Wallis [1] for the estimation of the annual runoff distribution in any Malaysian rivers by using hydrometric and climatic data of Malaysian gauged stations. The objectives of this study are to identify the homogeneous region and to compare between regional estimation and at-site estimation analysis.

2.0 METHODOLOGY IN REGIONAL FREQUENCY ANALYSIS BY USING L-MOMENTS

2.1 L-Moment Definition and Terminology

L-moments are statistics used to summarize the shape of a probability distribution and also define as linear combination of Probability Weighted Moments (PWMs) [5]. They are analogous to conventional moments in that they are used to calculate quantities analogous to the mean, standard deviation, skewness and kurtosis of data. In the L-moment field these terms are called L-mean, L-scale, L-skewness and L-kurtosis to distinguish them from the conventional moments and standardized moments. Standardized L-moments are called L-moment ratios [6].

For a random variable X, the first four population L-moments are [7]:

$$\lambda 1 = EX$$
$$\lambda 2 = (EX2{:}2 - EX1{:}2) / 2$$
$$\lambda 3 = (EX3{:}3 - 2EX2{:}3 + EX1{:}3) / 3$$
$$\lambda 4 = (EX4{:}4 - 3EX3{:}4 + 3EX2{:}4 - EX1{:}4) / 4, \qquad (1)$$

where Xk:n denotes the kth largest value in an independent sample of size n from the distribution of X.

The first two of these L-moments have conventional names:
$\lambda 1$ = mean, L-mean or L-location,
$\lambda 2$ = L-scale.

A quantity similar to the coefficient of variation, but based on L-moments is τ defined by

$$\tau = \frac{\lambda_2}{\lambda_1} \tag{2}$$

which is called the "coefficient of L-variation", or "L-CV".

A set of higher order scaled L-moments, or L-moment ratios, is defined by

$$\tau_r = \frac{\lambda_r}{\lambda_2}, \qquad r = 3, 4, \ldots \tag{3}$$

and conventional names for the third and fourth order L-moment ratios (r =3, 4) are
$\tau 3$ = L-skewness,
$\tau 4$ = L-kurtosis.

2.2 L-Moments Ratio Diagram (LMRD)

L-Moments ratio diagram is a graphical analysis of distribution fitting where several distributions can be compared in a single diagram. Theoretical relationship between $\tau 3$ and $\tau 4$ have been derived for various distribution [8]. The selection of a suitable parametric distribution to describe the data from several sites can be based on the proximity of the mean value of $\tau 3$ and $\tau 4$ for the region to a theoretical line or point as well as on the variability of the mean values.

2.3 Index Flood Method

The *T*-year event *XT* defined as the event of exceeded on average once every *T* years [9] is given as:

$$P[X > XT] = 1/T \tag{4}$$

The parameters of regional frequency distribution can b estimated using L-moment together with regional average sample L-moments ratios. Then, the *T*-year event at site *i* can be estimated as

$$XT,i = ui\ ZT \tag{5}$$

Where *ui* is the mean annual flood (MAF) at site *i*, and *ZT* is the regional growth curve.

2.4 Regional Frequency Analysis

There are five steps of the regional frequency analysis methodology which :

i. Screening of the data
ii. Identification of the homogeneous region
iii. Choose frequency distribution
iv. Estimation of the chosen parameters
v. Compute quintile estimation

Since these procedures are presented in detail by Hosking and Wallis [3], only a summary is reported below.

i. Screening of data

Test the gross outliers, inconsistencies, shifts, and trends [10]. Then, discordance measure is used to identify sites from the group of a given sites that are grossly discordance with the group as whole. The discordance measure is single statistics based on difference between L-Moment ratios of the site and the average L-Moment ratio of the group of same sites. These statistics can also be used to identify erroneous data.

ii. Identifying homogeneous regions

Assign the sites to region. Region defined as a set of sites in which the frequency distributions are considered to be appropriately similar. Region is the fundamental unit of the regional frequency analysis. The sites can be divided into region within the homogeneity criteria. It is exactly certified approximate homogeneity is sufficient enough to ensure that the regional frequency analysis is much more accurate compare to at site analysis.

iii. Choose the Frequency distribution

Single frequency distribution is fitted to the data from several sites of homogeneous region in regional frequency analysis. A distribution must be chosen which provides a good fit to the data because the true distribution of the runoff is not known. The parameter distributions that can be used to consider the quintile estimation in this study are Generalized Extreme Value (GEV), the Lognormal, Logistic, and Pearson Type 3. To help in selection of the appropriate distribution, Z-statistic was used. The Z-statistic is a goodness-of-fit measure for those parameter distributions that measures how good the theoretical L-Kurtosis of fitted distribution matched the regional average of the observed data.

iv. Parameter estimation

L-Moment algorithm is used to estimate the chosen distribution parameters and obtain the quintile estimate. It involves fitting the chosen distribution using L-Moment method of the distribution to the sample L-Moment derived from the observed data. Furthermore, the sample of L-Moment ratios from each site in the homogeneous region is weighted according to the length and combined to give regional average L-Moment ratios. Then, the regional mean is set and regional quintile estimates are derived.

v. Compute quintile estimates

To obtain the runoff estimation at ungauged sites, the regional quintile estimates derived from data at gauged sites within the region are interpolated to all ungauged sites in that particular region.

2.5 Discordancy Measures

This measure is used to identify site that are outliers with the group as a whole. If a single site does not appear to belong to the cloud of $\tau 3$ and $\tau 4$ points on the L- Moment diagram, a test of discordancy based on L- Moments can be used to determine whether it should be removed from the region. The test of discordancy is applied by calculating the D-statistics, defined terms of L-Moments.

$$Di = \frac{1}{3} N (ui - \bar{u})^{T} K^{-1} (ui - \bar{u}) \quad (6)$$

where ui = vector of L-moment ratios for station i,

K = covariance matrix of ui,
$\bar{u}$ = mean of vector ui.

The station i is declared to be discordant, if Di is greater than the critical value of the discordancy statistic given in a tabular form by [6].

2.6 Identification of Homogeneous Region using Heterogeneity Measure

Heterogeneity measure, H compares the inter-site variations in sample L-moments for the group of sites with what would be expected of a homogeneous region. The L-moment tests for heterogeneity fit a four-parameter Kappa distribution [11] to the regional data set, generate a series of 500 equivalent region's data by numerical simulation and compare the variability of the statistics of the actual region to those of the simulated series [1]. The inter-site variation of each generated region is computed and the mean and standard deviation of the computed inter-site variation is determined. Hence, heterogeneity measure is obtained as:

$$H = \frac{(V - \mu v)}{\sigma v} \quad (7)$$

where, V = weighted standard deviation of L-coefficient of variation values,
μV, σV = the mean and standard deviation of number of simulations of V.

The criteria for deciding heterogeneity of a region is as:
$H < 1$, region is acceptably homogeneous,

$1 \leq H < 2$, region is possibly heterogeneous,

$H \geq 2$, region is definitely heterogeneous.

2.7 Computer Programs for Method of L-Moments

All of the processes have been programmed by [12] (lmoments: version 3.04) based on FORTRAN-77. The FORTRAN-77 routines and subroutines are combined under a program which has been compiled and adapted into an executable form in this study [13].

3.0 STUDY AREA, AVAILABILITY AND ACQUISITION OF DATA

This study involves data acquisition and numerical modeling. The data acquisition involves acquiring the annual runoff data of selected location all over Malaysia from Department of Irrigation And Drainage, Ampang. Numerical modeling involved analyzing the annual runoff data to find the L-Skewness and L-Kurtosis from different sites of annual runoff data which has historical data for 20 years and above. The study area was divided into three homogeneous region which is southern, east coast and west coast region of peninsular Malaysia as shown in Figure 1. Figure 2 shows the flow of work done in order to construct the Regional Frequency Analysis of flow. The amounts of stations with homogenous data were 38 stations. Six (6) stations employed in REGION I (SOUTH), twenty three (23) stations employed in REGION II (WEST) and nine (9) stations employed in REGION III (EAST). Table 1 show the total sites and data involved in each state while Table 2 to Table 4 shows the Summary of selected Automatic Runoff Stations of R1, R2 and R3 of Peninsular Malaysia.

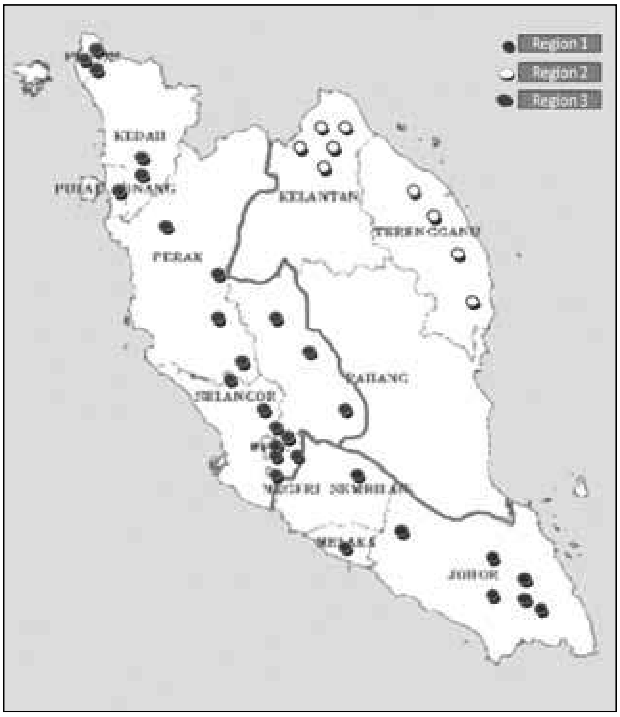

Figure 1: Selected hydrological gauge stations

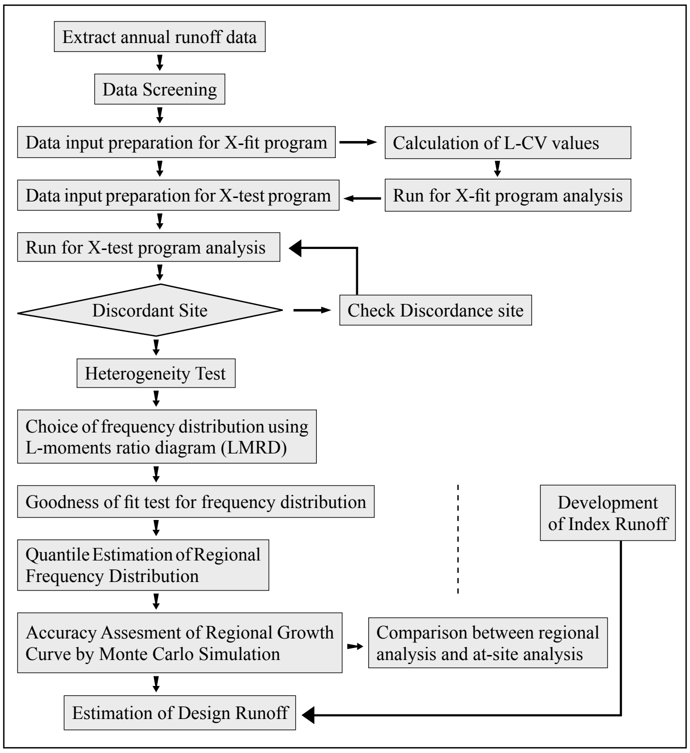

Figure 2: Constructing the Regional Flood Frequency Analysis for runoff

Table 2: Summary of selected Automatic Runoff Stations of R1 of Peninsular Malaysia

No.	Station Id.	Station Name	No. of years in Analysis
1	2527411	Muar at Buloh Kasap, Johor	44
2	2235401	Sg. Kahang at Bt.26 Jln Kluang	32
3	1931423	Sg. Sembrong at Bt.2 Air Hitam,Yong Peng	30
4	1836402	Sg. Sayong at JAM, Johor Tenggara	33
5	2322413	Sg. Melaka at Pantai Belimbing	50
6	3022431	Sg. Triang at Juntai, Negeri Sembilan	45

Region 1 (R1) – Johor, Melaka, and Negeri Sembilan (Southern of peninsular)

Table 3: Summary of selected Automatic Runoff Stations of R2 of Peninsular Malaysia

No.	Station Id.	Station Name	No. of years in Analysis
1	6502401	Sg. Jerneh at Titi Tampang, Perlis	27
2	6502432	Sg. Tasoh at Titi Baru, Perlis	20
3	6503401	Sg. Arau at Ldg. Tebu Felda, Perlis	27
4	5806414	Sg. Muda at Jeniang, Kedah	47
5	5405421	Sg. Kulim at Ara Uda, Pulau Pinang	47
6	5505412	Sg. Muda at Ldg.Victoria, Pulau Pinang	50
7	3913458	Sg. Sungkai at Sungkai, Perak	49
8	4212467	Sg. Cenderiang at Bt.32 Jln Tapah	38
9	4310401	Sg. Kinta at Weir G, Tg. Tualang	34
10	4611463	Sg. Kinta at Tg. Rambutan, Perak	49
11	5106433	Sg. Ijok at Titi Ijok, Perak	45
12	2816441	Sg. Langat at Dengkil, Selangor	50
13	2918401	Sg. Semenyih at Kg. Rinching, Selangor	36
14	2918443	Sg. Semenyih at Semenyih, Selangor	14
15	3615412	Sg. Bernam at Tanjung Malim, Selangor	50
16	3813411	Sg. Bernam at JAM.SKC, Selangor	49
17	3118445	Sg. Lui at Kg. Lui, Selangor	45
18	3116430	Sg. Klang at JAM. Sulaiman	37
19	3116432	Sg. Klang at Leboh Pasar, K. Lumpur	14
20	3116433	Gombak at Jln. Tun Razak	49
21	3519426	Sg. Bentong at JAM. Kuala Marong	41
22	4019462	Sg. Lipis at Benta, Pahang	45
23	4218416	Sg. Jelai at Kuala Medang, Pahang	29

Region 2 (R2) – Perlis, Kedah, Pulau Pinang, Perak, Selangor, Wilayah Persekutuan Kuala Lumpur and Pahang (West coast)

Table 4: Summary of selected Automatic Runoff Stations of R3 of Peninsular Malaysia

No.	Station Id.	Station Name	No. of years in Analysis
1	5621401	Sg. Sokor at Kg. Tegawan, Kelantan	15
2	5721442	Sg. Kelantan at JAM. Guillemard, Kelantan	50
3	5818401	Sg. Golok at Kg. Jenob, Kelantan	27
4	6019411	Sg. Golok at Rantau Panjang	45
5	6022421	Sg. Kemasin at Peringat, Kelantan	29
6	4232452	Sg. Kemaman at Rantau Panjang, Terengganu	35
7	5130432	Sg. Terengganu at G.Tanggol, Terengganu	49
8	5229436	Sg. Nerus at Kg. Bukit, Terengganu	29
9	5428401	Sg. Chalok at JAM. Chalok, Terengganu	32

Region 3 (R3) – Kelantan, Terengganu and Pahang (East coast)

4.0 RESULT AND DISCUSSION

The weighted mean of L-Skewness and L-Kurtosis were plotted into the L- Moment Ratios Diagram. This result was obtained by running the X-Test and X-Fit Program using FORTRAN Software.

Based on Figures 2 and 3, it can be summarized that Generalized Logistic Distribution (GLO) is the best distribution for regional frequency analysis for Regions 1 and 2. Figure 4 show that Generalized Extreme Value (GEV) is the best distribution for Region 3. The Goodness of fit Test (Z^{DIST}) should be less than or equal to 1.64 but if the value exceeded 1.64 the distribution with value Z^{DIST} close to it will be selected as a parent distribution. From Table 1, it is shown that for Region 1 and 2 represented by GLO distribution and for Region 3 represented by GEV distribution.

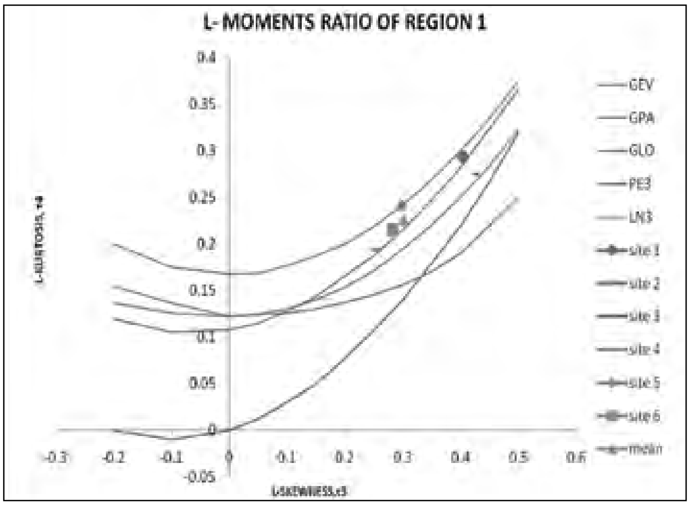

Figure 2: L-Moment Ratio Diagram of Region 1

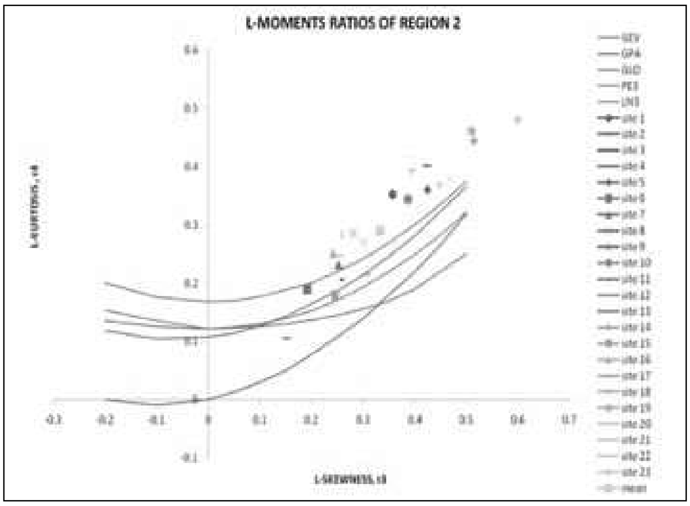

Figure 3: L-Moment Ratio Diagram of Region 2

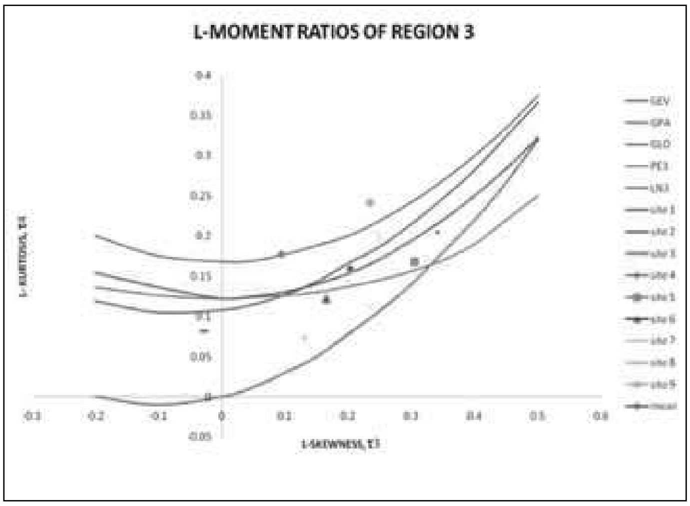

Figure 4: L-Moment Ratio Diagram of Region 3

Table 5: Goodness of fit Test (Z^{DIST})

Z^{DIST}	R1	R2	R3
Generalized Logistic	0.11[a]	-3.63[a]	1.66
Generalized Extreme Value	-0.59[b]	-4.66[b]	0.08[a]
Lognormal	-1.15[c]	-5.77[c]	-0.30[b]
Pearson Type III	-.2.11[d]	-7.65[d]	-1.09[c]
Generalized Pareto	-2.48	-7.66	-3.54[d]

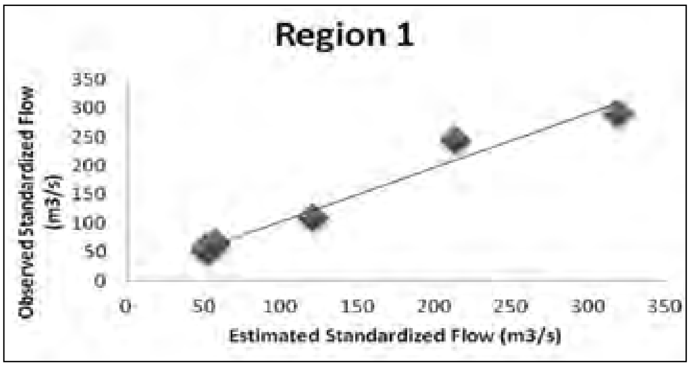

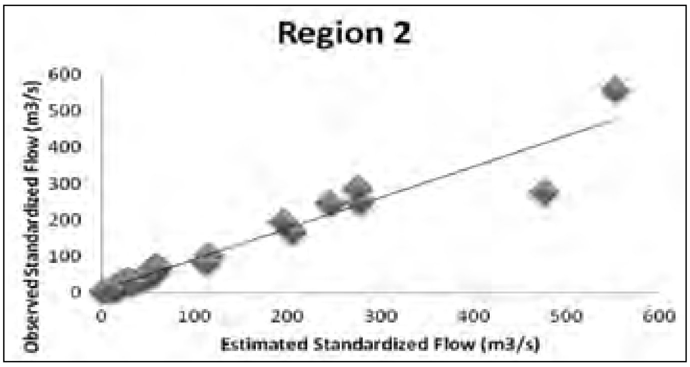

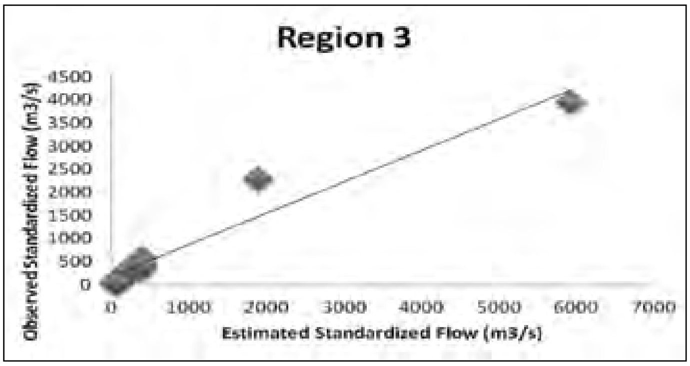

Figure 5: Comparison with regional and at-site analysis

5.0 CONCLUSION

In this study, the regionalisation frequency analysis is based on the Index flood approach. The index flood was replaced by the index runoff consist of two major parts which is the establishment of the regional growth curves or frequency curves and the estimation of the value of index runoff. This study focused on identifying the homogeneous region. The result presented in this study based on Goodness of Fit Test and the Probability plots indicates that the Generalized Logistic (GLO) and Generalized Extreme Value (GEV) distribution were found to be the most suitable distribution in Peninsular Malaysia.

The advantages of using regional frequency analysis approach are evident in many studies that have been done before [14];[15] and [16]. The regional L-Moment algorithm has been successfully implemented in most of the studies on frequency analysis. It is because by using L-Moment, it generally reduces sampling error. This approach reduces at site estimates errors. It can also be used to generate runoff information at an ungauged site.

6.0 ACKNOWLEDGEMENT

This study was carried out as a requirement for the degree of Master of Science in Civil Engineering Universiti Teknologi Mara (UiTM). The funding provided by the Research Management Institute Universiti Teknologi Mara [Dana Kecemerlangan, 600-IRDC/ST/DANA 5/3/Dst (20/2010)] and the organisations providing data to the project which is Department of Irrigation and Drainage (DID) Ampang are thanked. The authors wish to thank to all family and friends who help to done this research directly or indirectly. Contributions from all relevant parties involved in the study are gratefully acknowledged. ■

REFERENCES

[1] J.R.M. Hosking, and, J. R Wallis, Regional frequency analysis : an approach based on L-Moments, *Cambridge University Press*, Cambridge, U.K, 1997.

[2] N.F. Mohd. Halim, A. Baki, and I Atan, "Regionalisation Frequency Analysis of Annual Runoff in Malaysia", *Proceeding of Malaysian Science and Technology Congress* (MSTC 2010), Petaling Jaya, Malaysia, 9-11 November 2010.

[3] Abdullah A. Maimun, Alias Hashim and Jamal I. Daoud, "Regionalisation of low flow frequency curves for the Peninsular Malaysia", *Journal of Hydrology*, 381, pp 174-180, 2010.

[4] M.Z.M. Amin, "Regional flood frequency analysis in the East Coast of Peninsular Malaysia by L-moments approach", M.S thesis (unpublished), National University of Ireland, Galway, 2000.

[5] J.A. Greenwood, J.M. Landwehr, N.C. Matalas , and J.R. Wallis, "Probability weighted moments: Definition and relation to parameters of several distributions expressable in inverse form," *Water Resources Research*, 15(5), 1049, pp 81-105, 1979.

[6] J.R.M. Hosking and J.R. Wallis, "Some statistics useful in regional frequency analysis", *Water Resource Research*, 29(2), pp 271-281, 1993.

[7] J.R.M. Hosking, "The theory of probability weighted moments," *IBM Research*, Yorktown Heights, New York, IBM Research Report. RC 12210, 1986.

[8] J.R.M. Hosking, "L-moments: analysis and estimation of distribution using linear combinations of order statistics", *Journal of the Royal Statistical Society*, B,52(1), pp 105-124, 1990.

[9] Stedinger, J.R., Vogel, R.M., Foufoula-Georgiou, E., Frequency analysis of extreme events. *Handbook of Hydrology*. McGraw-Hill, New York, 1993.

[10] J.R. Wallis, D.P. Lettenmaier and E.F. Wood, "A daily hydroclimatological data set for continental United States," *Water Resources Research*, 27, 1657-63,1991.

[11] J.R.M. Hosking, "The four-parameter kappa distribution", *IBM Journal of Research and Development*, 38, 251-8, 1994.

[12] J.R.M. Hosking, "Fortran routines for use with the method of L-moments, Version 3.04". *Research Report* RC 20525, IBM Research Division, T.C. Watson Research Center, Yorktown Heights, N.Y, 2005.

[13] Basic Fortran Concepts. What is Fortran?, http://programming.ccp14.ac.uk/fortranresources/~cgp/prof77/node2. html, 2001

[14] R.M. Vogel, W.O. Thomas, and T.A. McMahon, "Flood-flow frequency model selection in southwestern United States". *Journal of Water Resources Planning and Management* 119 (3), pp 353-366, 1993.

[15] H. Madsen, C.P. Pearson, and D. Rosbjerg, *Comparison of annual maximum series and partial duration series method for modelling extreme hydrologic events* 2. Regional modelling Water Resources Research 33 (4), pp 759-769, 1997.

[16] S. Mkhandi and S. Kachroo, "Regional flood frequency analysis for southern Africa", *Southern African FRIEND, Technical Documents in Hydrology No. 15 UNESCO*, Paris, France, 1997.

PROFILES

ASSOC. PROF. IR. DR AMINUDDIN MOHD. BAKI currently is the Head Centre of Study Water Resource and Environmental System (WRES) Faculty of Civil Engineering, Universiti Teknologi MARA Shah Alam. His areas of expertise are Wastewater Engineering and Hydrology. He has involved in many Profesional Organization for example Member of MWA, WEF, IWA, ISRM, ISSMGE, MyWP, PHEAM, ASI, and MIM.

ASSOC. PROF. DR ISMAIL ATAN received his Msc (Engineering math) in 1990 and his Phd also in Engineering Math in 1998 both in the United Kingdom. He is now a senior lecturer in Faculty of Civil Engineering, Universiti Teknologi MARA Shah Alam. His areas of expertise is on Stochastic Hydrology.

NORA FARINA MOHD. HALIM currently is a Postgraduate Student in Faculty of Civil Engineering, Universiti Teknologi MARA Shah Alam. Area of interest is in Water Resource Engineering.

The Institution of Engineers, Malaysia

Bangunan Ingenieur, Lots 60/62, Jalan 52/4, Peti Surat 223 (Jalan Sultan), 46720 Petaling Jaya, Selangor Darul Ehsan
Tel : 03-79684001/2 **Fax :** 03-79577678 **E-mail** : sec@iem.org.my **IEM Homepage :** http://www.myiem.org.my

REFEREES FOR VETTING OF IEM PUBLICATIONS 2012/2013

The Standing Committee on Information and Publications is in the midst of compiling and updating the list of referees to assist in the vetting of articles received from members and non-members. The referees should preferably be at least Corporate Members of The Institution or graduates with higher degrees or with academics background.

The aim of appointing the referee is to ensure and maintain standard in the publication of the IEM quarterly Journal.

Members who are interested to be placed in the ***database of referees*** are to return the registration form to the IEM Secretariat, providing details of their degrees and particular expertise and experience in the engineering fields.

We need your generous services to look into the vetting and improving the IEM Journal articles received for Publications. An acknowledgement would be made at the end of the Sessions in either the Bulletin and Journal. Referees must be committed to return the papers within two weeks or a month from date of appointment made.

Thank you.

Principal Journal Editor
Standing Committee on Information and Publications

All submissions and correspondences are to be addressed to: -

JOURNAL EDITORIAL BOARD
Standing Committee on Information and Publications
The Institution of Engineers, Malaysia
Bangunan Ingenieur, Lots 60 & 62, Jalan 52/4
P.O. Box 223 (Jalan Sultan)
46720 Petaling Jaya, Selangor Darul Ehsan
Tel: 603-7968 4001/2 **Fax:** 603-7957 7678
E-mail: pub@iem.org.my/sec@iem.org.my
Website: http://www.myiem.org.my

DISCIPLINES / SUB-DISCIPLINES OF VETTER

Please tick (✓) the appropriate boxes.

- ❑ Agricultural
- ❑ Aerospace
- ❑ Aeronautical
- ❑ Chemical
- ❑ Civil
- ❑ Communication
- ❑ Electrical
- ❑ Electronics
- ❑ Environmental
- ❑ Industrial
- ❑ Manufacturing
- ❑ Marine
- ❑ Mechanical
- ❑ Mining
- ❑ Naval Architecture
- ❑ Petroleum
- ❑ Production
- ❑ Structural
- ❑ Others (*Please specify*) ____________________

AREAS OF INTEREST FOR VETTING OF PAPERS

Please tick (✓) the appropriate area of interest that you are able to vet the papers

- ❑ Acoustics
- ❑ Aerodynamics
- ❑ Air Conditioning
- ❑ Air Pollution Control
- ❑ Aircraft
- ❑ Airport Engineering
- ❑ Aluminum Design
- ❑ Arbitration
- ❑ Automation
- ❑ Automotive Engineering
- ❑ Biochemical Engineering
- ❑ Biotechnology
- ❑ Boiler Engineering
- ❑ Bridge Engineering
- ❑ Building Services
- ❑ Coastal Engineering
- ❑ Co-Generation
- ❑ Computer Engineering
- ❑ Concrete Design
- ❑ Concrete Technology
- ❑ Construction Management
- ❑ Control Engineering
- ❑ Drainage Engineering
- ❑ Dynamics Design
- ❑ Earthworks
- ❑ Edible Oil Refining
- ❑ Electrical Transmission
- ❑ Electrochemical
- ❑ Electrotechnology
- ❑ Energy Technology
- ❑ Engineering Education
- ❑ Environmental Engineering
- ❑ Fine Chemical
- ❑ Finite Element
- ❑ Fire Detection
- ❑ Fire Engineering
- ❑ Floods
- ❑ Food Processing
- ❑ Foundation Engineering
- ❑ Fuzzy Logic
- ❑ Gas Engineering
- ❑ Geotechnical
- ❑ Heat Exchanger
- ❑ Highway
- ❑ Hydraulics
- ❑ H.V. Electrical Distribution
- ❑ Industrial Engineering
- ❑ Industrial Transport
- ❑ Industrial Ventilation
- ❑ Information Technology
- ❑ Instrumentation
- ❑ Lighting System
- ❑ L.V. Electrical Distribution
- ❑ Management
- ❑ Mass Transit
- ❑ Manufacturing
- ❑ Mechanical Handling Equipment
- ❑ Metal Fabrication
- ❑ Metallurgy
- ❑ Micro Electronics
- ❑ Military Vehicles
- ❑ Mini Pressure Meters
- ❑ Mining Engineering
- ❑ Naval Architecture
- ❑ Navigation
- ❑ Oil and Gas Engineering
- ❑ Operation Research
- ❑ Palm Oil Industries
- ❑ Petrochemicals
- ❑ Petroleum Engineering
- ❑ Pharmaceuticals
- ❑ Piling
- ❑ Plumbing Engineering
- ❑ Pollution Control
- ❑ Ports and Harbor Engineering
- ❑ Power Electronics
- ❑ Power Generation
- ❑ Pressure Vessels
- ❑ Prestressed Concrete
- ❑ Project Management
- ❑ Public Administration
- ❑ Public Health Engineering
- ❑ Quarry Engineering
- ❑ Railways
- ❑ Reclamation Works
- ❑ Refrigeration
- ❑ Reinforced Concrete Beams
- ❑ Road Transport
- ❑ Robotics
- ❑ Roof Structures
- ❑ Room Temperature
- ❑ Safety Engineering
- ❑ Scaffolding Works
- ❑ Seepage
- ❑ Sewerage
- ❑ Shipbuilding
- ❑ Signal Processing
- ❑ Solar Energy Technology
- ❑ Steelworks Design
- ❑ Stream Turbine Power Plant
- ❑ Structural Analysis
- ❑ Structural Rehabilitation
- ❑ Survey Engineering
- ❑ Tailgates
- ❑ Telecommunication
- ❑ Thermal Engineering
- ❑ Timber Design
- ❑ Tool Engineering
- ❑ Transfer Tunnels
- ❑ Transportation Engineering
- ❑ Urban Planning
- ❑ Vehicles
- ❑ Vertical Transportation
- ❑ Waste Treatment
- ❑ Waste Water
- ❑ Water Resources Engineering
- ❑ Water Pollution Control
- ❑ Wind Engineering
- ❑ Others (*please specify*) ____________________

RESEARCHER / REVIEWERS DETAILS

Name : ______________________________

Membership No. : ______________ (*if applicable*)

Grade :
❑ **Graduate** ❑ **Member** ❑ **Fellow** ❑ **Affiliate**
❑ **Non-member** ❑ **Others (*please specify*)**
____
____

Qualifications : ______________________________

Addresses
(*Office*) : ______________________________
____
____
____

(*Residence*) : ______________________________
____
____
____

Contact No.
Handphone : ______________ **Office** : ______________ **Residence** : ______________

E-mail Address : ______________________________

Please mail all correspondences to the below. Please tick (✓) the appropriate boxes.

Mail to : ❑ **Office** ❑ **Residence**

Brief biodata (not longer than 50 words) (*to be appended with this Reply Slip*).

____
____
____
____

Have you ever reviewed submissions for publication in any Journal(s) before?

❑ **Yes** ❑ **No**

If YES, name the Journal(s) : Do you have papers published in any Journal(s)?

❑ **Yes** ❑ **No**

If YES, name the Journal(s) : ______________________________

Date : ______________ **Signature** : ______________

CALL FOR SUBMISSION OF IEM JOURNAL

The **IEM Journal** is an Engineering peer-reviewed journal published quarterly by The Institution of Engineers Malaysia. IEM Journal is dedicated to increasing the depth of research across all areas of engineering field: http://www.myiem.org.my/content/journal-122.aspx.

IEM Journal welcomes the submission of manuscripts that meet the general criteria of significance and scientific excellence in any of the Engineering field, and will publish:

- ❑ Original articles in basic and applied research
- ❑ Case studies
- ❑ Critical reviews, surveys, opinions, commentaries and essays

We invite you to submit your manuscript(s) in Times New Roman (12 point double spacing) to:

The Principal Journal Editor
Standing Committee on Information and Publications
The Institution of Engineers, Malaysia
Bangunan Ingenieur, Lots 60 & 62, Jalan 52/4
P.O. Box 223 (Jalan Sultan)
46720 Petaling Jaya, Selangor Darul Ehsan
Tel: 603-7968 4001/2 **Fax:** 603-7957 7678
E-mail: pub@iem.org.my/sec@iem.org.my **Website:** www.myiem.org.my

INFORMATION FOR AUTHORS

Submission of a contribution is taken to manifest the fact that the submission has not been submitted, accepted, published, or copyrighted elsewhere. To avoid publication delays, please send all manuscripts to the Editor and observe the following guidelines.

A. SUBMISSION OF PAPER

Authors are required to send four (4) copies of the manuscript and also short biodata/profiles of all author(s) with photo together with the softcopy (excluding via e-mail) upon submission. Each copy should be completed with keyword, illustrations (if any) and an abstract. Authors are also required to propose 3 reviewers (one of whom is international) for the manuscript.

Submissions should be made to the address below:

Chief Editor
The Institution of Engineers, Malaysia
Bangunan Ingenieur, Lots 60 & 62, Jalan 52/4
Peti Surat 223 (Jalan Sultan), 46720 Petaling Jaya, Selangor Darul Ehsan
Tel: 03 – 7968 4001 / 7968 4002 **Fax:** 03 – 7957 7678
E-mail: pub@iem.org.my

Three types of papers are solicited for the IEM Journal:

(1) **Regular Paper** – Presentation of significant research, developments or applications in any field of engineering or within the scope of the journal. Tutorials and surveys are also considered. For submissions, the length should be about 30 pages; double-spacing, single column with font of 12 (Times).

(2) **Brief Paper** – A concise description of new technical concepts or applications within the scope of the journal. Submission should be about 20 pages; double-spacing, single column with font of 12 (Times).

(3) **Technical Correspondence** – Letter to the Editor, comments on established engineering topics and discussion of published papers. Submission should be about 10 pages; double-spacing, single column with font of 12 (Times).

A minimum of 10 references, primarily to recent Journal paper is expected.

Citations of textbooks and web pages should be used very rarely. In order to verify of the IEM journal is the right Journal for manuscript submission authors may check if they are able link their to findings to other work published in the IEM Journal. Plagiarism is strictly prohibited for the IEM Journal.

NOTE ON FORMAT FOR THE MANUSCRIPT:
First submission for a review process: .pdf format in double spacing, single column, 12pt (Times) and pre-production (after reviewed): .doc format in double column, single spacing, 10pt (Times).

Manuscripts submitted as papers should state the significance of the problem in the Introduction.

Paper size should be of A4 (210 cm × 297 cm) with 2cm margins on the left, right, and bottom and 3cm from the top.

Enclose a signed letter giving your preferred address, telephone, fax number, and e-mail address (if available) for correspondence and return of proofs.

If the manuscript has been presented, published, or submitted for publication elsewhere, please also inform the Editor. Our primary objective is to publish technical materials not available elsewhere, but on occasion we publish papers of unusual merit that have appear or will appear before other audiences.

The language of the Journal is English. However, a paper in Bahasa Malaysia is also accepted and an abstract in English must be included.

Note that upon acceptance of an article for publication, the author is requested to submit a camera-ready format of the manuscript with single-spacing, double-column and font of 10 (Times). Illustrations and keywords of the paper should be included in the text. An electronic copy of the manuscript should also be submitted. The author is also requested to submit a passport-sized photograph and a short biography. This information will be sent to the author by the Editor.

B. STYLE FOR DRAFT OF MANUSCRIPT FOR REVIEW PROCESS

The draft of manuscript for a review process shall in word format.

The manuscript should be typewritten using double-spacing, font of 12 (Times); on one side of sheet only and in a single column format. The format for IEM Journal follows that of the IEEE Transactions (USA).

As we practice blind review, please do not put your name and address in the manuscript.

Provide an informative 100- to 250-words abstract at the head of the manuscript.

All sections should be numbered in Roman such as 1, 11, etc. with the title in capitals.

Sub-sections should be numbered in alphabet such as A, B, C, etc.

Sub-sub-sections (if any) should be numbered as A., A.2, etc.

Numbered all equations in round brackets ( ) flush to the right. The equation should be in the center.

References in the text should be cited each by a reference number in square brackets, e.g. [12] or [4-6], etc.

In the reference section, the references should be written as follows:

Style for papers: Reference Number, Author, first initials followed by last name, title (italics), location and publisher, year, chapter or page numbers, month, and year.

Style for books: Reference Number, Author, first initial followed by last name, title (italics), location and publisher, year, chapter or page numbers (if desired).

Sample format for references is as follows:

For paper
[3] M. Khalid, S. Omatu, and R. Yusof, "Temperature Regulations with Neural Networks and Alternative Control Schemes"' IEEE Trans on Neural Networks, Vol. 6, No. 3, pp. 572-582, May, 1995.

For book
[4] S. Omatu, M. Khalid, and R. Yusof, Neural-Control and Its Applications, London: Springer-Verlag, 1995.

If your paper is in Bahasa Malaysia, please provide an abstract in English.

C. STYLE FOR CAMERA READY MANUSCRIPT (PRE-PUBLICATION)

In the event of the paper being accepted, we will require the camera-steady manuscript to be submitted in a double column format, single-spacing and font of 10 (Times). Include all illustrations in between the text (if possible). An electronic copy should be submitted. We strictly prefer a document format camera ready manuscript for pre-publication.

D. STYLE FOR ILLUSTRATIONS

Try to include the illustrations in between the text.

Originals for illustrations should be sharp, noise-free and of good contrast.

Each illustration must be numbered such as "Figure 1, Figures 2-3, etc." and have a meaningful caption at the bottom. For tables, the caption must be at the top.

On graphs, show only the coordinate axes, or at most the major grid lines, to avoid a dense hard-thread result.

All lettering should be large enough to permit legible reduction of the figure to column width, perhaps as much as 4:1. Typing on figures is not acceptable.

Photographs should be glossy prints, of good contrast and gradation and any reasonable size.

Number each original on the back, or at the bottom of the front, and also indicate the author's name.

Upon acceptance of your paper submit a set of the figures and a list of the captions. An electronic softcopy must be submitted in a document format.

SUBSCRIPTION OF IEM JOURNAL

To subscribe Journal of IEM, please contact:

DIMENSION PUBLISHING SDN BHD (449732-T)
Level 18-01-03, PJX-HM Shah Tower
No. 16A, Persiaran Barat
46050 Petaling Jaya, Selangor Darul Ehsan.
Tel: +603 7493 1049
Fax: +603 7493 1047
E-mail: info@dimensionpublishing.com
Website: www.dimensionpublishing.com

Subscribe to IEM's Publications Now!

Yes! I would like to be a subscriber of The Institution of Engineers, Malaysia's publications

Name: ____

Mailing Address: ____

____ Country: ______________

Company/Institution: ____

Title: ____

Telephone No: ______________ Fax: ______________ Email: ______________________

☐ New Subscriber ☐ Renewal

Please commence my subscription from: ______________(month/year) Signature: ______________

To start your subscription of IEM's publications, complete this form and mail it back to the address below. For faster processing, fax it to: +603 7493 1047. Thank you.

What is your primary job title?

- ☐ Corporate Management (including chairman, president, proprietor, partner, director, vice president, general manager, division manager, import/export manager, other corporate title)
- ☐ Management (including project/contract/equipment/service/transport district manager, clerk of works, other technical or operating manager)
- ☐ Engineering/Design (including chief engineer, chief designer, civil/highway/mechanical/planning engineer, other engineering/design title)
- ☐ Buying/Purchasing (including chief buyer, buyer, purchasing officer, other buying/purchasing title)
- ☐ Titles allied to the field (architect, consultant, surveyor, research and development professor, lecturer, supervisor, superintendent, inspector or other allied title)
- ☐ Others (please specify) ______________

What type of organisation do you work in? *(Tick one box only)*

- ☐ Contractor
- ☐ Sub-contractor specialist
- ☐ Design and build contractor
- ☐ Consulting engineering/architectural/quantity surveying practice
- ☐ Mining/quarrying/aggregate production company
- ☐ Petroleum producer
- ☐ International/national authorities
- ☐ National/regional/local government
- ☐ Public utilities (electricity, gas, water, deck and harbour, other)
- ☐ Manufacturer
- ☐ Distributor/importer/agent
- ☐ Construction department of large industrial/Commercial concern
- ☐ Association/education establishment/research
- ☐ Construction equipment hire/rental company
- ☐ Project/construction management consultancy
- ☐ Others (please specify) ______________

What are the main activities of your organisation? *(Tick all that apply)*

Constructions of:	Manufacturer of:
☐ Roads/bridges	☐ Construction equipment
☐ Dams/reservoirs/irrigation	☐ Cement
☐ Harbours/offshore structures	☐ Other construction materials
☐ Foundations/tunnels	☐ Distribution
☐ Pipelines/refineries	☐ Construction equipment
☐ Structures/steel work	☐ Construction materials
☐ Building (commercial, industrial)	☐ Hire/rental of construction equipment
☐ Housing	☐ Design
☐ Construction management	☐ Earth-moving/open cast mining
☐ Deep mining	☐ Aggregate production

☐ Others (Please specify) ______________

Rate *(Please tick)*

- ☐ **RM234.00** - 12 issues of JURUTERA
- ☐ **RM117.00** - 6 issues of JURUTERA.
  Please specify the subscription month ______________
- ☐ **RM148.00** - 4 issues of quarterly Journal
- ☐ **RM95.00** - Annual IEM Directory (Hardcopy)
- ☐ **RM65.00** - Annual IEM Directory (CD-ROM)

Terms and Conditions:

1) The subscription is to be prepaid.
2) Please make cheque payable to **Dimension Publishing Sdn Bhd.**
3) Subscriptions are not refundable.
4) Magazine/s will be sent to the mailing address given.
5) Students are entitled for a 20% discount from the above subscription rate.
6) Students must submit a photocopy of the student identification card together with the payment.
7) The above rate is inclusive of delivery charges and applicable in Malaysia only.
8) Additional delivery charges will apply to overseas subscribers.

For subscription enquiries, please contact +603-7493 1049 or email to subscription@dimensionpublishing.com.

dimensionpublishing
The Choice of Professionals

DIMENSION PUBLISHING SDN. BHD. (449732-T)
Level 18-01-03, PJX-HM Shah Tower, No. 16A, Persiaran Barat, 46050 Petaling Jaya, Selangor Darul Ehsan, Malaysia
Tel +603 7493 1049 **Fax** +603 7493 1047 **Website** www.dimensionpublishing.com

EDITORIAL ADVISORY BOARD FOR IEM JOURNAL (MAY 2011 TO MARCH 2013)

Dear Readers,

If you have any comments or feedback concerning the Journal, please write in to *pub@iem.org.my* **within one month** from the publication of this issue.

PUBLICATION DISCLAIMER

The publication has been compiled by IEM and Dimension with great care and they disclaim any duty to investigate any product, process, service, design and the like which may may be described in this publication. The appearance of any information in this publication does not necessarily constitute endorsement by IEM and Dimension. They do not guarantee that the information in this publication is free from errors. IEM and Dimension do not necessarily agree with the statement or the opinion expressed in this publication.

We are pleased to announce that the articles in the IEM Journals have been indexed by other organisation *i.e. Linda Hall Library of Science, Engineering and Technology, Kansas City.*

THE INSTITUTION OF ENGINEERS, MALAYSIA
Bangunan Ingenieur, Lots 60 & 62, Jalan 52/4, P.O. Box 223 (Jalan Sultan), 46720 Petaling Jaya, Selangor.
Tel: 03-7968 4001/4002 Fax: 03-7957 7678 E-mail: sec@iem.org.my Homepage: http://www.myiem.org.my